VIRAL PROTEIN ENCAPSULATION FOR VACCINE VEHICLES:

CHARACTERIZATION AND *IN VITRO* STUDIES

A Dissertation

by

MIN-CHI HSIEH

Submitted to the Office of Graduate and Professional Studies of
Texas A&M University
in partial fulfillment of the requirements for the degree of

DOCTOR OF PHILOSOPHY

Chair of Committee,	Arul Jayaraman
Committee Members,	Robert C. Alaniz
	Zhengdong Cheng
	Victor Ugaz
Head of Department,	M. Nazmul Karim

December 2018

Major Subject: Chemical Engineering

ABSTRACT

Viral proteins are a potential candidate for subunit vaccine development as they are able to self-assemble into an authentic structure without the existence of an infectious genome. However, its poor immunogenicity limits its applications for vaccine delivery. Therefore, this work aims to develop an antigen-adjuvant complex to increase the immune response and cell viability with viral proteins, as well as investigate the mechanism of inflammasome signaling with the antigen-adjuvant complex *in vitro*.

Simian Virus 40 viral protein 1 (*SV40* VP1) viral protein with a size of ~20 nm in diameter was produced as a recombinant protein using a baculovirus expression vector system, and verified using SDS-Page and Western Blot analysis. *SV40* VP1 was then successfully encapsulated onto sacrificial $CaCO_3$ microparticles using layer-by-layer deposition of biodegradable dextran/poly-$_L$-arginine polyelectrolyte pairs. Zeta potential measurements, energy-dispersive spectroscopy, scanning electron and transmission electron microscopy confirmed the successful fabrication of the viral protein based polymeric multilayer capsule (VP-PMLC). Two approaches of viral protein encapsulation and different molecular weights (MW) of polyelectrolytes were investigated, and the highest encapsulation efficiency of 63% was observed using high MW polyelectrolyte pairs with protein deposited in the first layer.

In vitro release profiles were investigated with DC2.4 dendritic cells using fluorescent labeled dextran and 20nm fluorescent labeled silica beads to mimic the size of *SV40* VP1. Confocal microscopy demonstrated that all particles were engulfed within 4h, and while leakage of silica beads was observed within 24h by encapsulation of low MW polyelectrolytes,

fabrication with high MW of polyelectrolytes did not result in leakage of silica beads until 48h to 72h.

The overall cell viability was ~ 80% with a particle/cell ratio of ~20. The expression of co-stimulatory molecules, CD40 and CD86, was used to evaluate immune response with the antigen and adjuvant. It was observed that VP-PMLCs stimulate higher immune response in bone marrow-derived dendritic cells (BMDCs). An examination of the secreted cytokine profile from exposed BMDC cultures showed significant secretion of the pro-inflammatory cytokine IL-1β but no detectable increase in the levels of other pro-inflammatory cytokines such as IL-12 and TNF-α. We then verified that cathepsin B was required for IL-1β secretion, but the actin polymerization was not necessary.

Together, our results demonstrate that *SV40* VP1-based PMLCs are able to elicit stronger immune responses in dendritic cells while requiring lower doses of viral protein.

DEDICATION

To my parents, Ming-Yen Hsieh and Su-Jui Chen, my siblings,

my husband, Yan-Ru Lin, and my daughter, Emily Lin,

for all of their love, understanding and support

ACKNOWLEDGEMENTS

I would like to thank my committee chair, Dr. Jayaraman, and my committee members, Dr. Alaniz, Dr. Cheng and Dr. Ugaz, for their guidance and support throughout the course of this research. I also want to thank Dr. Pishko for all the support during my Ph.D. life.

Thanks also go to my friends and colleagues and the department faculty and staff for making my time at Texas A&M University a great experience. Finally, thanks to my mother and father for their encouragement and to my husband and daughter for their patience and love.

Moreover, much thanks to my co-worker Yufang Ding, a positive, hard-working girl who always encourages me and gives me so much hope, and my F2 friends, who always support me in my daily life! Further thanks go to Jing Zhou, Nitesh Sule and Rebekah Davis for their valuable discussions.

CONTRIBUTORS AND FUNDING SOURCES

This work was supervised by a dissertation committee consisting of Professor Arul Jayaraman and Zhengdong Cheng, Victor Ugaz of the Department of Chemical Engineering and Professor Robert C. Alaniz of the Department of Texas A&M Health Science Center.

All work for the dissertation was completed independently by the student.

There are no outside funding contributions to acknowledge related to the research and compilation of this document.

NOMENCLATURE

6xHis-tag	hexa histidine-tag
µl	microliter
µm	micrometer
µM	micromolar concentration
AcMNPV	autographa californica multicapsid nucleopolyhedrovirus
AIM2	Interferon-inducible protein AIM2
Bacmid	baculovirus shuttle vector
BCA	bicinchoninic acid
BEVS	baculovirus expression vector system
BMDC	bone marrow derived dendritic cell
BSA	Bovine Serum Albumin
CA-074 Me	CA-074 methyl easter
CaCO3	calcium carbonate
CCL3	chemokine (C-C motif) ligand 3
CD	cluster of differentiation
cm	centimeter
DAMP	damage-associated molecular pattern
DC	dendritic cell
DI	deionized
DNA	deoxyribonucleic acid
DS	dextran sulfate sodium salt

E. coli	escherichia coli
EDS	energy-dispersive x-ray spectroscopy
EDTA	ethylenediaminetetraacetic acid
FBS	fetal bovine serum
FE-SEM	field emission scanning electron microscope
FITC	fluorescent isothiocyanate
FSC	forward-scatter
GM-CSF	granulocyte-macrophage colony-stimulating factor
h	hour
HBsAg	Hepatitis B surface antigen
IFN-γ	Interferon-gamma
IL	interleukin
IPAF	NLR family CARD domain-containing protein 4
IPTG	Isopropyl β-D-1-thiogalactopyranoside
JAK-STAT	janus tyrosine kinase - signal transducer and activator of transcription
kb	kilobyte
KCl	potassium chloride
kDa	kilodalton
Lat. A	Latrunculin A
LbL	layer-by-layer
LDH	lactate dehydrogenase
LPS	lipopolysaccharide
ME	methyl ester

mg	milligram
MHC	major histocompatibility complex
min.	minute
ml	milliliter
mV	millivolt
MW	molecular weight
MWCO	molecular weight cut-off
NaCl	sodium chloride
ng	nanogram
Ni-NTA	nickel-nitrilotriacetic acid
nM	nanomolar concentration
NOD	nucleotide-binding and oligomerization domain
Ni-NTA	nickel-nitriloacetic acid
NLRP3	NOD-like receptor family, pyrin domain containing 3
nm	nanometer
PAMP	pathogen-associated molecular pattern
PEG	polyethylene glycol
PFA	paraformaldehyde
PFU	plaque-forming unit
pI	isoelectric point
PLARG	poly-L-arginine
PMLC	polymeric multilayer capsule

PYHIN	pyrin and haemat-opoietic interferon-inducible nuclear antigens with 200 amino-acid repeats
SDS-PAGE	sodium dodecyl sulfate polyacrylamide gel electrophoresis
Sf9	spodoptera frugiperda
SSC	side-scatter
STAT	signal transducer and activator of transcription
SV40	simian virus 40
TEM	transmission electron microscopy
TH1	type 1 T helper cells
TNF	tumor necrosis factor
Tris	tris(hydroxymethyl)aminomethane
UV	ultraviolet
VP	viral protein

TABLE OF CONTENTS

Page

LIST OF FIGURES

Page

LIST OF TABLES

Page

1. INTRODUCTION

1.1 Motivation

Vaccination is the most efficient way to control and prevent diseases. Currently, the most effective way is through parenteral immunization with booster doses. The inconvenience and patient noncompliance creates the need for more efficient vaccine fabrication strategies. Taken together, recent attention has been given to subunit vaccine, composed by part of pathogens.

Viral protein can assemble spontaneously through one or more viral protein units without the existence of viral genome and have properties similar to the responding virions [1]. This authentic structure provides the ability to mimic viral attachment and virion assembly, resulting in the capability of cellular and humoral immune responses for both viral and non-viral diseases[2]. Taking advantage of the versatile modification and safety approach, recombinant proteins are usually evaluated as a potential vaccine candidate. However, the viral protein alone serving as antigen showed lower immunogenicity by poorly presented to the immune systems, and the help from adjuvants are needed.

The toxicity and the failure to induce potent CD4 Type 1 T helper cells and CD8 cytotoxic T cell responses [3] present a problem for the conventional adjuvants. Biodegradable polyelectrolytes further show a potential candidate due to its variety. The existence of the polyelectrolytes may also slow the viral protein release profile, which resulted in enhancing the dendritic cell-binding probability and inducing stronger immune stimulation.

Therefore, by assembling viral protein onto biodegradable polyelectrolytes, this work aims to elaborate the structure, physicochemical properties and antigen encapsulation efficiency

of viral protein-based capsules. The cytotoxicity, release profile, immune response, cytokines and inflammasome signaling pathway towards mice dendritic cells *in vitro* are studied as well.

1.2 Specific aims and basic hypothesis

1.2.1 Fabrication and characterization of viral protein encapsulated polymeric multilayer capsule (VP-PMLC)

Recombinant viral protein encapsulated by polyelectrolytes is first fabricated in this research.

The *Simian Virus 40* viral protein 1 is harvested by a baculovirus expression vector system. The biodegradable polyelectrolytes, Dextran and Poly-$_L$-Arginine, are applied as polyanion and polycation, respectively. Through Layer-by-Layer technology, the viral protein fabrication with polyelectrolyte pairs is done by the electrostatic interactions. ξ-potential is then applied to monitor the surface charge on each layer, scanning electron microscopy; energy dispersive spectroscopy and transmission electron microscopy images gives evidences for the capsule morphology and the successful of the fabrication; confocal laser scanning microscopy is used by applying fluorescent labels towards polyelectrolyte to verify its structure; and viral protein encapsulation efficiency is measured by bicinchoninic acid protein assay kits

1.2.2 In vitro *immunity study on mice bone marrow derived dendritic cells*

Dendritic cells are immune cells that effectively link the innate and adaptive arms of the immune systems. They are considered a professional antigen-presenting cell population not only due to their ability to stimulate 100 to 3000 T cells but also because of their unique capacity to induce the activation and differentiation of naive T lymphocytes. As for particulate immune systems, dendritic cells showed the ability to take up more particles than macrophages [4]. Therefore, here we aim to investigate the *in vitro* properties of co-culturing viral protein-based polymeric multilayer capsules on mice bone marrow derived dendritic cells.

Several viral protein-based polymeric multilayer capsules are tested by either encapsulation through different molecular weight of polyelectrolytes or different approaches of viral protein encapsulation. The *in vitro* studies include 1) cell viability through lactate dehydrogenase cytotoxicity assay kits, 2) release profile through confocal laser scanning microscopy with fluorescent dextran and silica beads, and 3) surface immune level through surface markers, CD40 and CD86, by flow cytometry analysis on mice bone marrow derived dendritic cells.

1.2.3 In vitro *signal pathway study on mice bone marrow derived dendritic cells*

Cytokines are another crucial factor for immune response especially on the ability to activate adaptive immune systems. TNF-α, IL-12 and IL-1β are detected by mice bone marrow derived dendritic cells co-cultured with these viral protein-based polymeric multilayer capsules. The secretion level is then measured by ELISA assay kits. With positive cytokine secretion observed, *in vitro* inflammasome signaling pathway is then investigated.

2. LITERATURE REVIEW

The immune system is composed of special cells, proteins, tissues and organs to defend the body from attacks by microorganisms and pathogens. In order to function properly, the immune systems must be able to detect a wide range of pathogens and also distinguish between them and healthy tissue [5].

Vaccines, which are made of dead or weakened antigens, are the most efficient way to train the immune system. The amount of these antigens is not enough to cause an infection, but is still sufficient to induce innate immunity, which further activates adaptive immune responses to produce antibodies. After the threat has been cleared, many of the antibodies will be cleared from the body but this memory remains in immune cells. When the body encounters the specific antigen again, the memory cells produce antibodies quickly and eliminates the pathogen [6].

The most effective vaccines currently are attenuated vaccines based on parenteral delivery. Though these living vectors are able to activate innate immune systems and further develop robust memorized antibodies, the safety issues are still a concern. Therefore, vaccine design has shifted from containing the whole microorganism to only part of it.

2.1 Viral protein-based subunit vaccines

Vaccination is the most efficient way to control and prevent infections. The first vaccine was created in 1796 by Edward Jenner, the father of immunology, and successfully eradicated smallpox and demonstrated the power of the vaccine. Vaccines are generally classified as inactivated, live attenuated and subunit vaccines [7-9]. Inactivated vaccines, such as Polio vaccine and Hepatitis A vaccine, are made using dead pathogens. These microbes are killed by either heat, radiation or exposure to chemicals, resulting in lower risk but also less efficacy [10].

Live attenuated vaccines, such as Measles vaccine, Mumps vaccine, Rubella vaccine and Nasal-Spray Flu vaccine, contain a microbe variant that has been weakened in the lab. These vaccines are efficient and less toxic than live pathogens, but they are still able to replicate inside the human body [11, 12]. Subunit vaccines do not introduce pathogens that can replicate in the body, and are the focus of current research as they are safe and represent an effective approach for vaccine development [13]. Influenza vaccine and Hepatitis B vaccine are two vaccines that belong to this sub-category of vaccines.

Subunit vaccines are composed only by the antigenic parts of the pathogen, which are necessary to elicit a protective immune response, such as viral capsid protein antigens [14]. Viral capsid protein antigens are part of the virus which self-assemble into higher-order three-dimensional architectures and preserve the antigenic structure of virus immunogenes. Therefore, they are capable of invading and entering cells but do not lead to infection [1]. However, these peptide-based or highly purified protein components do not effectively activate the host innate immune response like a natural infection would do [15]. Although subunit vaccines represent a safe and effective means of vaccination, highly purified viral protein alone elicits weak induction of innate immunity in the host. Therefore, such vaccines require additional components known as adjuvant, that increases the level of innate immunity activation and enhances the immunogenicity of antigens used in vaccines [16, 17].

2.1.1 Antigens and adjuvants

Adjuvants, including inorganic, organic, macromolecules and bacteria, are chemical permeation enhancers that have been used to augment the immune response towards antigens by immune cells, inducing cytokine expression or activated antigen-presenting cells [3, 18]. They are capable of activating either innate or adaptive immune responses, but are themselves

immunologically inert. In the context of application to vaccine delivery, adjuvants have several advantages as they: (a) activate different signaling pathways [19], (b) serve as a depot barrier resulting in slow release [20], (c) minimize the amount of antigens needed [21], and (d) facilitate oral delivery[22, 23]. Currently, aluminum salts [24], oil-in-water emulsion MF59 [25], Freund's adjuvants [26], heat-labile enterotoxin [27], cholera enterotoxin [28], lipopolysacchride (LPS) [29], chemokine CCL28 [30] and oligodeoxynucleotide containing CpG motifs [31-33] are used as adjuvants in vaccine development. However, toxicity of the adjuvants and failure to induce potent CD4 Type 1 T helper cells (T_H1) and CD8 cytotoxic T cell responses are problems that limit the use of conventional adjuvants [3].

One proposed solution to improving the performance of adjuvants is the use of biodegradable and biocompatible polymers, including dextran, caprolactone [34], inulin [35], and chitosan [36]. For example, though chitosan has not been confirmed to stimulate an immune response, it affects antigen release because of its intrinsic ability to open tight junctions and adhere to the mucosal surface [28, 37]. Though the mechanism by which PMLCs induce an immune response is still unclear, evidence shows that PMLCs, composed of Poly-$_L$-Arginine/Dextran polymers (P_LARG), play a crucial role in mediating dendritic cell activation *in vivo* [38]. Evidence also shows that P_LARG provides strong enhancement of the mucosal specific IgA response *in vivo* [39, 40]. These studies illustrate the advantages of using biodegradable polymers as adjuvants.

With an antigen-polymer complex, the uptake mechanism of antigen-presenting cells might be different from that of the antigen itself. The antigen-polymer complex can be phagocytosed [41] and processed through proteasomes, activate the inflammasome pathway via

secretion of the cytokine IL-1β, acts as a ligand for toll-like receptors, or directly interact with B cells [3].

2.1.2 Viral protein characteristics

A virus is a small infectious agent that replicates only inside the living cells of other organisms. It is composed mainly of nucleic acids surrounded by a protective coat of protein, also called as capsid protein [2]. A virus might be composed of several viral proteins, but the capsid protein is the only one which is able to form the viral cover without the genome from identical protein subunits. Therefore, the viral protein alone is not infectious, is capable of delivering viral genomes into targeted cells, and thus is a promising tool for the delivery of genes, drugs, and pharmaceuticals [42-44].

The most well-known and commercial subunit vaccine is the Hepatitis B vaccine. Hepatitis B vaccine was first commercially available in 1982, and composed of Hepatitis B surface antigen (HBsAg) purified from the plasma of patients with chronic Hepatitis B virus infection [45]. The source of HBsAg has now been replaced with heterologous expression of the HBsAg gene using yeast or mammalian cells to eliminate concerns associated with the use of human blood products [46]. The HBsAg protein is adsorbed to aluminium hydroxide or aluminium phosphate, and is used as the adjuvant for better immunization. While effective, three injections are needed to prevent Hepatitis B infection [47]. Therefore, there is significant interest in developing subunit vaccines that have the effectiveness of the Hepatitis B vaccine but require fewer injections.

In this work, Simian Virus 40 (*SV40)* Viral Protein 1, the capsid protein of *SV40,* is chosen as the antigen due to its long-term gene expression in target cells and its capability to efficiently incorporate larger transgenes *in vitro* with safety and flexibility than the capacity of

the *SV40* wild-type [48]. *SV40* belongs to the *Polyomavirus* family and was isolated in 1960 as a contaminant of human polio vaccines originating from monkey cells harvested during the 1950s [49, 50]. *SV40*, which could abortively infect and transform mice cells *in vitro*, does not replicate in mice cells [51]. However, whether *SV40* can cause human tumors has been a highly controversial issue for over 50 years. There is inadequate evidence to support widespread *SV40* infection in the human population or a direct role for *SV40* in human cancer treatment [52-54]. Though *SV40* is still under investigation as a human virus, *SV40* VP1 virus-like particle is considered to be safe for use as a vaccine vehicle [55].

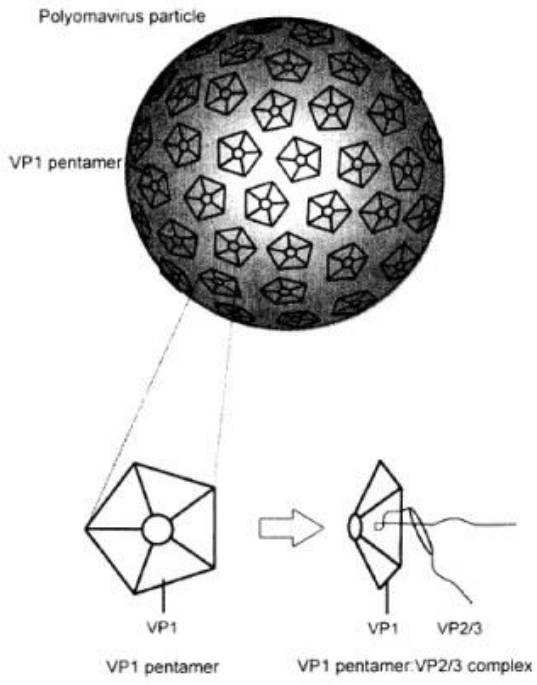

Figure 1. The general architecture of *Polyomavirus*, reprinted with permission [56].

SV40 is a small, non-enveloped, double-strained deoxyribonucleic acid (DNA) virus with a diameter of 45 nm and a circular genome of ~ 5 kb, which encodes three viral proteins, viral protein 1 (VP1), viral protein 2 (VP2) and viral protein 3 (VP3) [56, 57]. As shown in Figure 1, the outer shell contains 360 monomers of the major capsid protein VP1, arranged in 12 pentavalent and 60 hexavalent pentamers with an isoelectric point (pI) equals to 6.8 [56, 58]. It unexpectedly forms three different types of connections in the T = 7d icosahedral surface lattice, which is inconsistent with the quasi-equivalent bonding theory [59]. The structure of *SV40* VP1 is a jellyroll β-barrel with extending amino- and carboxy-terminal arms [56]. Each VP1 monomer forms extensive contacts with its neighbors, VP2 and VP3; the amino-terminal (N-terminal) arm of VP1 binds DNA and faces the interior of the capsid and the carboxy-terminal (C-terminal) arm ties the 72 pentamers together by disulfide bridge. *SV40* VP2 and VP3 have the same sequences in their C-terminus but differ in their N-terminus composition [56]. The *SV40* genome, ses, presents within the viral regulation region and plays a crucial role for replication [60].

SV40 VP1 serves as capsid protein is responsible for the attachment to the host cells. The journey of a virus traveling from the cell surface to the nucleus contains mainly four distinct steps [61]: receptor binding, targeting to the endoplasmic reticulum, endoplasmic reticulum membrane penetration and nuclear entry.

First, *SV40* virions bind to the cell surface via the ganglioside and Major Histocompatibility Complex (MHC) class I. Because there are 360 binding sites in each *SV40*, the *SV40*-GM1 interaction is relatively strong. Second, after binding, *SV40* virions enter the cell by caveolae-mediated endocytosis and travels to the endoplasmic reticulum. Third, in the endoplasmic reticulum, the viruses penetrate the membrane either through endoplasmic

reticulum-associated degradation-mediated cytosol transport or viroporin-mediated nuclear entrance. Finally, *SV40* can travel through the cytosol to nuclear pores [56, 61, 62].

As a subunit vaccine, the capsid protein alone can form virus-like particles without the needs of viral genome, showing more authentic conformation of viral antigens than other subunit vaccines. Besides its structural function, virus-like particles alone possess a receptor-binding domain [63], a nuclear localization signal domain, a DNA-binding domain, as well as a calcium-ion-binding domain [64]. These aspects are crucial in mimicking viral attachment and virion assembly, resulting in the ability to stimulate efficient cellular and humoral immune responses for both viral and non-viral diseases [2]. Therefore, the *SV40* VP1 viral protein was used in this work.

SV40 VP1 is small, non-infectious, and capable of self-assembly [65]. The repeated units of *SV40* VP1 viral protein and its highly organized structure further facilitates the formation of mono-dispersed capsules easily. These capsules can be engineered at their internal, external or inter subunit interfaces at specific locations, allowing for highly controlled surface properties [66]. Also, several studies have investigated different factors and mechanisms of *SV40* VP1 self-assembly and disassembly, which has led to their use in several applications [48, 67]. The mechanism of dissociation and re-assembly of *SV40* VP1 viral protein is also well studied [67-70]. Moreover, *SV40* VP1 viral protein can non-specifically target cells, induce non-preexisting immune response in humans and provides many binding sites on the viral protein surface [71]. These properties make *SV40* VP1 an ideal candidate for the development of vehicles for vaccine delivery [72].

SV40 VP1 virus-like particle was first produced by the *Escherichia coli* (*E. coli*) bacterial system. It demonstrated the ability to assemble into an empty capsid-like structure

spontaneously, with a size and morphology similar to the wild-type *SV40* (*wtSV40*) [73]. However, this system may not be ideal for scale up and lack posttranslational modifications, such as phosphorylation, sulfation, methylation, acetylation and hydroxylation, that occur only in eukaryotic cells [74]. Therefore, the eukaryotic baculovirus expression vector systems (BEVS) is considered to be a better production system for *SV40* VP1 as it provides more benefits [75]. These advantages include: 1) ability to harvest larger amount of recombinant proteins, 2) having correct protein folding because of production in eukaryotic cells, 3) narrow host range for infection, 4) can be terminated easily and 5) more amenable to scale-up [76]. Furthermore, it can also be potentially used for investigating the transportation to the nucleus and protein-protein interactions [77]. Therefore, there are broad applications for virus-like particles. For instance, they can be used as a tool for providing the natural structure for studying virus-host interactions, investigating the assembly factors between major and minor proteins and performing fundamental research about the virus and the vaccines. Though they target cells in a non-specific manner, their ability to be easier modified to bind ligands, such as human Epidermal Growth Factor [78, 79] or tumor lysate [80], making them a potential candidate for tumor vaccine vehicles.

Nevertheless, most virus-like particles already in use as vaccine vehicles show poor activation of immunogenic pathways and need adjuvants for enhancement of immune responses. Evidence shows that *SV40* VP1 viral protein is presented as a natural adjuvant on cytotoxic T lymphocytes (CTL) induction. Therefore, *SV40* VP1 viral protein is a promising alternative for use in vaccine platforms [55].

2.1.3 Polymeric multilayer capsule (PMLC) self-assembly technology

Several approaches can be used to encapsulate antigens into particulate platforms, such as reverse micro-emulsion [81, 82], spray drying [83], and Layer-by-Layer (LbL). Considering recent advances in antigen encapsulation through polymers [84], the LbL technique further provides a more flexible and variable means to encapsulate antigens.

The LbL technique, first introduced by Gero Decher in the early 1990s, is based on sequential adsorption of oppositely charged polyelectrolytes onto a solid, charged surface via electrostatic interactions [85]. It is a well-known, reproducible and versatile technique for encapsulating a wide range of particles and makes it easier to control wall thickness, composition, physical, chemical surface properties and controlled-release profile [86]. This method can be applied in drug encapsulation [86-91], sustained release dosage form [92], gas barrier [93] and biosensors, etc. As for vaccine delivery applications, the polyelectrolyte shells can further protect antigens for other delivery routes, such as mucosal delivery [23, 94].

Originally, LbL was applied on charged planar substrates, such as silicon wafers. The LbL procedure can be divided into two steps (Figure 2) [85]. First, the charged planar substrate is immersed into an oppositely charged polyelectrolyte solution for a certain time, then removed and washed with deionized water to remove excess polyelectrolyte. This causes the polyelectrolyte to absorb to the substrate surface and reverses the surface charge of the substrate due to electrostatic charge. Second, the substrate is immersed into the second polyelectrolyte solution, which has a different charge from the first polyelectrolyte, then removed and washed with deionized water (DI water) to remove excess polyelectrolyte. Once again, the second polyelectrolyte absorbs to the substrate surface and reverses the surface charge of the substrate. These two steps can be repeated until the desired numbers of layers are achieved to meet the

thickness, composition or surface function needs. Besides electrostatic interactions, other interactions, including hydrogen bonding, hydrophobic interaction, covalent bonding, biospecific interactions, stereocomplex formation or van der Waals forces can also be used to absorb materials onto the particle surface through LbL build-up [95].

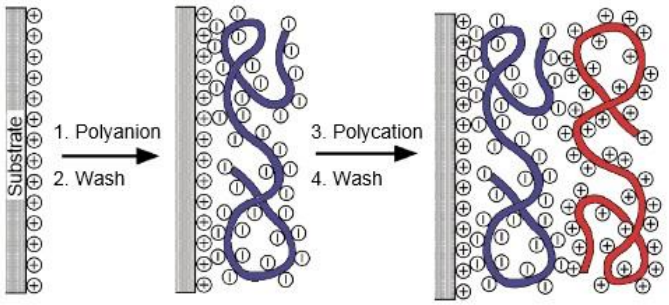

Figure 2. Schemes of Layer-by-Layer (LbL) adsorption procedures, reprinted with permission. [85]

Recently, more applications of LbL are merging in the fields of pharmaceuticals and biotechnology, to form forming nano- or microparticulates for use in vaccine delivery and controlled-release [89]. LbL has also been extended to colloidal systems, with the encapsulated macromolecules including DNA, enzyme [96], proteins [38, 97-99], live *E. coli* [100], lipids or other bioactive materials.

The procedure to build PMLCs is almost the same as the original LbL approach, but the problem is that the macromolecules are too small to be centrifuged down with normal speed. Therefore, a sacrificial core, such as calcium carbonate ($CaCO_3$) [98], Cadmium carbonate [101], and Manganese carbonate crystals [102], is applied to facilitate centrifugation and removed later in the process.

PMLCs are fabricated in three steps: first, the antigen is encapsulated in the sacrificial porous micro-templates; second, these micro-templates are coated with alternating anioic and cationic polyelectrolytes until desired properties are reached; finally, the sacrificial core is decomposed at relatively mild conditions to form the macromolecule PMLCs [98]. PMLC fabrication techniques can be applied to a broad range of polyelectrolytes and biomolecules, such as the protein encapsulation [99], live *E. coli* encapsulation [100] and enzyme encapsulation [96]. Moreover, it can strongly increase antigen delivery towards professional antigen presenting cells, such as dendritic cells, macrophages and B cells. The existence of the polyelectrolytes may also slow the viral protein release profile which can result in enhancing the dendritic cell activation and stronger immune stimulation.

In this work, calcium carbonate is chosen as the sacrificial core. $CaCO_3$ microparticles were fabricated by colloidal crystallization from supersaturated solution, which led to the formation of uniform spherical porous microparticles with a narrow size distribution. Variable sizes of $CaCO_3$ microparticles can be generated by varying fabrication conditions, such as the agitation speed, the agitation time or salt concentration [103]. $CaCO_3$ microparticles were formed by directly mixing calcium chloride and sodium carbonate under vigorous stirring and initiated by heterogeneous precipitation. After crystals formed, the terminated step was then applied by centrifugation and followed by thoroughly washed with DI water.

A wide variety of materials can be deposited, providing an easier way to control the thickness and meet requirements for surface modification. Biodegradable polyelectrolytes are currently broadly applied for therapeutic applications, as they can be degraded by cells and eliminated from the body [87, 104]. This work used dextran sulfate (DS) as the polyanion and

Poly-L-Arginine (P_LARG) as the polycation, which can be enzymatically degraded both *in vitro* [105, 106] and *in vivo* [107].

Dextran is a complex, branched glucan composed of chains of variable length [108]. As a sodium salt, dextran is a strong negatively charged polymer with a pKa value of 6.4, average molecular weight (MW) over 500 kDa, and is soluble and stable in water with a broad range of pH values. The chemical structure of dextran is shown in Figure 3a. Due to the repulsion of the negatively charged sulfate groups, the DS sulfate polymer is fully extended in low ionic strength solutions. On the other hand, P_LARG is a cationic poly-amino acid with a pKa value of 12 and average MW over 70 kDa, provides durable high positive charges with a broad range of pH values and assembles into stable and non-aggregated capsules. The chemical structure of P_LARG is shown in Figure 3b. P_LARG has also been demonstrated to disturb cell membranes and rapidly be phagocytozed by dendritic cells. However, P_LARG alone does not evoke T cell responses and can be used for booster function [109].

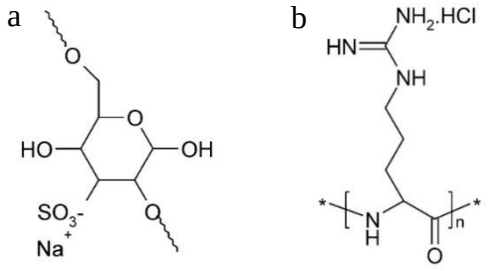

Figure 3. Chemical structures: (a) Dextran-Sulfate (DS) sodium salt and (b) Poly-L-Arginine (PLARG).

In order to increase the uptake by professional antigen-presenting cells, templating of antigens in nano- or microparticulate carriers by entrapment into the polymer network has been adopted [3, 41]. This is especially true for antigens in the 0.1 to 10 μm size range, which is similar to the dimension of pathogens, and shows potential to be recognized by dendritic cells [110]. For example, ovalbumin encapsulated by DS/P_LARG PMLCs, DS/P_LARG polyelectrolytes were encapsulated by dendritic cell *in vivo* with high efficiency and resulted in better antigen presentation to $CD4^+$ and $CD8^+$ cells [38].

Several factors, such as the thickness, numbers of layers, pH of the medium, surface charge, particle size, and surface properties, are important for antigen-polyelectrolyte fabrication [111-114]. The thickness of the shell is mainly determined by the property of polyelectrolytes and the number of layers we desired [111]. The influence of the surface charge on the outer layer of capsule is still unclear. Some studies propose that, particles with positively charged surface possessed an inherent adjuvanticity due to the electrostatic interaction with negatively charged membrane [112]. However, other studies showed that negatively charged surface, ~-20 mV, which show similar surface charge of bacterial and mammalian cells, leads to higher uptake behavior by immune cells [113]. As for the size factor, though dendritic cells are known to be able to engulf particles ranging from 0.1 to 10 μm in diameter, particle size ranging from 1-3 μm display higher uptake efficiency [114]. Moreover, the curvature or the roughness of the particle surface is another important factor that needs to be considered.

Together, several biomacromolecule encapsulated by P_LARG/DS capsules provide evidence to support that P_LARG/DS as adjuvants could strongly increase antigen delivery towards professional antigen-presenting cells [38]. However, no studies investigating viral protein-based encapsulation have been carried out.

2.2 Immune responses

2.2.1 Immune system

The two main classes of immunity are innate immunity and adaptive immunity. Innate immunity provides an immediate response to pathogens and alerts our bodies while, adaptive immunity is able to develop a specific army to eliminate pathogens [5].

The innate immune system is also a non-specific system providing immediate defense against infection. These cells, such as natural killer cells, mast cells, eosinophils, basophils and phagocytic cells, including macrophages, neutrophils, and dendritic cells, circulate in the blood and are able to recognize potentially harmful, non-self particles agents such as bacteria, viruses, pollen, dust or toxic chemicals. The non-self particles which are infectious and cause an immune response are termed as antigens, such as bacteria *a*nd viruses. The immune response can be induced by the entire non-self particle or by part of it [5].

The adaptive immune system, also called acquired immune systems, is an antigen-specific immune system. The adaptive immune system is composed of highly specialized cells, including B-cells and T-cells, and is aimed to eliminate pathogens or prevent their growth [5]. Adaptive immunity provides immunological memory after an initial response to a specific pathogen leads to an enhanced and quicker response to subsequent encounters with that pathogen [5]. Having antibodies ready in advance before pathogen infection is the primary benefit of vaccination; however, lymphocytes, which are able to produce specific antibodies and kill pathogens, are not normally circulating in the bloodstream [5]. Therefore, a connector between innate and adaptive immune systems is required.

Dendritic cells were first discovered in 1973 by the Steinman group, and are the initiator and modulator of adaptive immune systems [115]. Also, dendritic cells are the most potent

antigen presenting cells due to their ability to uptake, process and present foreign pathogens [116]. They are located in tissues such as the gut, circulate in the bloodstream and can contact external environments through the skin, the inner mucosal lining of the nose, lungs, stomach, and intestines [117]. Since dendritic cells are located in tissues that are common points for initial infection, they can identify threats and act as messengers for the rest of the immune systems by antigen presentation. Immature dendritic cells, serve as the first line of defense and circulate through the bloodstream [5]. Either directly activated by conserved pathogen molecules or indirectly by inflammatory mediators, dendritic cells mature and are able to elicit cytokines to recruit and activate adaptive immunity, such as T helper cells, to produce the specific antibody and eliminate pathogens.

In order to activate naïve lymphocytes from innate immunity, three signals are required: an antigen signal through the T cell receptor or B cell receptor, a co-stimulatory signal, such as CD40, CD86, and a cytokine signal. Once lymphocytes receive these three signals from antigen-presenting cells, effector T cells, and B cells, they differentiate and are activated [118]. Macrophages, dendritic cells, and B cells are the only cell types that can express specialized co-stimulatory molecules required to activate naïve T-cells [5]. However, differnet cells stimulate T-cells through different mechanisms. Dendritic cells can take up, process and present antigens from all types of sources, are only present in the T-cell areas, and overwhelmingly drive the initial clonal expansion and differentiation of naïve T cells into effector T-cells. However, macrophages and B cells specialize in processing and presenting antigens from intracellular pathogens and soluble antigens, and interact mainly with already primed effector CD4 T cells [5].

Immature dendritic cells migrate through the bloodstream to take up particulate matter by phagocytosis [119]. Though they then degrade the pathogens, their main role in the immune system is not the clearance but maturation [120]. Mature dendritic cells activate T lymphocytes by displaying antigens on their surface and also provide other signals to alert of the specific antigen. This is the reason dendritic cells are also called antigen presenting cells. In certain conditions, macrophages can also act as antigen-presenting cells [121], but dendritic cells also function in initiating the adaptive immune response.

2.2.2 Particulate design for stronger immune response on dendritic cell

Immature dendritic cells endocytose through a variety of mechanisms and include nonspecific uptake by constitutive macropinocytosis [38], specific uptake via receptor-mediated endocytosis [122], and phagocytosis [123]. Soluble protein or peptide antigens in the solution internalized by dendritic cells via macropinocytosis show weak immunity due to poor antigen presentation; however, the particulate form is able to greatly improve the cross-presentation efficiency via phagocytosis leading to stronger immune response [124, 125]. In order to induce strong immune response through particulate form, several factors such as surface modification [126, 127], shape[128], surface curvature[129], surface charge [112, 113], size [130, 131], the addition of IL-1β [132] are important. Because of the potential for use these materials in vaccine development, we focus on immunogenic and targeting of dendritic cells. This is because dendritic cells are the most potent antigen-presenting cells and play a vital role in the initiation of immune responses.

2.3 Inflammatory signaling pathways

2.3.1 Cytokine secretion

Cytokines are molecules that are used for cell signaling or cell-to-cell communication, and can be grouped by structure or receptors. The cytokines secreted by dendritic cells in response to activation of pattern recognition receptors include Interlukin-1β (IL-1β), Interlukin-12 (IL-12) and Tumor necrosis factor alpha (TNF-α) [133].

IL-1β belongs to IL-1 family, the hematopoietins, the TNF family, and the type I interferons, and can be activated by innate immunity [134]. IL-12, known as a T cell-stimulating factor, is able to induce lymphocytes to produce IFN-γ and is able to amplify the activation of T_H1 cells through Janus tyrosine kinase-signal transducer and activator of transcription (JAK-STAT) intracellular signaling pathway [135]. TNF-α is a major pro-inflammatory cell signaling protein involved in early inflammatory events and is one of the cytokines that make up the acute phase reaction [136].

The IL-12 family of heterodimeric cytokines includes IL-12, IL-23, IL-27, and IL-35. The first three of these cytokines are produced primarily by dendritic cells, macrophages, and monocytes, while IL-35 is produced by regulatory T and regulatory B cells [137]. Each of the IL-12 family cytokines consists of two subunits: an alpha chain (p19, p28, or p35) with a four alpha-helix bundle structure and a beta chain (p40 or EBI3) that is homologous to the soluble class I cytokine receptor chains [138].

IL-12 is a secreted heterodimeric cytokine that contains disulfide-linked p35 and p40 subunits, produced by macrophages, dendritic cells, monocytes, langerhans cells, neutrophils, keratinocytes, microglia, and non-germinal center B cells [138]. It acts through a receptor complex that contains the ligand binding IL-12 R β1 and the signal transducing IL-12 R β2. IL-

12 can enhance cytotoxic activity and induce Interferon-gamma (IFN-γ) production in natural killer cells, T-cells and dendritic epidermal T-cells [138]. In conjunction with IL-23 and IL-27, IL-12 promotes the development of a T_H1 immune response; however, while T_H1 cells continue to respond to signals during in infection, IL-12 is also needed to continuously sustain the effectiveness of differentiated T_H1 cells [138].

2.3.2 Inflammasome activation

The inflammasome is a multiprotein signaling complex belonging to the nucleotide-binding and oligomerization domain (NOD)-like receptor family, and is expressed not only in immune cells but also in other types of cells, such as astrocytes, epithelial cells, fibroblasts, keratinocytes and neurons [139]. There are mainly four types of inflammasomes: NOD-like receptor family, pyrin domain containing 1 (NLRP1), NLRP3, NLR family CARD domain-containing protein 4 (IPAF) and Interferon-inducible protein AIM2 (AIM2) [140]. Due to their components they can be separated into two groups: the NLR family including NLRP1, NLRP3 and IPAF, as well as the pyrin and haematopoietic interferon-inducible nuclear antigens with 200 amino-acid repeats (PYHIN family), like AIM2 [140].

The NLRP3 inflammasome is activated by a wide range of stimuli including pathogen-associated molecular patterns (PAMPs), such as viral RNA, damage-associated molecular patterns (DAMPs), such as ATP, fiber/particles, such as alum, metabolic products, such as monosodium urate crystals and environmental hazards, such as UV radiation. NLRP3 inflammasome is the most widely characterized and implicated in inflammasome diseases [141, 142]. Activation of NLRP3 inflammasome leads to the processing and secretion of IL-1β and IL-18, which in turn trigger an inflammatory response. These proinflammatory cytokines have been

shown to stimulate cytokine production by T_H1, T_H2 and T_H17 cells and consequently contribute to immune activation [143].

The NLRP3 inflammasome has been described by three models: the channel model [144], the lysosomal rupture model [145] and the cellular stress model [146]. The channel model describes the direct activation of the NLRP3 inflammasome through entry of hydrophilic molecules into the cytosol [142]. This model, however, fails to explain activation of the NLRP3 inflammasome through particulates that are too large to reach the cytosol through the newly formed pores. The lysosomal rupture model, proposed for particulates, suggests that phagocytosis of large crystals, particles or molecules leads to swelling and rupture of the lysosome and subsequent leakage of lysosomal enzymes into the cytosol [145]. The cellular stress model, which leads to the generation of reactive oxygen species aligned with changes in intracellular potassium concentration, has also been shown to contribute to inflammasome activation by particulates such as silica or alum [147].

Particulate vaccine delivery systems have been reported to act as adjuvants and to help promote immune responses through a variety of mechanisms such as enhanced uptake by dendritic cells, prolonged antigen presentation through a depot effect or targeting of specific cell compartments [104]. Recent studies showed that particulate systems with variant physicochemical properties could activate NLRP3 inflammasome through lysosomal damage, stimulate IL-1β secretion *in vitro* and further suggested that the NLRP3 inflammasome could be a common mechanism of action for particulate vaccine adjuvants [131]. However, not all particulate vaccine delivery systems can activate the NLRP3 inflammasome, and it was observed that CNP or alum, but not cubsomes or IFA, activate the NLRP3 inflammasome when given in combination with toll-like receptor-agonist [148]. The factors influencing activation of the

NLRP3 inflammasome are surface charge [148], surface complexity [149], morphology [150], the level of phagocytosis [151], and the timing of the addition of toll-like receptor-agonist [148, 152].

3. FABRICATION AND CHARACTERIZATION OF VIRAL PROTEIN ENCAPSULATED POLYMERIC MULTILAYER CAPSULE

We hypothesize that viral protein-based particulate vaccine platform comprising of viral protein and biodegradable polymers provides safe and efficient method for inducing immune response in dendritic cells. In this chapter, recombinant *SV40* VP1 viral protein was encapsulated into P_LARG/DS through electrostatic interactions, and the physicochemical properties of the antigen-adjuvant complex were studied.

3.1 Introduction

Simian Virus 40 VP1 viral protein, a small, non-enveloped, double-strained DNA virus, belonging to the *Polyomavirus family* was chosen as the virus antigen. Previous work has shown that epitope modified *SV40* VP1 virus-like particle presents as a natural adjuvant on cytotoxic T lymphocytes [55]. The capability of long-term gene expression in targeted cells and efficient incorporation of larger transgenes *in vitro* makes it a potential candidate for vaccine delivery with safety and flexibility than the capacity of the *SV40* wild-type [48].

Since subunit vaccines formed by a portion of the pathogens shows poor immunogenicity [153, 154], the antigen-adjuvant capsule was fabricated with the properties for biocompatibility and dendritic cell targeting. This subunit vaccine vehicle was constructed into a $CaCO_3$-based PMLC using the LbL technique. *SV40* VP1 was used as a model viral protein due to its low immune response, small and authentic viral structure, as well as its antigenic properties. Biodegradable poly-$_L$-arginine/dextran sulfate polyelectrolyte pairs as adjuvants were used as they are capable of providing better biocompatibility and the ability to target dendritic cells. The size, structure, and physicochemical properties of the assembled viral protein-based

polyelectrolytes were characterized using scanning electron microscopy, transmission electron microscopy, confocal laser scanning microscopy, zeta potential measurements and protein encapsulation efficiency.

3.2 Materials and Methods

3.2.1 Materials

The *E. coli* strain containing recombinant *Autographa californica* multicapsid nucleopolyhedrovirus (AcMNPV) with the viral protein 1 gene of *SV40* virus and a hexa histidine-tag (6xHis-tag) were purchased from Capital Bioscience Inc.

Reagents for bacterial culture were purchased as below. Ampicillin, Sodium Salt was purchased from AMRESCO, Miller broth was purchased from Difco, Agar powder was purchased from Alfa Aesar and Glycerol and bicinchoninic acid (BCA) protein assay kits were purchased from Thermo Fisher Scientific. Dimethylformamide (DMF) was purchased from Sigma-Aldrich. *E. coli* DH10Bac™ E. coli strain, kanamycin, gentamicin, tetracycline, bluo-gal, Isopropyl β-D-1-thiogalactopyranoside (IPTG), Qiagen endoFree plasmid maxi kits, cellfectin® II reagent and Alexa Fluor 680 labeled dextran, 10kDa were all purchased from Invitrogen.

Regaents for insect cell culture were purchased as given below. *Spodoptera frugiperda* (*Sf9*) insect cells, Grace's insect medium, and Western Blot secondary antibody, goat anti-rabbit antiserum conjugated to Alkaline Phosphatase were purchased from Invitrogen. Trypan blue, sodium phosphate monobasic and sodium phosphate dibasic hydrate were purchased from Sigma-Aldrich. Gibco Glutamax supplement, Penicillin-Streptomycin (10,000 U/mL), Nickel-Nitriloacetic Acid (Ni-NTA) resin and purification column were purchased from Thermo Fisher Scientific.

For LbL ecapsulation, calcium chloride, sodium carbonate, dextran sulfate sodium salt (DS, MW>500kDa and MW: 6.5-10kDa), poly-$_L$-arginine (P_LARG, MW>700kDa and MW: 5-15kDa) and potassium chloride (KCl) were purchased from Sigma-Aldrich.

Ethylenediaminetetraacetic acid (EDTA) and sodium chloride (NaCl) was purchased from BDH Chemicals. Instant blue stain for SDS Page was purchased from C.B.S. Scientific Co. Inc. Polyethylene glycol (PEG) virus precipitation kits and Western Blot primary antibody, rabbit anti-*SV40* VP1 polyclonal antibody were purchased from Abcam. Imidazole and Tween 20 were purchased from Acros Organics. Potassium dihydrogen phosphate was purchased from Alfa Aesar. 2% uranyl acetate and 10nm formvar and 1nm carbon with 400 square mesh grid (FCF400-Cu) were purchased from Electron Microscopy Sciences. 10K Microsep Advance Centrifugal Devices with Omega membrane was purchased from Pall Corporation.

Ultrapure water used for all experiments was obtained from a Millipore system with a specific resistance 18.2MΩ/cm.

3.2.2 Methods

3.2.2.1 Spodoptera frugiperda (Sf9) cell culture

Spodoptera frugiperda insect cell line is a clonal isolate derived from the parental *Spodoptera frugiperda* cell line IPLB-Sf-21-AE, and is a suitable host for expression of recombinant proteins from baculovirus expression vector systems. *Spodoptera frugiperda* insect cell line was grown as a monolayer culture at 27^{o}C in Grace's insect medium, supplemented, containing lactalbumin hydrolysate, yeastolate, L-glutamine and sodium bicarbonate with 5% fetal bovine serum (FBS) and antibiotics.

3.2.2.2 Simian Virus 40 (SV40) VP1 Viral Protein Harvest by baculovirus expression vector system (BMES) System

The recombinant Autographa californica multicapsid nucleopolyhedrovirus (*AcMNPV*) containing the VP1 gene of *SV40* with an N-terminal addition of 6xHis-tag was used to produce *SV40* VP1 viral protein, shown in Figure 4.

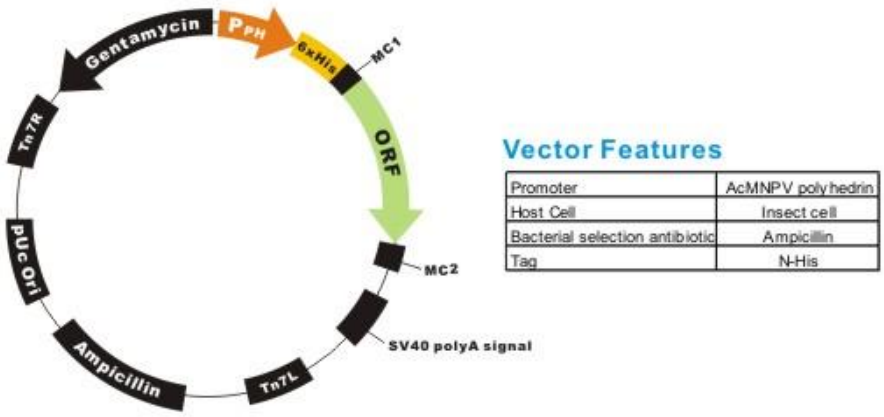

Figure 4. Donor plasmid for generating recombinant *SV40* VP1 viral protein.

The competent *E. coli*, strain *DH10Bac*™ was used as a host for DNA plasmid to harvest baculovirus shuttle vector (bacmid). *DH10Bac*™ cells contains a bacmid with a mini-attTn7 target site and a helper plasmid, pMON7124, which encodes the transposase and confers resistance to tetracycline. Once the DNA plasmid was transformed into *DH10Bac*™ cells, transposition occurs between the mini-Tn7 element on the DNA plasmid and the mini-attTn7 target site on the bacmid to generate a recombinant bacmid, shown in Figure 5 [155]. This

transposition reaction occurs in the presence of transposition proteins supplied by the helper plasmid.

The above process was carried out following the detailed protocol available in the Invitrogen, Max Efficiency *DH10B* Competent Cells manual, Invitrogen, Bac-to-Bac® Baculovirus Expression System manual, and EndoFree Plasmid Maxi kit manual.

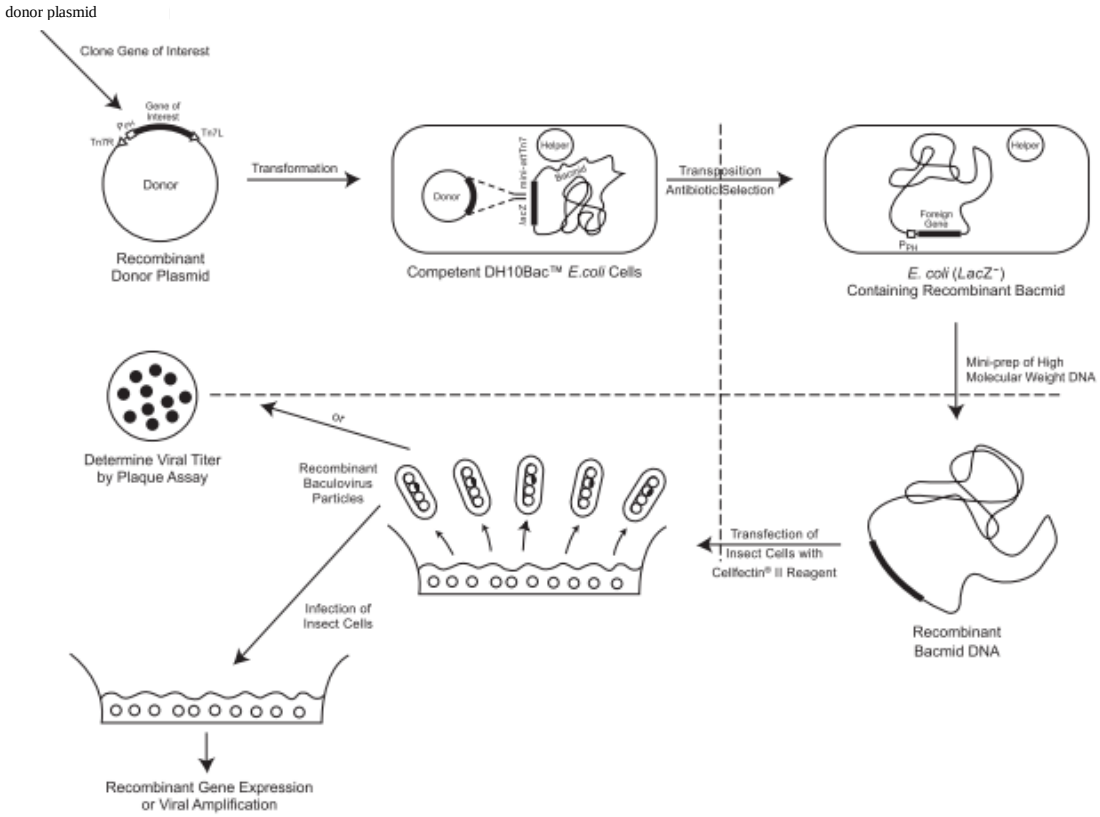

Figure 5. Diagram of the baculovirus expression vector system (BEVS), reprinted with permission [155].

The concentration and growth of the *E. coli* was monitored by measuring absorbance at a wavelength at 600 nm, shown as OD_{600}. The bacmid DNA was verified by blue-white screening

on selective plates containing the 50μg/ml kanamycin, 7μg/ml gentamicin and 10μg/ml tetracycline, as well as the reagents, 100μg/ml blue-gal, and 40μg/ml IPTG. Additionally, the purification of either plasmid DNA or bacmid DNA was preceded by Qiagen endoFree plasmid maxi kits and the concentration was then determined by Nanodrop, exposed to ultraviolet light at a wavelength of 260 nm, shown as A_{260}. The recombinant plasmid DNA and bacmid DNA stock were stored in -80ºC freezer for long-term preservation.

Once recombinant bacmid DNA was harvested, *Sf9* transfection was carried out. Monolayer cell culture of *Sf9* cell was first infected by recombinant bacmid DNA through cationic lipid, cellfectin® II reagent, with a density of $8x10^5$ cells/well at 27ºC. Once signs of infection, such as the detachment of cells from flasks or cell lysis, were observed, the medium containing viral protein was harvested. The supernatant was then collected as the P1 viral stock and separated from the cell debris by centrifugation at 500 x *g* for 5 min. The viral titer ranged from approximately 1×10^6 to 1×10^7 plaque-forming units/ml (pfu/ml).

The infection was repeated with fresh *Sf9* cells using the P1 viral stock with a cell density of $2x10^6$ cells/well to obtain the P2 viral stock. The cultures which were infected by the P2 viral stock were harvested after signs of infection were observed, approximately 3 days post-infection. The cells were then collected by centrifugation at 500 x *g* for 5 min. Any unlysed viral protein was then released by carrying out three cycles of freeze-thawing and the cell debris was removed by centrifugation at 3,000 x *g* for 15 min. The supernatant was then purified on a nickel-nitrilotriacetic acid (Ni-NTA) resin based on binding of the 6xHis-tag.

Ni-NTA Agarose is a nickel-charged affinity resin that can be used to purify recombinant proteins containing a 6xHis sequence. Proteins bound to the resin may be eluted with either low pH buffer or by competition with imidazole or histidine. Purification can be performed under

both native and denaturing conditions. Ni-NTA uses the chelating ligand nitrilotriacetic acid coupled to a cross-linked 6% agarose resin that is suitable for use in batch and gravity flow applications.

The harvested recombinant protein was stored at -80^{o}C. The concentration of protein was measured by the BCA protein assay.

In order to harvest higher concentration of viral protein, PEG virus precipitation kits and 10K molecular weight cut-off (MWCO) spin tube were used as described in the user manuals.

3.2.2.3 Simian Virus 40 (SV40) VP1 Viral Protein Identification Analysis

SV40 VP1 viral protein production was confirmed by sodium dodecyl sulfate polyacrylamide gel electrophoresis (SDS-PAGE), Western Blot analysis and transmission electron microscopy (TEM) images.

SDS-PAGE and Western Blot analysis were used to verify the identity of viral protein. Viral protein containing protein supernatants were resolved on 12% SDS-PAGE minigel using the Tris-Glycine buffer system, and visualized by instant blue stain. Gels were imaged on Gel Doc^{TM} EZ imager (Bio-Rad). Western Blot was utilized to confirm the identity of viral protein. The viral protein was first resolved by using SDS-PAGE as mentioned above, and then transferred to a nitrocellulose membrane by using the Quadra Mini-Vertical Slab Gel/Blotting System. Membranes were blocked in a solution of 5% dried milk powder in Tris-buffered saline containing 0.1% tween 20 and then probed with a 1:1000 dilution of the rabbit anti-*SV40* VP1 polyclonal antibody. A 1:5000 dilution of the secondary antibody (goat anti-rabbit IgG conjugated to Alkaline Phosphatase) was used and protein bands were visualized by developing the membrane with chemiluminescent substrate in conjunction with exposure to X-ray film.

The on-grid method of negative staining by 2% uranyl acetate was used to visualize small viral protein and determine its size with TEM. First, 400 mesh grids were treated with plasma to make them hydrophilic. Next, 2 µl of viral protein was placed on copper-coated grids, allowed to adsorb to the grid for 30 seconds and the excess removed by blotting with a filter paper. The samples were then negatively stained with a 2% uranyl acetate, incubated for 45 seconds, the extra medium removed, and then air-dried for 1 min. Lastly, the samples were examined with a JEOL 1200 EX TEM operating at 100 kV.

3.2.2.4 Fabrication of Calcium carbonate ($CaCO_3$) Microparticles

Polymeric multilayer capsules were built on $CaCO_3$ microtemplates as a sacrificial core. $CaCO_3$ microparticles were synthesized according to Volodkin et al. [103] by rapidly adding 0.33M Na_2CO_3 solution into an equal volume of 0.33M solution of $CaCl_2$ at room temperature. After intense agitation on a magnetic stirrer with 650 rpm for 30 seconds, the precipitate was filtered for 30 min. The solution containing $CaCO_3$ microparticles was centrifuged and the pellet thoroughly washed with DI water. The average size of $CaCO_3$ microparticles was ~ 4 µm in diameter. In order to fabricate smaller $CaCO_3$ microparticles, the agitation time was increased from 30 s to 60 s, while keeping the other steps unchanged. This resulted in $CaCO_3$ microparticles with average size ranging from 1 to 4 µm in diameter and ~ 95% yield.

3.2.2.5 Polymeric Multilayer Capsule (PMLC) Encapsulation

The layer formation was constructed by LbL technique. Dextran sulfate and Poly-L-Arginine were prepared as the polyanion and polycation, respectively. The concentration of DS and P_LARG was 2 mg/ml and 1 mg/ml, respectively, dissolved in 0.5 M NaCl (pH 6.0). The PMLC fabrication experiment process is shown in Figure 6.

$CaCO_3$ microspheres were freshly made as described above, and resuspended in 10 ml NaCl solution. Macromolecule capsules were built up by adding 0.25 mg/ml viral protein together with 1 ml P_LARG (positively charged PE solution) onto the $CaCO_3$ microtemplates at a protein/$CaCO_3$ weight ratio of 4%. Suspensions were thoroughly agitated on a shaker for 20 minutes at room temperature and followed by centrifugation and sonication with 0.5M NaCl. To avoid particle aggregation, the centrifuged pellets were vortexed every time before the addition of next layer and after decanting the supernatant. The same process was alternatively applied to 1 ml DS and 1 ml P_LARG solution alone, until 5 layers were deposited (2.5 bi-layers). The core removal step was carried out using 0.05 M EDTA. After 30 min agitation, the capsules were centrifuged, the supernatant was removed, and resuspended in fresh EDTA. The EDTA core removal step was repeated an additional two times. The resultant suspensions of PMLCs were washed twice with DI water and finally stored at 4^{o}C in 0.5M NaCl. The concentration of viral protein was then measured by the BCA protein assay kit and quantified using the infinite M200 Pro microplate reader (Tecan).

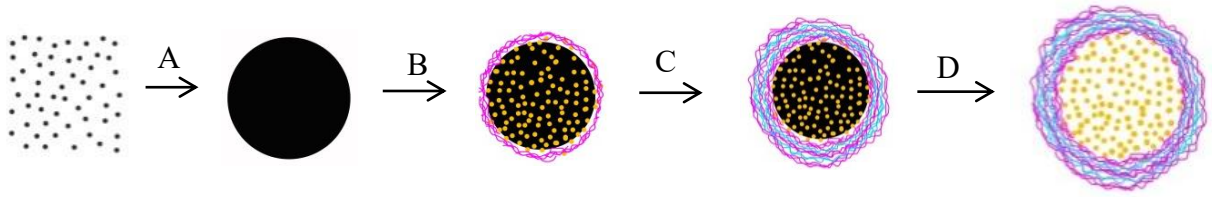

Figure 6. Scheme of PMLCs fabrication. Step A: $CaCO_3$ crystallization, Step B: Protein precipitation, Step C: Encapsulation by Layer-by-Layer technology, Step D: Core dissolution.

We evaluated the effect of varying the MW of the polymers on PMLC formation. Different capsules were formed using different combination of the polyelectrolytes, as shown in Table 1.

Additionally, in order to study the influence of the distribution of viral protein, 2VP-PMLC was fabricated. The fabrication scheme used for 2VP-PMLC was similar to VP-PMLC, only that the viral protein concentration was different and an addition viral protein layer was used. Viral protein was co-precipitated with P_LARG both in the first and third layers but only with half amount of viral protein to keep the same total concentration of the viral protein.

To study the *in vitro* release profile of the VP-PMLCs, 20 nm fluorescent silica bead was used to mimic the size distribution of the viral protein. Alexa Fluor 488 labeled dextran (10 kDa) and Fluorescein labeled dextran (500kDa) were applied as the second layer.

3.2.2.6 Polymeric Multilayer Capsule (PMLC) Identification Analysis

Surface and elemental analysis was analyzed by field emission scanning electron microscope (FE-SEM) and Energy-dispersive X-ray spectroscopy (EDS). One drop of sample was first applied on the silicon wafer, and air dried overnight. Then samples were conducted with a JEOL JSM-7500F, an ultra-high resolution FE-SEM equipped with a high brightness conical field emission gun and a low aberration conical objective lens. The sample preparation for EDS was the same as FE-SEM, and the analysis was done with an Oxford EDS system equipped with X-ray mapping and digital imaging.

Zeta-potential measurements was used with the microparticles during LbL encapsulation. 50 µl of samples were suspended in 1 mM fresh prepared KCl and the electrophoretic mobility measured by Malvern Zetasizer Nano series.

Confocal Laser Scanning Microscope (CLSM) was used to investigate the distribution of polyelectrolyte via LbL fabrication. In order to understand the microparticle structure, Alexa Fluor 680 labeled dextran, with MW of 10 kDa and ~4.6 nm in diameter [156] was applied to 2nd layer of PMLCs. One drop of well-suspended Alexa Fluor 680-labeled-VP-PMLC was spread and placed on a glass slide. Confocal micrographs were taken with an Olympus FV1000 Confocal Microscope, equipped with a 100x oil immersion objective with a numerical aperture of 1.4. Data were analyzed by FV10-ASW software. Alexa Fluor® 680 was detected at an excitation wavelength of 633 nm.

3.3 Results

3.3.1 SV40 VP1 harvest

SV40 VP1 viral protein was harvested through a baculovirus expression vector system (BEVS) *Sf9* insect cell line. Before transfection by the BEVS system, the bacmid was first harvested by growing DH10Bac™ *E. coli* overnight, followed by purification using EndoFree® Plasmid kits. The OD_{600} value was 1.3 and the final mass of the purified recombinant bacmid was approximately 30 µg.

The *Sf9* insect cell line is a clonal isolate derived from the parental *Spodoptera frugiperda* cell line IPLB-Sf-21-AE. It is a suitable host for expression of recombinant proteins from the baculovirus expression vector system. The bacmid was transfected using the cellfectin II cationic lipid reagent. Compared to mammalian expression system, the baculovirus expression vector system provided an easier way to amplify the viral stock to obtain higher viral titers, as described in the Materials and Methods section (3.2.2.2 SV40 VP1 Viral Protein Harvest by BEVS System).

At three days post-infection of 2 x 10^7 *Sf9* cells cells, approximately 0.5 mg of the purified recombinant *SV40* VP1 viral protein was harvested by using 0.4 ml P2 viral stock with a titer ranging from 1 x 10^7 to 1 x 10^8 pfu/ml. In order to increase the viral protein concentration, PEG virus precipitation kits were used to increase P2 viral titer on bacmid, and 10K molecular weight cut-off (MWCO) spin tube was used to concentrate the *SV40* VP1 viral protein to reach a concentration up to 0.4 mg/ml.

The size of the *SV40* VP1 viral protein was then verified by TEM with negative stain. Negative staining is achieved when heavy staining ions are repelled by the charged groups of the specimen and tracking the trace of the biological molecules. Some well-known negative stains include ammonium molybdate, uranyl acetate, uranyl formate, phosphotungstic acid, osmium tetroxide, osmium ferricyanide [157] and auroglucothionate. Figure 7 illustrates the morphology of *SV40* VP1 viral protein and shows the size is uniformly around 20 nm in diameter.

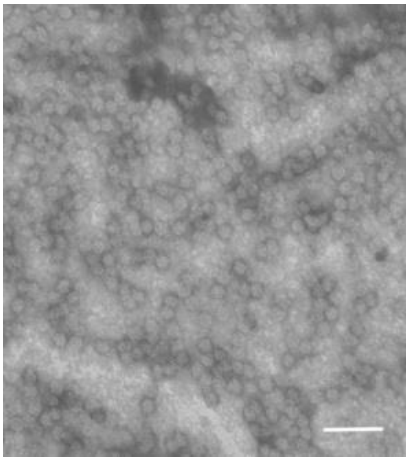

Figure 7. Electron micrograph image of *SV40* VP1 viral protein with negative stain. Scale bar, 100nm.

Viruses have the ability to enter the human cells. The capsid protein, e.g. viral protein 1, is especially important as it is responsible for attachment to host cells. Moreover, the capsid protein is capable of self-assembling into a virus-like particle which is authentic as the wild-type viral capsid protein even without the existence of the infectious genome. This makes virus-like particles a potential candidate for vaccines. However, using different solvent conditions, such as pH, calcium addition and ionic strength, the capsid proteins could be assembled into different unit numbers [158]. In this study, taking advantages of smaller particles, *SV40* VP1 capsomeres were applied as a model viral protein.

The identification of *SV40* VP1 viral protein was then examined by SDS-PAGE and Western Blot, shown in Figure 8. From Figure (8a), with the comparison to standard MW protein label, the SDS-PAGE gel shows that the molecular weight of the *SV40* VP1 viral protein is around 49 kDa. Moreover, based on lane W from the SDS-PAGE gel shown in Figure (8a), there is no protein loss is observed in the washing steps; however, compared lane L to lane VP, the color and the thickness of the lane reveals that more viral protein remained on the gel. Therefore, though Ni-NTA resin provided a convenient way to purify 6xhis-tag proteins, the harvesting efficiency was not high. From Figure (8b), the VP1 viral protein was verified by Western Blotting. These results demonstrate that *SV40* VP1 capsomere was successfully formed using the baculovirus expression vector system.

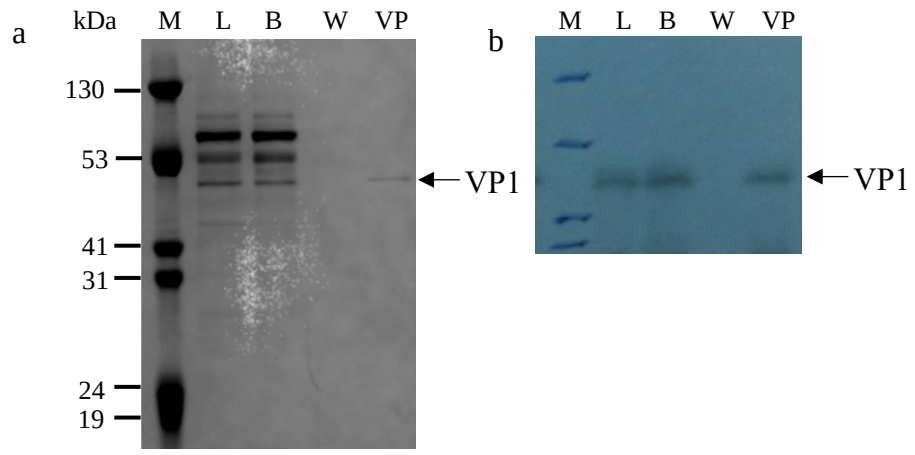

Figure 8. Expression of the *SV40* VP1 viral protein in insect cells. Viral protein was harvested 3 days post-infection with the recombinant *AcMNPV* expressing *SV40* VP1. An extract of ~10^7 *Sf9* infected cells were analyzed through Ni-NTA resin-purified. (a) SDS-PAGE gel of resin-purified *SV40* VP1 was stained with instant blue stain. Lanes of a 12% SDS-PAGE gel were loaded as followed. M: molecular weight markers; L: cell lysates before purification; B: supernatant after cell lysates bond to the Ni-NTA resin; W: supernatant of Ni-NTA wash buffer with bond cell lysates resin; VP: cell lysates after purification. (b) Western blot of resin-purified *SV40* VP1 was detected with rabbit anti-*SV40* VP1 polyclonal from a 12% SDS-PAGE.

3.3.2 Fabrication of viral protein-based polymeric multilayer capsule

Polymeric multilayer capsules (PMLCs) were first developed in 2004 [98]. This approach of encapsulation provides a safer, versatile as well as stable method for enzymatic assays [100], drug delivery [105, 107, 159-168], and vaccine delivery [38, 41]. This formulation helps avoid harsh conditions for core removal, like extreme pH [167, 169], or oxidizing agents [170]. Antigen-loaded PMLCs were synthesized as shown in Figure 9. Dextran and Poly-$_L$-Arginine were used as the polyanion and polycation, respectively for LbL encapsulation.

3.3.2.1 Porous structure of viral protein-based polymeric multilayer capsule (VP-PMLC)

Highly homogeneous and porous inorganic $CaCO_3$ microparticles were crystallized from colloidal aggregation of primary $CaCO_3$ nanoparticles. By directly mixing and vigorously

stirring soluble salts containing Ca^{2+} and CO_3^{2-}, an amorphous nanoprecipitate was formed instantly leading to a microparticle nucleus. The crystal growth was then transformed slowly by recrystallizing into rhombohedral calcite crystals in DI water. To get $CaCO_3$ microspheres, the recrystallization was then terminated by filtering and washing with DI water. The morphology of $CaCO_3$ microparticles (Figure 9) was an even uniform spherical microparticles that were ~4 μm in diameter.

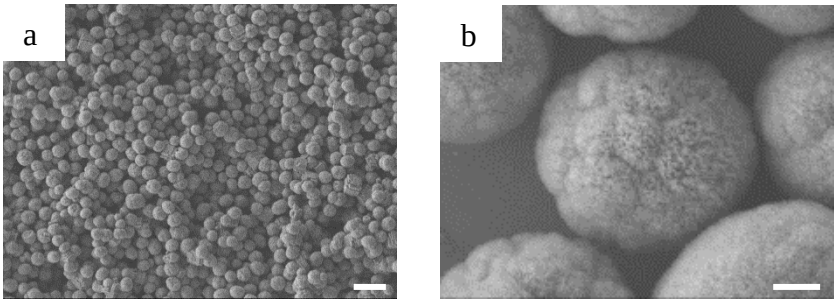

Figure 9. Scanning electron microscopy images of $CaCO_3$ microparticles with an average size of 4 μm: (a) in overview, scale bar, 10 μm (B) single particle, scale bar, 1 μm.

The properties of the microparticles were altered by changing the conditions of formation. The speed and time of stirring were two factors that altered the size of nuclei. The longer the time or the higher the speed of agitation, the smaller size of the nuclei formed due to more intermixing of salts, which further resulted in smaller sized crystals. Therefore, under the same salt concentration and the speed of agitation, when the agitation time increased from 30 s to 60 s, the size of $CaCO_3$ changed from 4 μm monodisperse porous spherical microparticles to 1 to 4 μm polydisperse porous spherical microparticles. The results are in agreement with Volodkin et al. [103]; by using this approach, a narrow range of size distribution of $CaCO_3$ porous

spherical microparticles could be achieved only with the sizes ranging from 3 to 20 μm in diameter. The SEM images were shown in Figure 10.

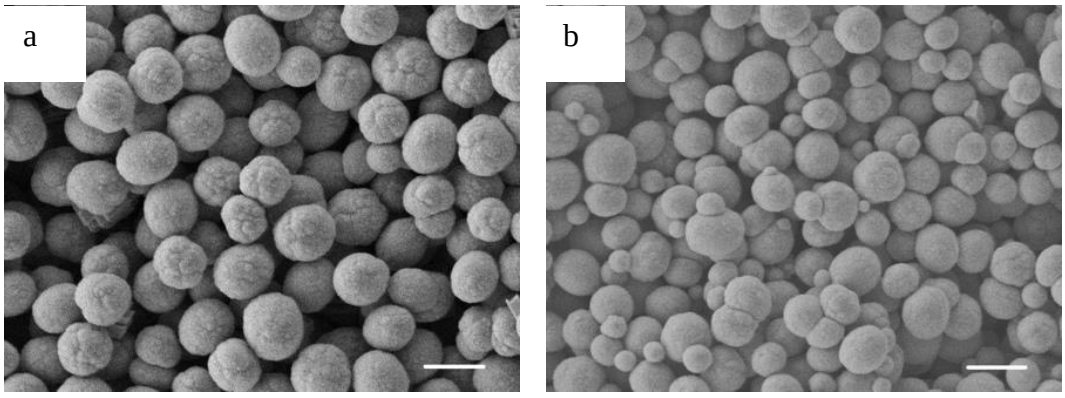

Figure 10. Scanning electron microscopy images of $CaCO_3$ microparticles fabricated by different preparation conditions. (a) By 30 seconds of irritation, the mean size of $CaCO_3$ microparticles was 4 μm mono-disperse porous spherical; (b) By 60 seconds of irritation, the mean size of $CaCO_3$ microparticles was 1 to 4 μm poly-disperse porous spherical. Scale bar, 5 μm.

Viral protein precipitated together with positively charged polyelectrolyte were then applied onto $CaCO_3$ templates. The surface charge of the $CaCO_3$ microparticles and *SV40* VP1 viral protein was approximately -22.4 mV and -4.5 mV, respectively, measured by ξ-potential measurements in KCl solution. The data of the slightly negatively charged *SV40* VP1 viral protein was consistent with predictions that with a pI of 6.8 [58], the VP1 protein presented negative to neutral surface charges in a pH 6 solution. Despite being negatively charged, the boundaries, which indicate the position of the $CaCO_3$ surface, showed preferential sites for viral protein to initiate accumulation, resulting in surface-mediated nucleation followed by precipitation. Therefore, the $CaCO_3$ microparticles served to absorb viral proteins onto internal surfaces.

P_LARG, a positively charged polyelectrolyte, was chosen as the first layer and co-precipitated with negatively charged viral protein for better encapsulation rate. After protein precipitated onto the $CaCO_3$ microtemplates, oppositely charged PEs were applied sequentially. When considering the outermost layer for vaccine vehicle design, booster injection and cell targeting performance played crucial factors. Due to the negatively charged cell surface, a positively charged polyelectrolyte shows potential to induce more non-specific interactions [171]. Moreover, it has been shown that poly-$_L$-arginine can be used for repeated vaccination and resulted in no antibody or T cell responses [109]. Therefore, in this study, the VP-PMLCs were designed as the 2.5 bi-layer PLARG/DS capsules by sequential application of oppositely charged polyelectrolytes, with the last layer being a P_LARG layer. Alternating charges of zeta-potential measurements during the adsorption of each layer were determined, providing the evidence of the successful adsorption of polyelectrolytes on each layer, shown in Figure 11.

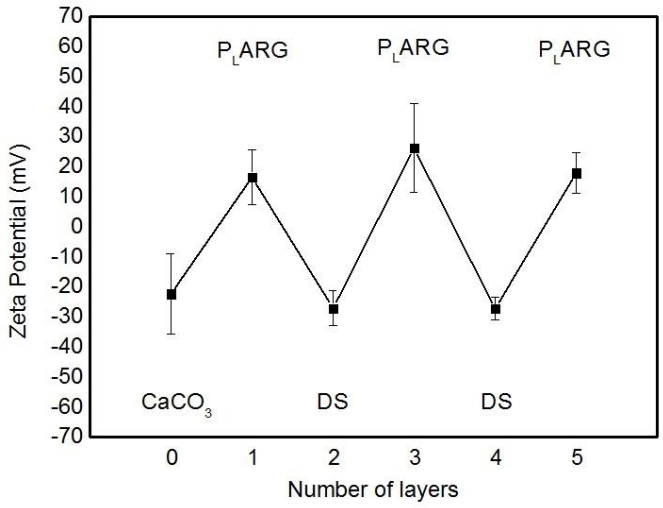

Figure 11. ξ-potential versus layer number for the layer-by-layer self-assembly of Dextran and Poly-$_L$-Arginine on $CaCO_3$ sacrificial core.

The SEM image in Figure 12 shows the morphology after encapsulation of five polyelectrolyte layers onto 4 μm $CaCO_3$ core. Compared to the untreated $CaCO_3$ microspheres, shown in Figure 9(b), a rougher surface was observed as surface coating but the porous surface still could be seen.

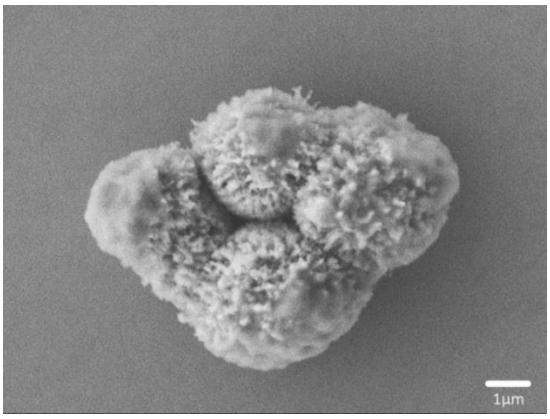

Figure 12. Scanning electron microscopy images of VP-PMLCs treated by 5 layers of polyelectrolytes, scale bar, 1 μm.

Alexa Fluor 680 labeled Dextran with MW of 10 kDa was further applied to the 2nd layer for distribution studies, while keeping the other layers of polyelectrolytes the same. After achieving 2.5 bi-layer VP-PMLCs, confocal laser scanning microscope images were taken and the intensity of fluorescence was analyzed to observe the localization of fluorescent Dextran inside the microcapsules, shown in Figure 13.

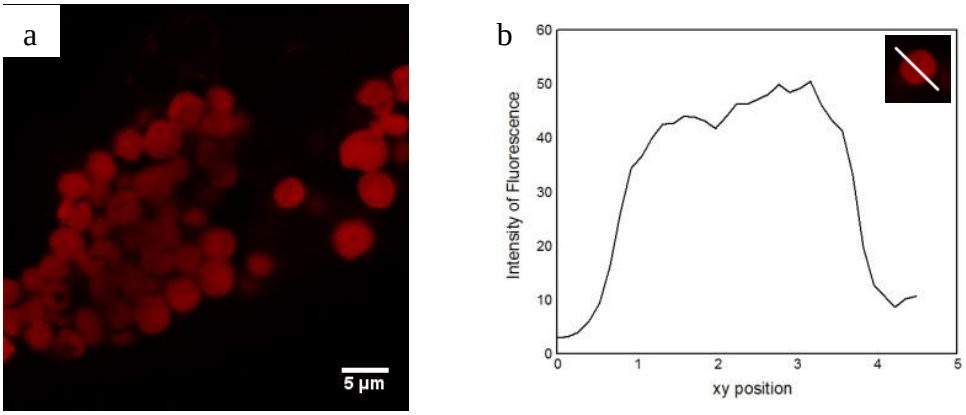

Figure 13. (a) Confocal laser scanning microscope images of VP-PMLCs encapsulated with Alexa Fluor 680 labeled DS in 2nd layer by using 4 µm $CaCO_3$ microparticles; (b) the intensity of fluorescence profile.

The confocal laser scanning microscope images suggested that fluorescent Dextran deposited as the 2nd layer still could penetrate through P_LARG layer and deposit at the center of the $CaCO_3$ microparticles uniformly. Additionally, Volodkin *et al*. found that the pore size distribution of 4µm $CaCO_3$ particles was between 20-60 nm [172]. The size of *SV40* VP1 capsomere is around 20 nm in diameter. Moreover, taking advantages to the high surface area of $CaCO_3$ microplates, it is reasonable to believe the *SV40* VP1 can be deposited within the $CaCO_3$ microparticles uniformly.

Core dissolution was applied by treating with EDTA (Figure 14). Compared to other sacrificial models that use harsh conditions like extreme pH value, organic solvents or oxidizing agents for core removal, washing with EDTA provide a mild condition that results in lesser loss in particles. EDTA has the ability to sequester metal ions, such as Ca^{2+} and Fe^{3+} etc. After binding to EDTA, the metal ions remain in solution but exhibit diminished activity. In brief, core

dissolution could be achieved by the formation of water-soluble complex between Ca^{2+} and EDTA.

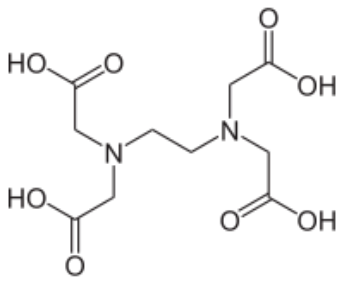

Figure 14. Chemical structure of ethylenediaminetetraacetic acid (EDTA)

The surface charge of the final capsule was 10 ± 6 mV, resulting in non-aggregated capsules. Core decomposition was demonstrated by TEM, SEM, and EDS, as shown in Figure 15. Figure (15a) and (15b) show TEM images before and after core removal. Before core removal, the particles show a solid, dark color; however, after core removal, the particles become semi-transparent. Figure (15c) and (15d) also show that the particle size shrank after core decomposition. However, neither TEM nor SEM images could accurately demonstrate complete core removal level. Therefore, we used EDS for core removal detection. The Ca^{2+} peaks in the EDS spectra show the existence of the $CaCO_3$ core, shown in Figure (15e) and (15f). The high peaks seen in EDS, shown in Figure (15e), demonstrated the existence of the $CaCO_3$ microparticles before core dissolution and that no Ca^{2+} was detected after core decomposition (Figure 15f).

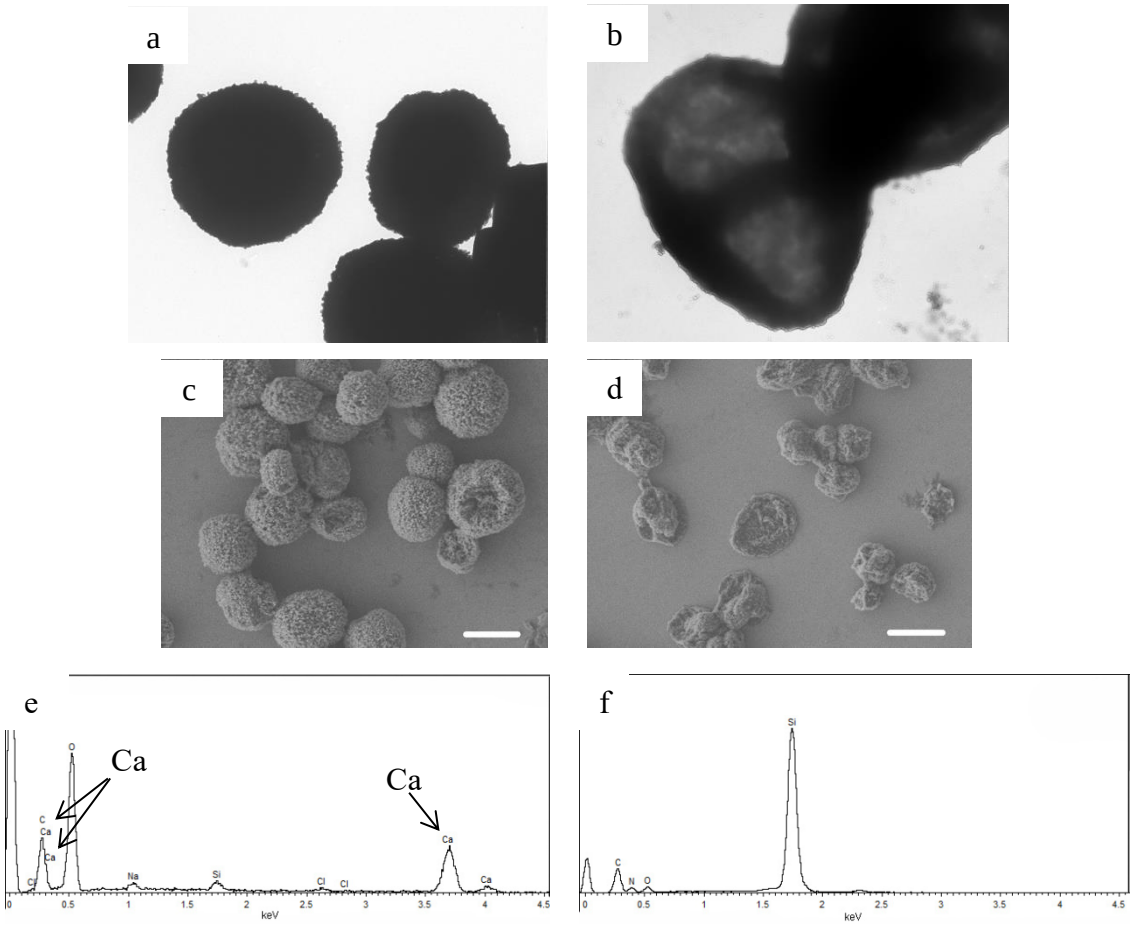

Figure 15. Transmission electron microscopy images, scanning electron microscopy images and energy-dispersive spectroscopy of VP-PMLCs (a, c, e) before and (b, d, f) after core decomposed. Scale bar, 3 μm.

Together the ξ-potential, TEM, SEM, EDS and CLSM analysis show that the VP-PMLCs could be successfully fabricated using the LbL technique. Moreover, after encapsulation with polyelectrolytes, these VP-PMLCs have been reported to be stable and show no further recrystallization for at least one week at room temperature [172].

3.3.2.2 Encapsulation efficiency of viral protein-based polymeric multilayer capsule (VP-PMLC) by different molecule weight of polymers

Protein encapsulation efficiency is defined as the amount of protein encapsulated by PMLCs. It is a crucial factor in determining the successful assembly of VP-PMLC. The protein encapsulation efficiency was calculated as follows:

E = [(Amount of encapsulated protein)/(Total amount of fed protein)] x 100%

Parameters affecting protein encapsulation efficiency include the selection of polyelectrolyte pairs and their molecular weight, number of layers, the approaches of protein adsorption, the size of protein, and pH of the system. In this work, the protein encapsulation efficiency was addressed by varying MW of polyelectrolytes and using different methods for viral protein adsorption.

To study on the mechanism of protein encapsulation and release, two approaches of fabrication were used: (i) viral protein encapsulated together with P_LARG in the 1st layer onto $CaCO_3$ microparticles ($CaCO_3$/VP/P_LARG), followed by layer-by-layer assembly until 2.5 bi-layer P_LARG/DS shell was formed, denoted as "VP-PMLC", and (ii) "2VP-PMLC" where viral protein adsorbed together with P_LARG in both of the 1st and 3rd layers, followed again by layer-by-layer assembly until 2.5 bi-layer P_LARG/DS was formed. The encapsulation efficiency from both approaches was then compared between P_LARG/DS polyelectrolyte pairs with different molecular weight (Table 1).

Table 1. Design of polymeric multilayer capsules

Denotation	Composition
$(PMLC)_H$	$[CaCO_3 - (P_LARG)_H] - (DS)_H - (P_LARG)_H - (DS)_H - (P_LARG)_H$
$(PMLC)_C$	$[CaCO_3 - (P_LARG)_H] - (DS)_H - (P_LARG)_L - (DS)_L - (P_LARG)_L$
$(PMLC)_L$	$[CaCO_3 - (P_LARG)_L] - (DS)_L - (P_LARG)_L - (DS)_L - (P_LARG)_L$
$(VP\text{-}PMLC)_H$	$[CaCO_3 - VP - (P_LARG)_H] - (DS)_H - (P_LARG)_H - (DS)_H - (P_LARG)_H$
$(VP\text{-}PMLC)_C$	$[CaCO_3 - VP - (P_LARG)_H] - (DS)_H - (P_LARG)_L - (DS)_L - (P_LARG)_L$
$(VP\text{-}PMLC)_L$	$[CaCO_3 - VP - (P_LARG)_L] - (DS)_L - (P_LARG)_L - (DS)_L - (P_LARG)_L$
$(2VP\text{-}PMLC)_H$	$[CaCO_3 - VP - (P_LARG)_H] - (DS)_H - [VP - (P_LARG)_H] - (DS)_H - (P_LARG)_H$
$(2VP\text{-}PMLC)_L$	$[CaCO_3 - VP - (P_LARG)_L] - (DS)_L - [VP - (P_LARG)_L] - (DS)_L - (P_LARG)_L$

After encapsulation, the viral protein is located inside the particles. However, due to the porous structure, the protein concentration of VP-PMLCs can still be determined by the micro BCA protein assay. The concentration of viral protein inside particles under the different conditions (different MW of polyelectrolytes or different methods for encapsulation) is shown in Table 2.

Table 2. Concentration and encapsulation efficiency of SV40 VP1 Viral Protein in 2.5 Bi-Layer of Polymeric Multilayer Capsules[a]

Capsule Loading Approach	$(VP\text{-}PMLC)_L$	$(VP\text{-}PMLC)_H$	$(2VP\text{-}PMLC)_L$	$(2VP\text{-}PMLC)_H$
Protein Concentration (mg/ml)	0.145	0.158	0.088	0.133
Encapsulation Efficiency (%)	58%	63%	35%	53%

[a.] Total initial amount of *SV40* VP1 viral protein was 0.25 mg in each sample. Each data presents a mean value of three independent experiments with standard deviation less than 5%.

Table 2 shows that polyelectrolyte pairs comprised of high MW provides higher retaining ability in comparison with those composed of low molecular ones. The highest encapsulation efficiency of PMLCs is around 63% and is observed with $(VP\text{-}PMLC)_H$. This can be attributed to the increasing entanglement and viscosity of high molecular weight polyelectrolytes. Although a smaller pore size can be attained with a shorter deposition time; however, the relationship between pore size and MW of polyelectrolytes depends on the polymer itself. For example, higher MW of polycyclic aromatic hydrocarbons show larger pore size, but opposite results were observed with poly(acrylic acid) [173].

Adding viral protein in different layers could also influence the viral protein encapsulation efficiency. Table 2 shows that 2VP-PMLC has a lower viral protein concentration inside the particle than VP-PMLC. However, since different antigen encapsulation efficiency was obtained with the different capsules, the antigen amount after normalization to the particle number is comparable (~0.008 - 0.01 mg/$20x10^5$ particles). This means that even with the same amount of $CaCO_3$ core and viral protein at the beginning, different final particle amounts were obtained, and further confirmed that the ability of the encapsulation efficiency on each single capsule is similar.

In order to further investigate on protein loss, the protein concentration of supernatants from each wash step was measured (Figure 16).

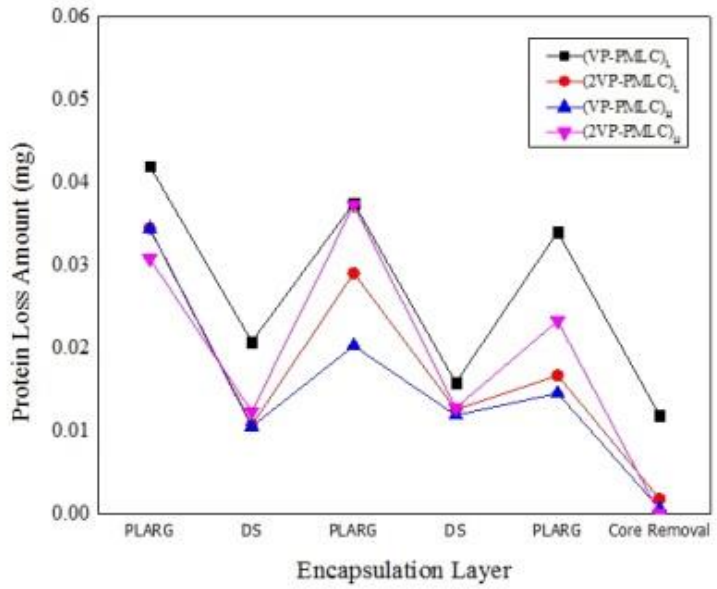

Figure 16. Protein loss measurement applied on supernatants from each wash step. Initial protein amount was 0.25 mg in total.

Recent studies presented that $CaCO_3$ synthesized together with protein ($CaCl_2$/Na_2CO_3/protein) led to more protein loss after core dissolution [38, 174]. However, by co-precipitating protein and P_LARG directly onto $CaCO_3$ crystals ($CaCO_3$/VP/P_LARG), protein loss was minimized in the core dissolving process, shown in Figure 16. This might be attributed to fewer interactions between the viral protein and calcium ions. By using this approach, it could be predicted that more viral protein would either penetrate into the center of porous $CaCO_3$, or adhere onto the surface of $CaCO_3$ microparticle and polyelectrolytes. Therefore, it was reasonable to observe more protein loss in either the 1st layer of P_LARG for VP-PMLCs or both 1st and 3rd layers of P_LARG for 2VP-PMLCs. Therefore, 2VP-PMLC provided two viral protein addition layers that might decrease the encapsulation efficiency. Except for viral protein co-

precipitation step, protein was released immediately after the deposition steps, but little loss was found in the following washing steps.

In comparison with dextran and Poly-$_L$-Arginine polyelectrolytes, it was shown that more protein was lost in P_LARG layers. For example, for the VP-PMLC series, P_LARG fabricated as the 3rd and 5th layers resulted in almost twice protein loss than Dextran in the 2nd and 4th layers, except for the 5th layer on high MW of PMLCs. As for high MW of capsules, the 5th layer of protein loss is barely seen, showing that high MW of PMLCs are able to secure viral protein inside the particles then low MW of PMLCs on the 5th layer.

Therefore, we conclude that layers with low MW of P_LARG/DS polyelectrolyte pairs, viral protein or P_LARG showed a higher protein loss. Since VP-PMLC presented higher encapsulation efficiency than 2VP-PMLC, a certain amount of protein appears to be lost at each protein co-precipitation step. To attain higher encapsulation efficiency, high molecular weight polyelectrolyte pairs with a one-time protein loading should be used.

3.4 Summary

SV40 VP1 viral protein of ~20 nm diameter were successfully harvested by baculovirus expression vector system in insect cells. Viral protein-based polymeric multilayer capsules serving as vaccine vehicle was successfully developed for the first time. P_LARG/DS polyelectrolyte pairs, as well as *SV40* VP1 viral protein were assembled onto $CaCO_3$ sacrificial porous microparticles through LbL fabrication, followed by EDTA core removal. The VP-PMLC was a porous sphere, with diameters ranging from 1-4 μm in diameter and a positively charged surface. To optimize protein encapsulation efficiency, two capsule formulations and varying molecular weight of P_LARG/DS polyelectrolyte pairs were investigated. In this study, the viral protein capsules that achieved the highest protein encapsulation efficiency of ~63% was by using

high molecular weight polyelectrolyte pairs with protein deposited together in the first layer (VP-PMLC)$_H$. But when normalized to the total number of particles, the encapsulation efficiency in each single capsule was similar.

4. *IN VITRO* IMMUNITY EVALUATION OF PMLC PARTICLES

The results in Chapter 3 showed successful fabrication and characterization of *SV40 VP1* viral protein-based PMLCs. This Chapter discusses *in vitro* studies with immune cells to evaluate their effectiveness for vaccine delivery.

4.1 Introduction

The primary goal of a vaccine is to prepare the body to clear an infectious agent without allowing disease symptoms to be expressed. When a person is immunized, APCs recognize any pathogens and produces specific antibodies to clear the antigens and protect the body against further infection [175, 176]. However, if there are no antibodies for the antigen, it will take several days for the body to recognize the antigen, generate antibodies, and to mount an antibody response to clear the pathogen from the body. While this may not be very significant for some viral pathogens, for other pathogens like the measles virus [177] or whooping cough bacteria [178], a delay in initiating antibody-mediated immune response can have significant consequence and even lead to mortality. This underscores the importance of vaccines.

In order to generate antibodies, cells of the adaptive immune system need to be stimulated by components of the innate immunity system [116, 179]. Therefore, the first defense line of immunity is stimulation of antigen presenting cells like dendritic cells are the bridge between innate and adaptive immunity and would be the cells that respond first to a vaccine.

In this Chapter, results from *in vitro* studies on co-incubation PMLCs with either bone marrow derived dendritic cells or murine DC2.4 dendritic cell line are shown. The effect of PMLCs on dendritic cells was assessed based on *in vitro* release profile of fluorescent particles,

cell viability measurements, and expression of the CD40 and CD86 surface marker proteins in dendritic cells upon stimulation.

4.2 Materials and methods

4.2.1 Materials

The DC2.4 dendritic cell line was provided by Dr. Robert Alaniz at the Texas A&M Health Science Center. Primary bone marrow derived dendritic cell were isolated and cultured from marrow of C57BL/6 mice that were kindly donated by Dr. Alaniz's lab from their ongoing experiments.

Gibco Glutamax supplement, Penicillin-Streptomycin (10,000 U/mL), BCA protein assay kits and Lactate dehydrogenase (LDH) cytotoxicity assay kits were purchased from Thermo Fisher Scientific.

Antibodies for flow cytometry analysis are listed below: rat anti-mouse CD16/CD32 (mouse BD Fc block), Alexa Fluor 700 hamster anti-mouse CD11c, APC rat anti-mouse CD40 and PE-Cy7 rat anti-mouse CD86 were purchased from BD Biosciences. Recombinant mouse granulocyte-macrophage colony-stimulating factor (GM-CSF) was purchased from BD Biosciences as well.

Alexa Fluor 488 labeled dextran (10kDa) and Fluorescein labeled dextran (500kDa) were purchased from Invitrogen. LPS from *E. coli* O55:B5 and 2-well chamber slides were purchased from Sigma-Aldrich. Cy5-labeled 20 nm silica beads were purchased from NANOCS INC. RPMI 1640 without L-glutamine was purchased from Lonza.

Ultrapure water used for all experiments was obtained from a Millipore system with a specific resistance 18.2MΩ/cm.

4.2.2 Methods

4.2.2.1 Mice Bone Marrow Cell Isolation

Bone marrow cells were flushed out of the femurs and tibias into complete medium and pipetted vigorously to make a single cell suspension, and then passed through a 70 μm cell strainer. Cells were centrifuged at 1300 rpm for 10 min and resuspended in ACK lysis buffer. After 4 min incubation at room temperature, cells were washed twice with complete growth medium, resuspended in growth medium, and ready for culture.

4.2.2.2 Mice bone marrow derived dendritic cells harvest

A single-cell suspension of mice freshly isolated bone marrow stem cell was seeded at a density of ~$2x10^6$ cells/petri dish in 10 ml culture of RPMI 1640 medium containing 10% FBS, 2mM glutaMax, 100 U/ml penicillin/streptomycin and 20ng/ml GM-CSF. Cells were differentiated into BMDCs at 37ºC in 5% CO_2 environment for 6 days.

At day 2, half of the culture medium was replenished, while taking care to exclude monocytes. At day 4, an additional 10 ml of fresh culture medium was added. At day 6, cells were centrifuged at 300 x *g* for 8 min. The cell pellet contained immature BMDCs that was used in subsequent experiments.

4.2.2.3 DC2.4 dendritic cell line harvest

DC2.4 dendritic cells were maintained at 37ºC in 5% CO_2 environment with the same growth medium as BMDCs but with 5% FBS. Medium was replenished every three days till cells reached ~80% confluence. For routine passaging, cells were trypsinized, centrifuged at 300 x *g* for 10 min at room temperature, and resuspended in growth medium at the desired cell density.

4.2.2.4 Lactate dehydrogenase (LDH) cytotoxicity assay kit

The lactate dehydrogenase (LDH) cytotoxicity assay kit was used to estimate cell viability, based on the levels of LDH in the cell culture supernatant. Since LDH is an intracellular enzyme, any LDH in the supernatant must have been released from a dead cell; therefore, cultures will lower viability would have higher levels of LDH in the supernatant. The optimized protocol given by the manufacturer was used for the assay.

All experiments were run in triplicate. BMDCs were seeded in the 96-well flat bottom culture plates at a density of ~10^4 cells/well. Two ratios of PMLCs or VP-PMLCs to cells were tested (20:1 and 100:1) and the viral protein concentration was 0.1 mg/ml. BMDCs co-treated with viral protein and particles were incubated at 37ºC in 5% CO_2 environment for 24h.

4.2.2.5 Release profile by confocal laser scanning microscope

Confocal Laser Scanning Microscope (CLSM) was used to investigate the distribution of microparticles after cell phagocytosis. In order to visualize microparticles *in vitro*, fluorescent materials - Alexa Fluor 488 labeled dextran (10kDa), Fluorescein labeled dextran (500kDa), and 20nm Cy5-labeled silica beads - were used to fabricate microparticles. For five layers of encapsulation, fluorescent dextran was used in the 2^{nd} layer to investigate particle structure and the breakdown of particles. The 20 nm fluorescent silica beads were used to mimic the viral protein for release. Before carrying out *in vitro* release experiments, ξ-potential and SEM were applied to verify the structure of the fluorescent particles as described in 3.2.2.6 (Polymeric Multilayer Capsule Identification Analysis section).

After verification, fluorescent particles were then co-cultured with DC2.4 dendritic cells in multiple two-well chamber slides in parallel. The DC2.4 dendritic cell density was ~2x10^4 cells/cm^2, and the particles to cell ratio was 20:1. Cells were incubated at 37ºC in 5% CO_2 for up

to 72h. At 4, 24, 48, and 72h, the culture medium was aspirated from one set of cultures, the cells washed twice with PBS, and fixed with 4% PFA in the dark for 15 min.

The slide chamber was placed on the stage of a Olympus FV1000 Confocal Microscope with a numerical aperture of 1.4. The excitation wavelength was 488 nm for detecting Alexa Fluor 488 labeled 10 kDa dextran, 515 nm for Fluorescein labeled 500kDa dextran, and 633 nm for detecting 20nm Cy5-labeled silica beads.

4.2.2.6 Flow cytometry analysis by antigen targeting to mice bone marrow derived dendritic cells (BMDCs)

Antigen targeting to BMDCs was evaluated by flow cytometry using the following antibodies: Alexa Fluor 700 hamster anti-mouse CD11c, APC rat anti-mouse CD40 and PE-Cy7 rat anti-mouse CD86. BMDCs were seeded in 96-well round bottom culture plates with a density of ~10^5/well. LPS (1000 ng/ml) was used the positive control, and the ratio of PMLCs, VP-PMLCs to cells was 20:1 and the viral protein concentration was 0.1 mg/ml. Co-treated BMDCs were then cultured at 37^{o}C in 5% CO_2 for another 24h.

After 24h, the treated BMDCs were centrifuged at 300 x *g* for 3 min, followed by two PBS wash steps. Before incubating with antibodies, 100 µl of 100X Fc block dilution in 10% PBSA was added to each well to minimize non-specific binding. The plate was then incubated on the ice for 10 min, followed by a PBSA wash. Antibodies were prepared at 1:100 dilution in PBSA, and added 50µl into each well. Cells were incubated in the dark on ice for 30 min, washed twice with PBSA, and fixed with 200 µl of 1% PFA. The cells were fixed for 20 min in the dark on ice, centrifuged, and re-suspended in PBSA for flow cytometry. Data acquisition was performed by using BD Fortessa X-20 in the TAMSHC College of Medicine Cell Analysis Facility using the manufacturer supplied FlowJo software.

4.3 Results

4.3.1 Cell viability through BMDC

Since an antigen alone might be toxic to cells, PLMCs were used to form matrix microcapsules. A polycation was used as the outermost layer to provide more non-specific cell targeting ability. However, Fisher et al. reported that polycation with high MW, high charge density, and flexibility, could cause higher cytotoxicity [180]. Therefore, the VP-PMLCs with different molecular weights of P_LARG/DS polyelectrolyte pairs were used to study cell viability using BMDCs. The cell viability of bone marrow derived dendritic cells after exposure to 3μm in diameter microparticles for 24h was evaluated. *In vitro* cell compatibility studies and LDH release is shown in Figure 17.

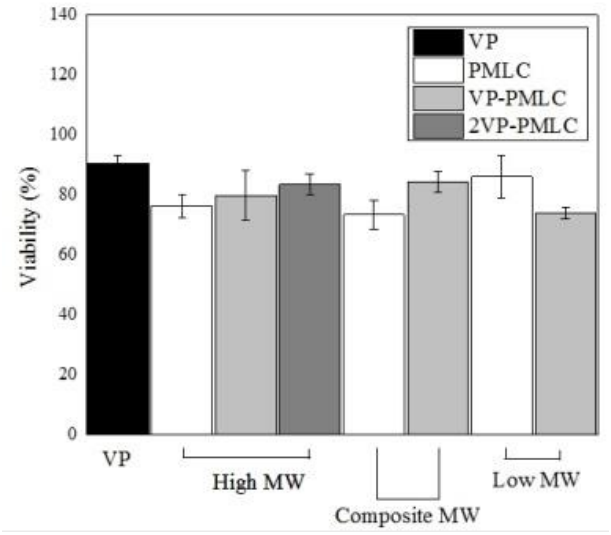

Figure 17. Viability of BMDCs incubated with PMLCs with particle/cell ratio 20:1. Cytotoxicity was evaluated by co-culturing mice BMDCs with either VP (black color), PMLCs (white color), VP-PMLCs (light grey color) and 2VP-PMLCs (dark grey color), respectively, for 24h. The viral protein concentration was 0.1 μg/ml and the ratio of particle to cell was 20. Two molecular weights of P_LARG/DS polyelectrolyte pairs were applied to encapsulate the viral proteins for cytotoxic studies.

BMDC cells co-cultured with 0.1 mg/mL of VP showed relatively high viability. This could be due to the nature of *SV40* VP1 viral protein, as although it can transform mouse cells *in vitro*, it is not able to induce tumor growth [181]. Therefore, at this concentration, *SV40* VP1 viral protein was not toxic to BMDCs. Compared to different MW of PMLCs, $(PMLC)_H$, $(PMLC)_C$ and $(PMLC)_L$ with a microparticle to cell ratio of 20:1 (shown in Figure 17 as white columns), low MW of capsules showed higher viability than high MW ones. Similar observations were made with VP-PMLC (Figure 17, light grey color columns). This finding also supports the results from Fisher et al, who mentioned that high MW of polymers tend to be more toxic [180].

Next, PMLC, VP-PMLC, and 2VP-PMLC were compared to study the viability influence caused by different locations of viral protein. The first group (high MW PMLC) shown in Figure 17 shows that the presence of the viral protein caused lower cytotoxicity; this was also observed in composite MW, as well as low MW PMLC. Taking the capsule number into consideration, the viral protein concentration in each capsule ranged from 0.008 to 0.01 mg/ml while the concentration of viral protein alone is 0.1 mg/ml.

The same experiment was repeated with the ratio of particle/cell increased to 100 and keeping the viral protein concentration at 0.1 mg/ml. Figure 18 shows the cytotoxicity in BMDCs for 24h. Comparing to Figure 17, Figure 18 shows an overall reduction in viability, with the averaged viability decreases to 70%. The trend observed in Figure 17 still can be found in Figure 18; however, due to the large amount of particles, the influence of MW of the polymers and the location of viral protein on viability is not obvious.

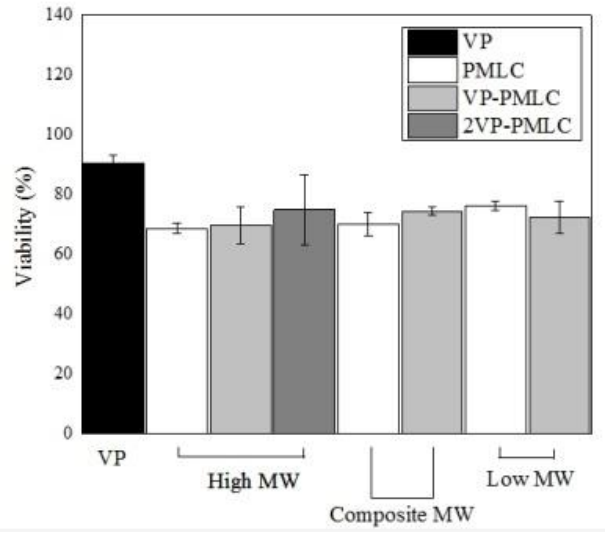

Figure 18. Viability of BMDCs incubated with VP (black color), PMLCs (white color), VP-PMLCs (light grey color) and 2VP-PMLCs (dark grey color), respectively, for 24h. The viral protein concentration was 0.1 mg/ml and the ratio of particle to cell was 100:1. Two molecular weights of P_LARG/DS polyelectrolyte pairs were used to encapsulate the viral proteins for cytotoxic studies.

Altogether, BMDCs co-cultured with a ratio of 20 PMLC/cell for 24h, resulted in an average viability of 80%, and the viability decreased to 70% with a ratio of 100 PMLC/cell, which is similar to prior reports [107]. These results showed that VP-PMLC could be developed as a safe vaccine delivery vehicle for vaccine delivery systems.

4.3.2 Release profile through confocal laser scanning microscope (CLSM)

Dendritic cells are able to take up microparticles through either phagocytosis or macropinocytosis [123]. In order to understand how efficient BMDCs would uptake the particles, as well as the influence of the MW of polymer shells on uptake, we designed a set of experiments for visualizing particle release. In order to visually study release behavior,

fluorescently labeled reagents were used. The encapsulation procedures were the same as regular particles, as described above.

Due to the electronic interaction between viral protein and polyelectrolytes, we hypothesize that silica beads that are similar in size to the viral protein can be used to mimic viral protein release. Therefore, we replaced *SV40* VP1 with 20 nm diameter Cy5-labeled silica beads. The 2nd layer of dextran was switched to fluorescent dextran, with MW of either 500 kDa, denoted as $(DS\text{-}F)_H$, or 10 kDa, denoted as $(DS\text{-}F)_L$. The surface charge of each material was measured by Malvern Zetasizer Nano series and the results are shown in Table 3.

Table 3. The surface charge of assembly materials

Surface Charge	***$CaCO_3$***	***Silica bead***	***$(P_LARG)_H$***	***$(P_LARG)_L$***	***$(DS)_H$***	***$(DS)_L$***	***$(DS\text{-}F)_H$***	***$(DS\text{-}F)_L$***
Mean (mV)	-24.83	-45.53	24.47	32.83	-29.53	-9.47	-22.27	-10.40
Standard deviation	0.86	1.85	10.43	6.29	10.56	6.36	4.47	5.37

The differences between the normal and fluorescent particles are the fluorescent silica beads, as well as the fluorescent dextran in the 2nd layer. As can been seen in Table 3, the surface charge of low MW of fluorescent-dextran showed less negative charge than high MW of fluorescent-dextran, which showed the same trend as regular dextran polyelectrolyte. The surface charge of silica beads in pH 6.0, 0.5M NaCl is around -45 ± 0.86mV, while the *SV40* VP1 viral protein is around -4.5 ± 4mV. The successful of encapsulation were confirmed by ξ-potential analysis, as shown in Figure 19.

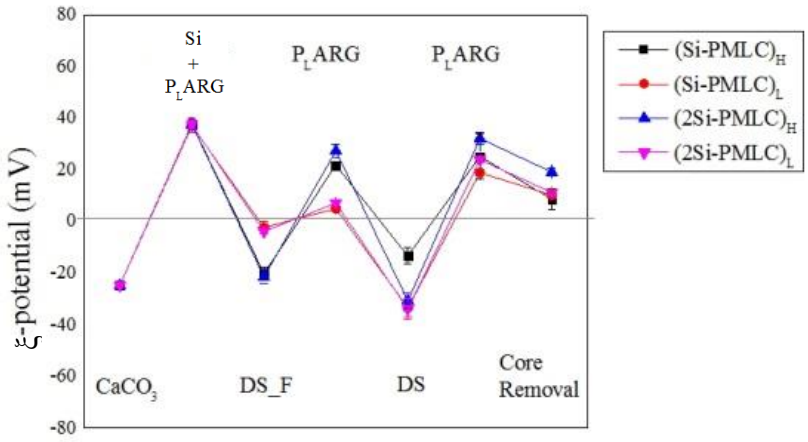

Figure 19. ξ-potential verification of the encapsulated fluorescent silica bead PMLCs with 2.5 bilayers.

Figure 19 shows that the less negatively charged DS, like $(DS)_L$ and $(DS\text{-}F)_L$ also have less particles charged on the surface. However, the addition of silica beads in different layers, either in the 1st layer, Si-PMLC, or both in the 1st and 3rd layers, 2Si-PMLC, does not show a significant difference from the surface charge analysis. Overall, the pattern seen with the potential shows the success of the encapsulation by alternatively applying positively and negatively charged polyelectrolytes onto the particles.

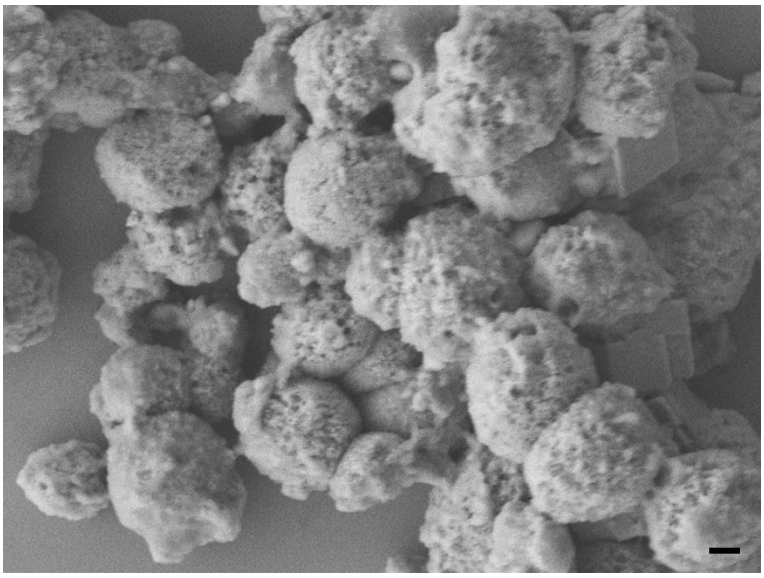

Figure 20. SEM images of $CaCO_3$ microparticles fabricated with fluorescent silica beads with high MW of polymer electrolytes. Scale bar, 1 μm.

Before core removal, the $(Si\text{-}PMLC)_H$ were dried overnight and imaged in a dry state. For $(Si\text{-}PMLC)_H$, the SEM images shown in Figure 20 additionally provides evidence of the success of encapsulation. The porous structure and the size of the particles are the same as normal PMLCs. Similar behavior was observed with other particles such as $(Si\text{-}PMLC)_H$, $(Si\text{-}PMLC)_L$, $(2Si\text{-}PMLC)_H$ and $(2Si\text{-}PMLC)_L$ as well. Together, the ξ-potential (Figure 19) and the SEM analyses (Figure 20) further confirmed the success of the Si-PMLC encapsulation.

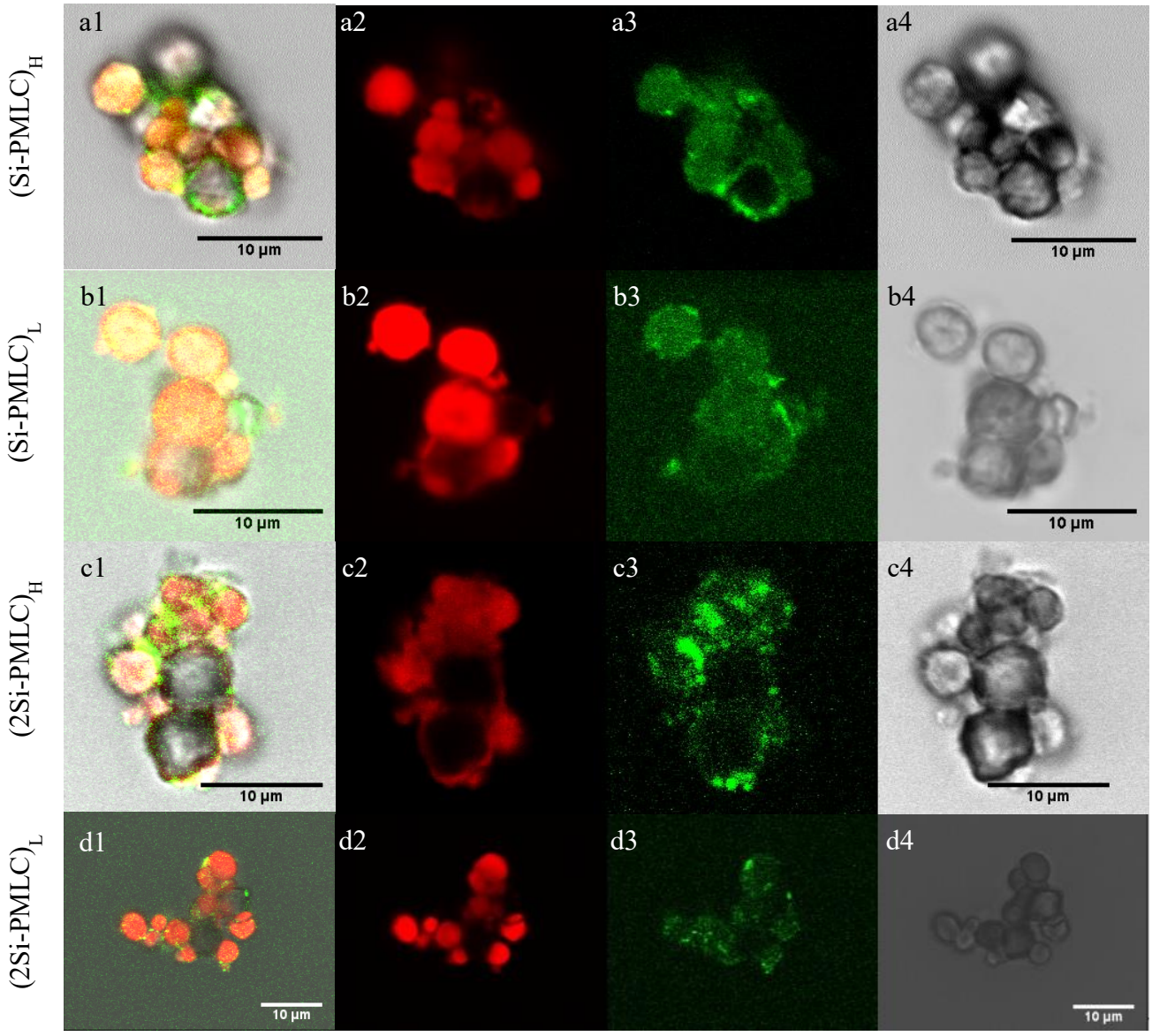

Figure 21. Fluorescent particles were fabricated by encapsulation of 20 nm Cy5-labeled silica beads with DS/P_LARG polyelectrolytes. The fluorescent shell was formed by Alexa Fluor 488 labeled DS located in 2nd layer. Confocal laser scanning microscope images were applied before core removal on (a) (Si-PMLC)$_H$, (b) (Si-PMLC)$_L$, (c) (2Si-PMLC)$_H$ and (d) (2Si-PMLC)$_L$, respectively. As for the number denotation, (a1) both PMLC encapsulated fluorescent silica beads (red fluorescence), as well as fluorescent DS (green fluorescence), were represented, (a2) the red fluorescence showed the distribution of DS in 2nd layer; (a3) the green fluorescence indicated the 20nm silica beads, while (a4) whole particles without fluorescence were presented. Scale bar, 10 µm

After the fluorescent Si-PMLCs were fabricated, confocal laser scanning microscope was used to study their intracellular distribution. The effect of different MW of polymers and different locations of silica beads were studied. The fluorescent silica beads were in 20 nm in diameter, used to mimic the *SV40* VP1 viral protein. The 500 kDa and 10 kDa fluorescent DS was served as high and low MW of polyelectrolytes at the 2^{nd} layer, respectively. Volodkin et al. reported that the average pore size of $CaCO_3$ particles ranging from 3 to 15 μm in diameter is around 25 nm [103]. The diameter of DS with MW 2,000 kDa is ~56 nm, and the diameter was ~3.4 nm with 4 kDa Dextran [172].

Comparing Figure (21a) to (21b) and Figure (21c) to (21d), the core-shell structure is only partially displayed in high MW polyelectrolyte pairs. However, most of the high MW and all of the low MW of capsules are able to penetrate to the center of core. A similar conclusion can also be drawn from the fluorescence intensity data. From Figure (21a), we further found that the polyelectrolyte shell is ~ 400 nm.

Figure (21a3) and (21b3) show that the fluorescent intensity is a solid circular image, which indicates an even distribution and suggests that the penetration phenomenon was seen in Si-PMLC. When applied on 2Si-PMLC, shown as Figure (21c3) and (21d3), the distribution of silica beads is more spread and gathered on the shell. This suggests that 2Si-PMLC facilitates localization of viral protein onto the shell and could be used for instant release.

After characterizing fluorescent microparticles, experiments were conducted using DC2.4 dendritic cells to study the release profile *in vitro*. The experiment set up is shown as Figure 22.

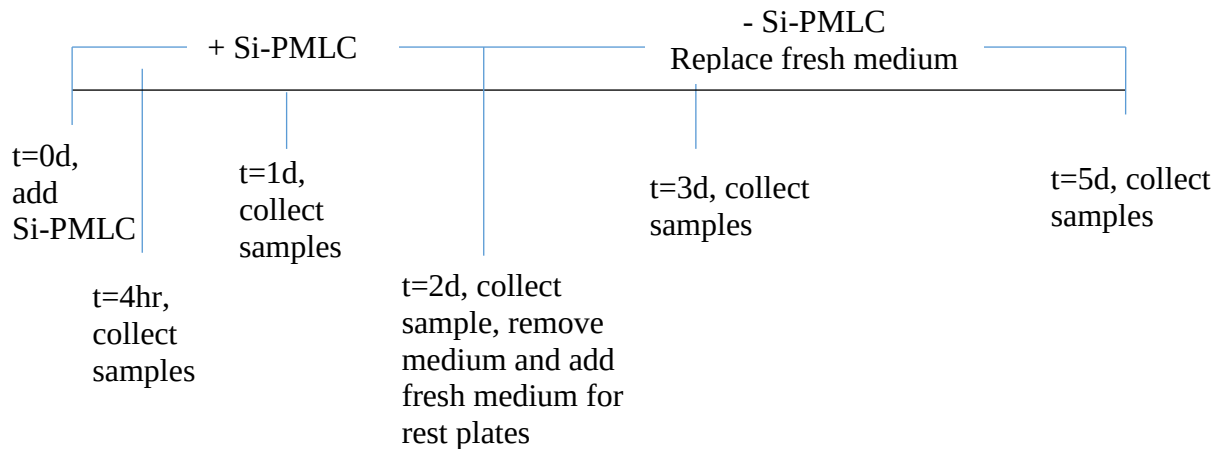

Figure 22. Time line for the *in vitro* release profile experiment using the DC2.4 cell line.

DC2.4 dendritic cells were co-incubated with different capsules, such as $(Si\text{-}PMLC)_H$, $(Si\text{-}PMLC)_C$, $(Si\text{-}PMLC)_L$, $(2Si\text{-}PMLC)_H$ and $(2Si\text{-}PMLC)_L$. Cells were collected, fixed, and then imaged using CLSM at different time points to observe their fluorescent intensity.

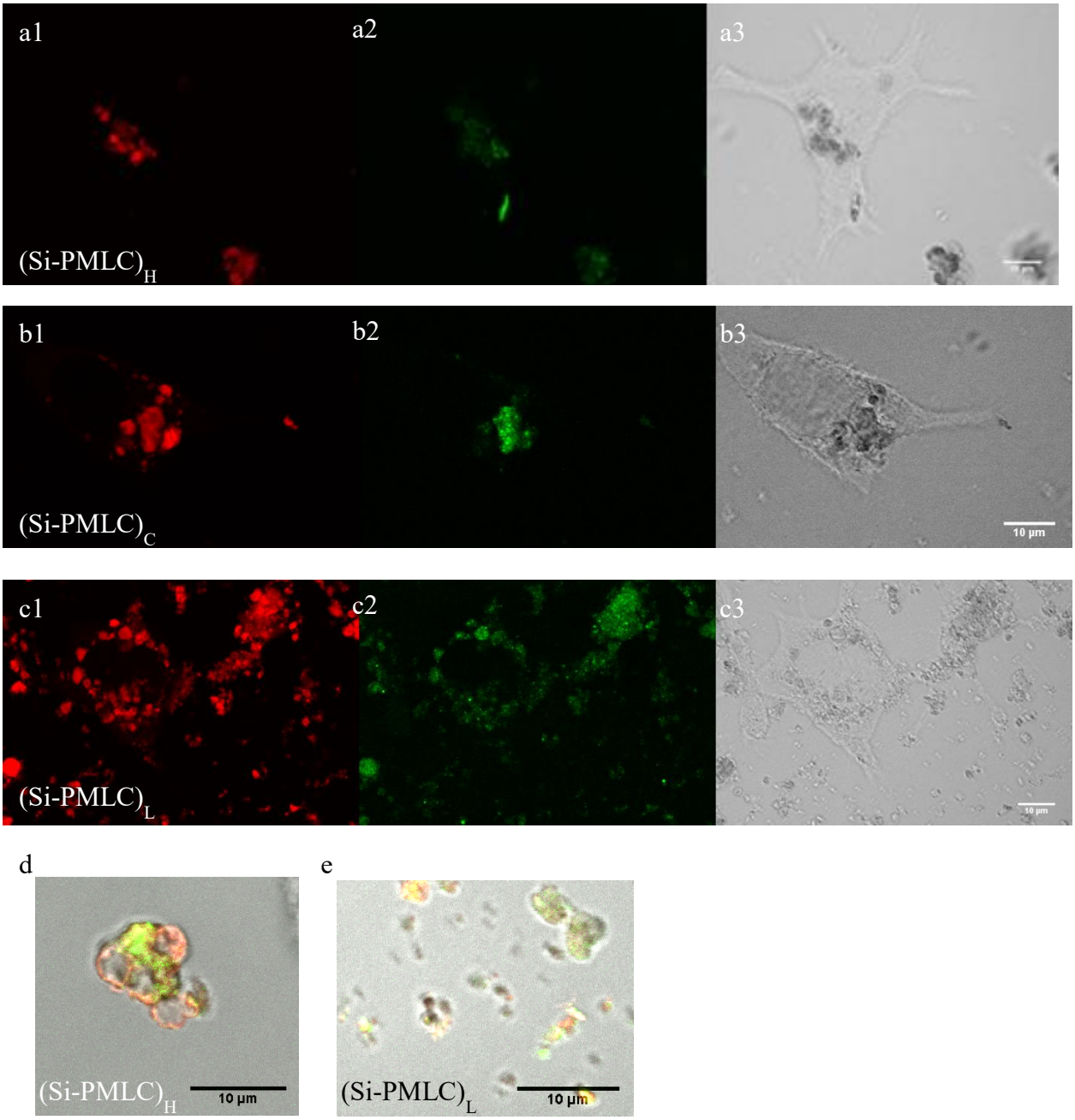

Figure 23. *In vitro* interaction between DC2.4 dendritic cells and Si-PMLCs. Confocal laser scanning microscope images were used to determine microparticle release profile co-incubated with (a) $(Si\text{-}PMLC)_H$, (b) $(Si\text{-}PMLC)_C$, as well as (c) $(Si\text{-}PMLC)_L$, at 37°C in 5% CO_2 humidified environment for 4h. (a1) the red fluorescence shows Alexa Fluor 680 labeled DS; (a2) green fluorescence indicates 20nm Cy5-labeled silica beads; (a3) both PMLC encapsulated fluorescent silica beads, as well as fluorescent DS, are presented. A close-up image of the fluorescent intensity with $(Si\text{-}PMLC)_H$ and $(Si\text{-}PMLC)_L$ is shown in is shown in Figure (d) and Figure (e), respectively. Scale bar, 10 µm.

DC2.4 dendritic cells were first seed in a two-well chamber slide, and then co-incubated with $(Si\text{-}PMLC)_H$, $(Si\text{-}PMLC)_C$ and $(Si\text{-}PMLC)_L$ particles. The fluorescence release profile was studied using CLSM. Figure 23 shows that most of the particles were engulfed by DC2.4 dendritic cells within 4h. The fluorescent intensities in Figures (23d) and (23e) are different, and show that low MW polyelectrolytes of capsules are able to break into small pieces within 4h. However, this was not observed with high MW polyelectrolytes. The core-shell structure was also found in Figure (23d), which shows the core-shell structure on $(Si\text{-}PMLC)_H$ clearly even after the core removal.

A potential limitation of this *in vitro* experiment is that the culture medium has to be changed every other day, leading to removal of microparticles from the culture. Since most of particles were engulfed within 4h (Figure 23), this might not be a problem and suggest that the release activity can be studied over longer periods of time.

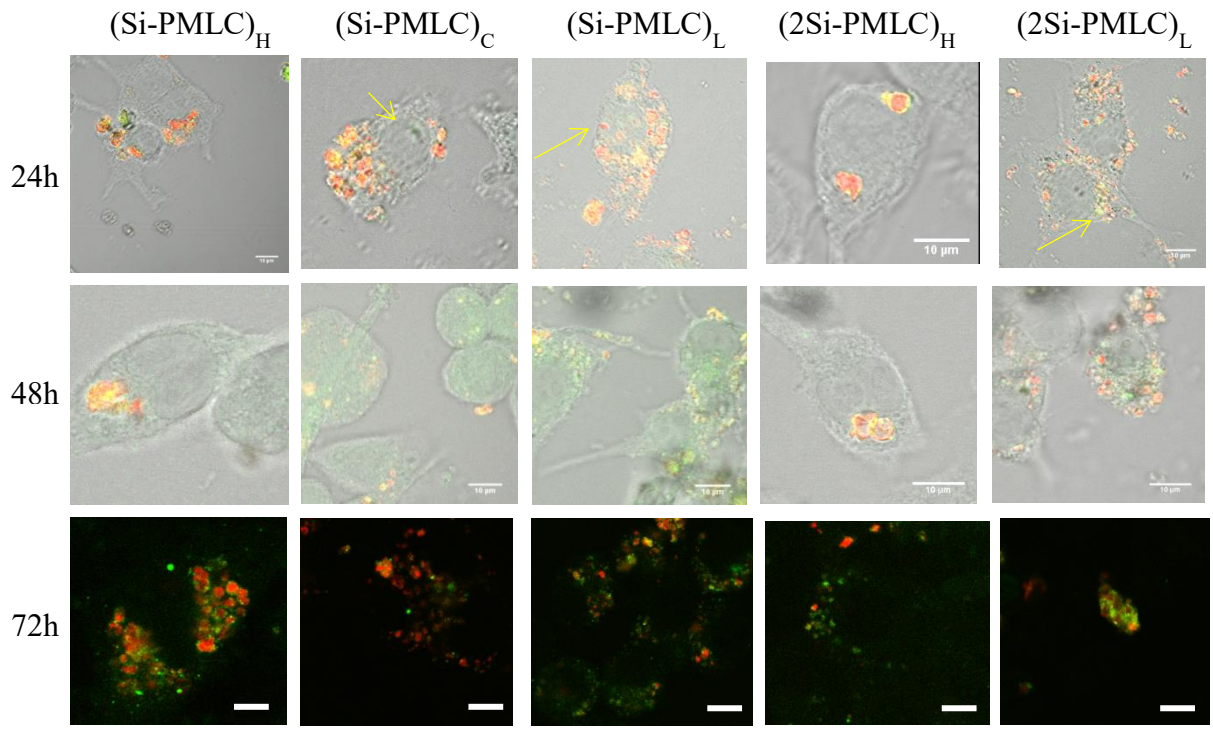

Figure 24. *In vitro* interaction between DC2.4 dendritic cells and Si-PMLCs. Confocal laser scanning microscope images were used to determine microparticle release profile co-incubated with $(Si\text{-}PMLC)_H$, $(Si\text{-}PMLC)_C$, $(Si\text{-}PMLC)_L$, $(2Si\text{-}PMLC)_H$, as well as $(2Si\text{-}PMLC)_L$, at 37°C in 5% CO_2 humidified environment for 24h, 48h and 72h, respectively using a two-well chamber slide. Red fluorescence shows the Alexa Fluor 680 labeled DS, green fluorescence indicates 20nm Cy5-labeled silica beads, while the yellow color showed the combination of red and green. The yellow arrow indicates area with green fluorescence alone. Scale bar, 10 µm.

Longer duration experiments were designed to investigate the release profile. DC2.4 dendritic cells were co-incubated with $(Si\text{-}PMLC)_H$, $(Si\text{-}PMLC)_C$, $(Si\text{-}PMLC)_L$, $(2Si\text{-}PMLC)_H$, as well as $(2Si\text{-}PMLC)_L$, for 24h, 48h and 72h, respectively. The fresh culture medium was replaced on day 2. Cells were then fixed using 4% PFA and studied using CLSM.

Figure 24 confirms that most of the microparticles were engulfed by DC2.4 dendritic cells. In row 1, after co-culturing for 24h, the leakage of silica beads are found in $(Si\text{-}PMLC)_C$, $(Si\text{-}PMLC)_L$ and $(2Si\text{-}PMLC)_L$ (indicated by the yellow arrow). The green fluorescence

illustrates the location of silica beads, after the combination of red and green, the green color in the Figure also presents the existence of silica bead alone. Therefore, we found that the silica beads encapsulated by low MW of polymers, as well as the composite MW of polymers, were able to release within 24h. In row 2, more green color was found in $(Si\text{-}PMLC)_C$, $(Si\text{-}PMLC)_L$ and $(2Si\text{-}PMLC)_L$, meaning that more silica beads were released by 48h. However, for high MW of capsules, the images of $(Si\text{-}PMLC)_H$ and $(2Si\text{-}PMLC)_H$ are still more yellow and red, meaning the silica beads and the DS are still in the same location inside the cells.

In row 3, the images show more red and green color separately; the green color is even present outside the red color, meaning the silica beads are no longer inside the shells and have leaked out. Surprisingly, at 72h, with $(Si\text{-}PMLC)_H$, the red color is still very solid, and the shell does not appear to be broken like the low MW capsule. The same conclusions can be made from $(Si\text{-}PMLC)_C$ and $(2Si\text{-}PMLC)_H$ particles.

In this experiment, by encapsulating silica beads in different locations, such as $(Si\text{-}PMLC)_H$ vs. $(2Si\text{-}PMLC)_H$ and $(Si\text{-}PMLC)_L$ vs. $(2Si\text{-}PMLC)_L$, no significant differences in the release profiles were observed. This suggests that the factors controlling the leakage of 20 nm particles from P_LARG/DS shell are related to the shell structure than the location.

Altogether, as for the release profile of Si-PMLCs, we found that the silica beads assembled by low MW and composite MW of capsules were able to leak out within 24h; however, it took 72h for silica beads encapsulated by high MW of polymers to release, shown in Figure 25. So, with 2.5 layered P_LARG/DS shell, silica beads could be released during 24-72h. Moreover, low MW capsules tend to break down easily, while the high MW capsules still retain their shape. This trend was also seen in a previous study that demonstrated that high MW

PMLCs were deformed after 8 days of injection; however, the PMLCs started to degrade after 16 days [107].

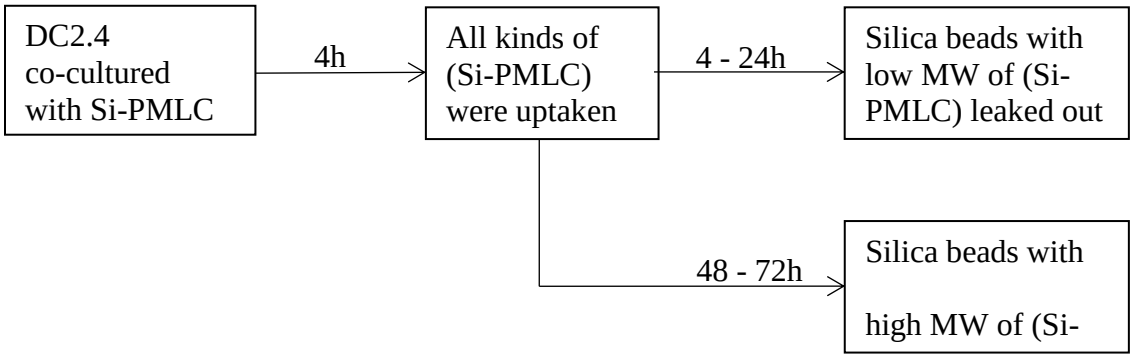

Figure 25. Scheme to summary the release activity through the overall Si-PMLC behavior

4.3.3 Stimulation and maturation of BMDC

Immature dendritic cells circulate throughout the body, and look for foreign proteins. Once they engage foreign proteins they mature through uptake, process and present antigens to the cell surface, and also release signals to stimulate adaptive immunity that leads to development of memorized antibodies [5, 182]. We investigated the efficiency of immune response induction and dendritic cell maturation resulting from co-culturing dendritic cells with VP-PMLCs using flow cytometry.

We previously demonstrated that PMLCs could be engulfed by dendritic cells *in vitro*. In order to successfully prime naïve T cells to generate antibodies, multiple molecule signals are required. A primary signal is the binding of cognate antigen in MHC-restricted manner to an antigen receptor expressed by T and B lymphocytes. Multiple secondary signals involve the engagement of co-stimulatory molecules expressed by T and B lymphocytes with their respective

ligands [116]. The co-stimulatory surface markers that we profiled are CD40 and CD86 on BMDCs.

CD40 belongs to the tumor necrosis factor receptor family and is expressed by B cells, dendritic cells, macrophages and basal epithelial cells under inflammatory conditions [183, 184]. CD40 signaling induces dendritic cells to mature and achieve all of the necessary characteristics to effectively trigger T-cell activation and differentiation by engaging the surface of dendritic cells to promote cytokine production, induce co-stimulatory molecules and facilitate cross-presentation of antigen [185, 186]. Therefore, CD40 plays an important role in the initiation and progression of cellular and humoral adaptive immunity.

CD86 belongs to the CD28/B7 family and is expressed by monocytes, activated B cells and dendritic cells. The expression of CD86 presents one of the most important T-cell co-stimulatory molecules and plays a major role in the activation of T cells, leading to their proliferation and cytokine production [187, 188]. These immune molecules can also be affected by the addition of an adjuvant, substances that enhance immunogenicity of antigens. With the addition of adjuvant, the antigen-adjuvant particles are capable of inducing a stronger immune response [38, 72, 88, 94]. Moreover, different adjuvants would lead to different immune responses, and the co-stimulatory molecule upregulation levels might also show differences [189]. Therefore, different adjuvants were prepared in our study. The method of stimulating surface markers was as described in the materials and methods section. A brief time line of the experiment design is presented in Figure 26.

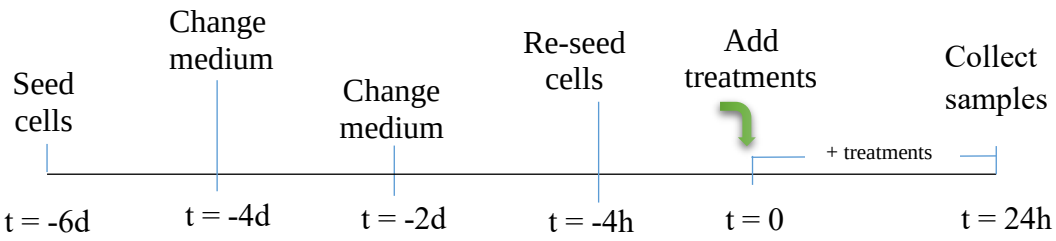

Figure 26. Time line for the *in vitro* immune response experiment

In this experiment, we aimed to investigate the efficiency of BMDC stimulation by different antigens *in vitro* in response to viral protein, polymer microparticles, and viral protein capsules. As negative and positive controls, we co-incubated BMDCs with plain growth medium or LPS, respectively. Figure 27 (a1) and (b1) show that after 24h co-culture, more than 80% of BMDCs were still alive. The levels of CD11c (Figure 27a2. and 27b2) which suggests the presence of mature BMDCs were used to gate cells. Figure (27b3) and (27b4) further show the levels of CD40 and CD86 upon stimulation which show that BMDCs can be activated by LPS.

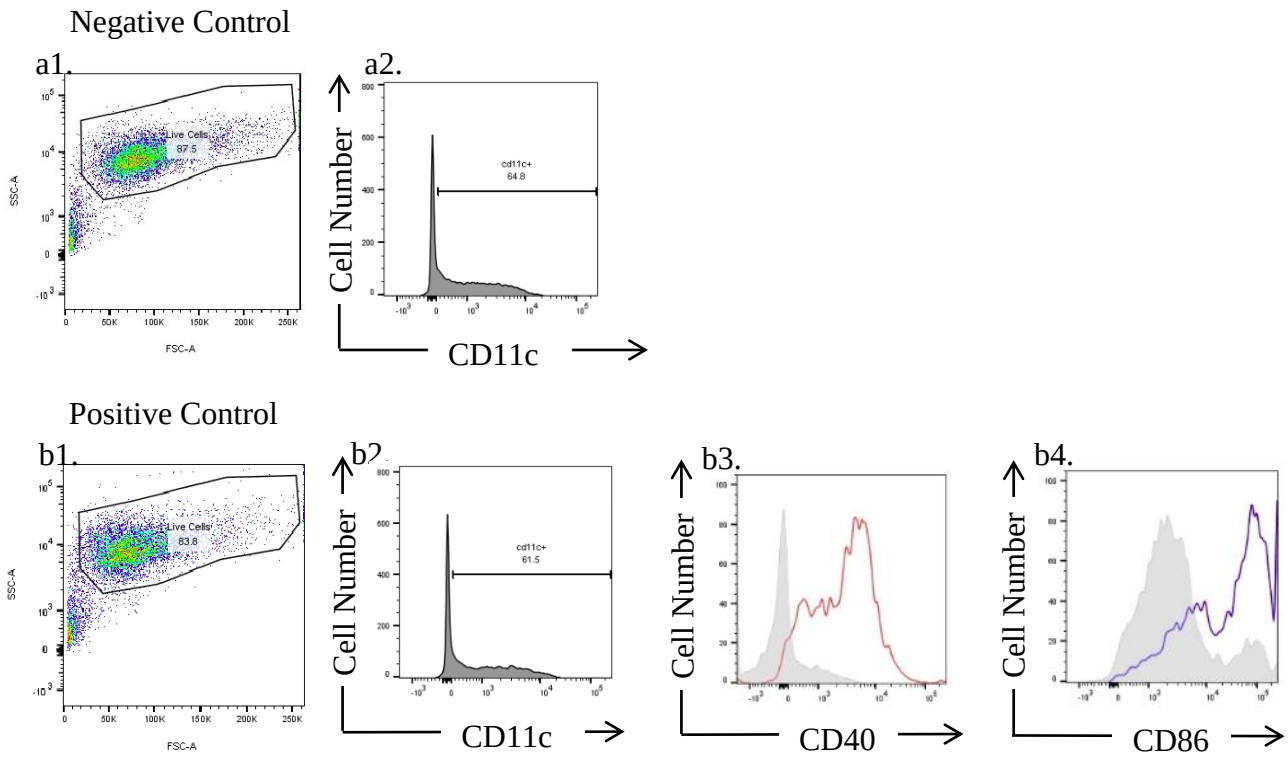

Figure 27. Activation marker expression by BMDCs was observed with negative and positive controls. Primary BMDCs were generated from C57BL/6 mice. After 6 days of culture from mice bone marrow cells and further 24h treatment, the maturation level was detected by flow cytometry analysis. (a) Without any treatment, negative control. (b) BMDC co-incubated with 1000 ng/ml LPS, positive control. (a1), (a2), (b1), (b2) Live BMDCs were selected based on the distribution of FSC-SSC and the expression of CD11c. (b3), (b4) Flow cytometry analysis of BMDC maturation was induced by LPS. The gray color presents the stimulated levels of CD40 and Cd86 on negative control. One representative experiment from three independent experiments with similar results is shown.

The *SV40* VP1 viral protein was co-incubated with freshly harvested BMDCs at different concentrations (10 μg/ml, 50 μg/ml and 100 μg/ml). After intercellular staining, changes in the expression of CD40 and CD86 were used to evaluate the extent of BMDC stimulation. Figure 28 shows that after being gated by $CD11c^{+}$, the CD40 and CD86 levels suggest that after 24h stimulation, *SV40* VP1 alone could induce BMDC maturation.

Compared to Figure 28, (a2) and (a3), the CD40 upregulation level on 10μg/ml and 50μg/ml is similar. The same conclusion can be made based on the stimulation of CD86 stimulation, Figure 28, (c2) and (c3). The mean fluorescent intensity of CD40 and CD86, shown as Figure (28b) and (28d), also indicate that compared to the 100 μg/ml, the stimulation level of viral protein concentration with 10 μg/ml and 50 μg/ml is much lower. However, when the viral protein concentration went up to 100 μg/ml, shown as Figure 28, (a1) and (c1), the stimulation level is comparable to the one co-incubated with LPS, shown as Figure 27, (b3) and (b4).

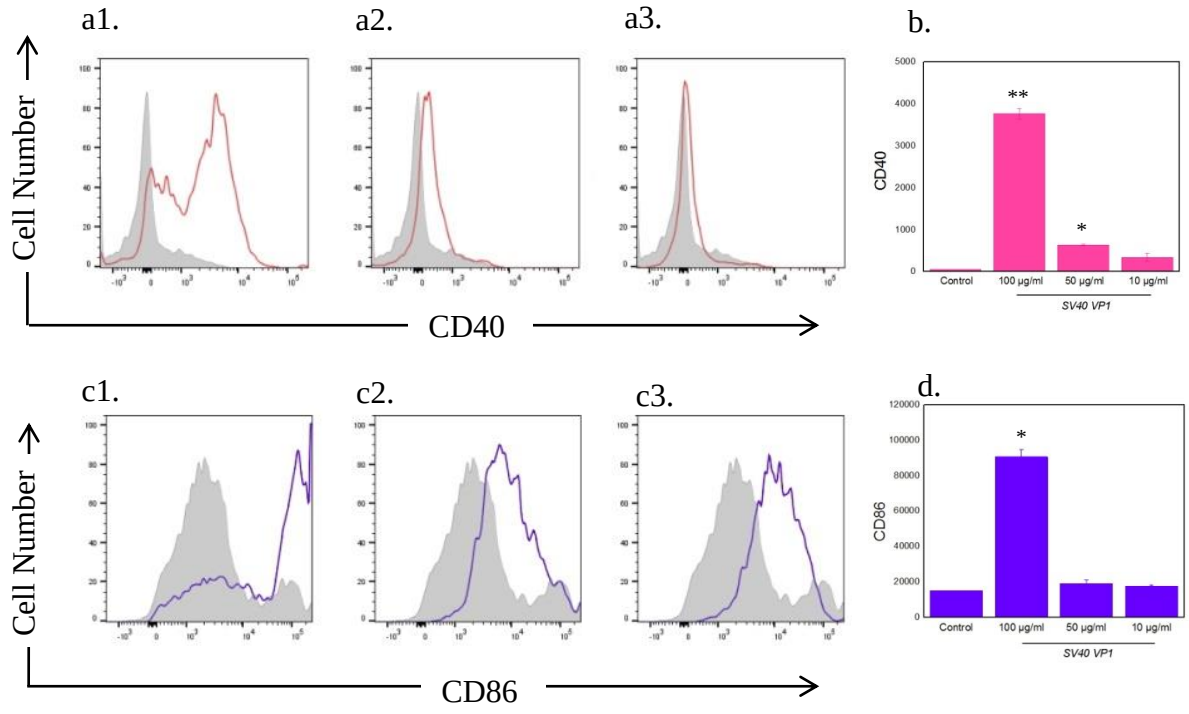

Figure 28. *In vitro* interaction between BMDCs and *SV40* VP1 viral protein was analyzed by flow cytometry. Freshly isolated BMDCs were co-incubated with viral protein in different concentrations, 100μg/ml (a1, c1), 50μg/ml (a2, c2) and 10μg/ml (a3, c3) for 24h. Cells were then stained with surface markers- CD11c, CD40 and CD86. Figure (a1), (a2) and (a3) show the CD40 level, gated by $CD11c^+$, while the gray color indicates the negative control. Figure (b) shows their mean fluorescence intensities individually. Similarly, Figure (c1), (c2) and (c3) present the CD86 level, gated by $CD11c^+$, while Figure (d) indicates their mean fluorescent intensity, respectively. One representative experiment from three independent experiments with similar results is shown. $*p < 0.05$, $**p < 0.01$.

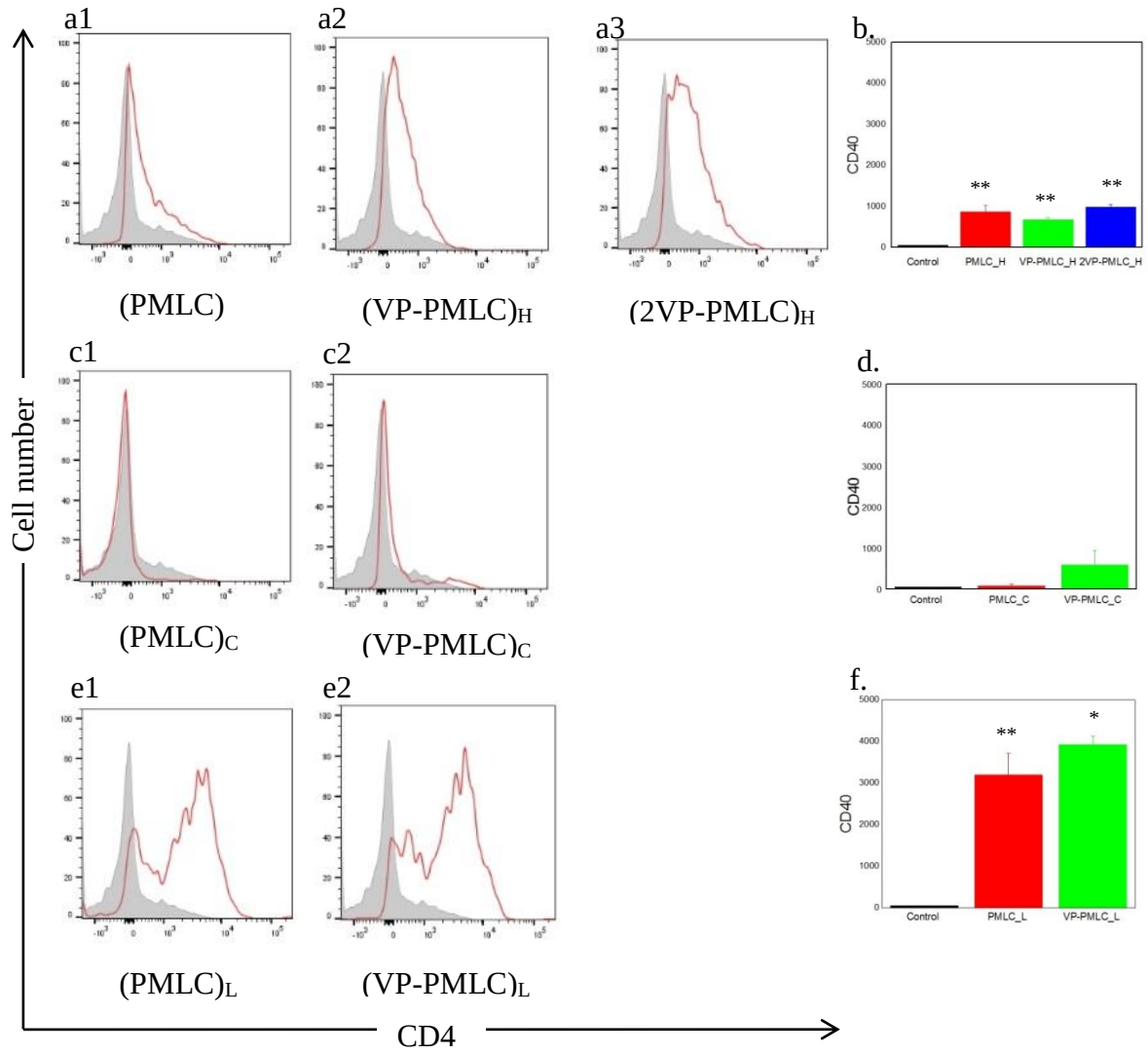

Figure 29. *In vitro* interaction between BMDCs and either PMLCs or VP-PMLCs was analyzed by flow cytometry. Freshly isolated BMDCs were co-incubated with different capsules at a capsule to cell ratio of 20:1 for 24h. Cells were then stained with surface markers- CD11c, CD40 and CD86. Figures show the expression of CD40 in different conditions after being gated by $CD11c^{+}$ expression. The histogram and mean fluorescent intensity of CD40 upregulation level are showed, respectively by co-incubated mice BMDCs with ((a) and (b) high MW of PMLCs, ((c) and (d)) composite MW of PMLCs and ((e) and (f)) low MW of PMLCs. The gray color indicated the stimulated level of CD40 on negative control. Different antigen capsules were performed by encapsulating different MW of polymers showed in each row. From left to right, the investigation went by PMLC alone, VP-PMLCs, as well as 2VP-PMLC, indicated as 1, 2 and 3, respectively. One representative experiment from three independent experiments with similar results is shown. *$p < 0.05$, **$p < 0.01$.

CD40 is a co-stimulatory molecule belonging to the tumor necrosis factor superfamily and is essential in activation of dendritic cells. In order to study the immune response induced by viral protein capsules, BMDCs were co-incubated with either capsules or viral protein capsules for 24h, and the expression of CD40 detected by flow cytometry. Figure (29a) and (29b) represent the CD40 upregulation level and the mean fluorescent intensity of $CD11c^{+}$ gated BMDCs, which were co-incubated with high MW of PMLCs, denoted as $(PMLC)_H$. The numbers, 1, 2 and 3, indicate the capsules alone, viral protein capsules and viral protein capsules with two-layer encapsulation of viral protein, respectively. Figure (b) represents the PMLCs composed by composite MW of polymer, denoted as $(PMLC)_C$. Figure (c) represents the PMLCs composed by low MW of polymer, denoted as $(PMLC)_L$. The gray color shown in Figure (29a), (29c) and (29e) illustrates the CD40 level of negative control.

The influence of the maturation level on mice BMDCs with the addition of viral protein and its distribution within the capsules is discussed below. In Figure 29, row a, (a1) represents the CD40 signal after BMDCs co-incubated with $(PMLC)_H$, compared to the negative control, the gray curve, the curve is shifted a little to the right. When compared to Figure 29 (a2), the expression of CD40 is higher for $(VP\text{-}PMLC)_H$, suggesting that the combination of viral protein and capsules was able to stimulate stronger immunity. In this experiment, the capsule to cell ratio was set at 20:1 with a viral protein concentration of 10μg/ml. Figure 28 (a3) shows that BMDCs co-incubated with 10μg/ml viral protein alone was barely able to activate DCs. However, the combination of viral protein with the adjuvant stimulates higher immune response, based on CD40 expression. More evidence for higher stimulation levels of CD40 expression on encapsulation form was provided by Figure (29c), (29d), (29e) and (29f). These results show that VP-PMLC elicited a stronger immune response than PMLCs.

Comparing Figure 29 (a2) to (a3), we found that, $(2VP\text{-}PMLC)_H$ elicited a higher immune response than $(VP\text{-}PMLC)_H$, suggesting that the viral protein located in the outer layer might be more accessible to DCs. Interestingly, Figure 24 shows that the silica beads were not released from high MW of capsules until 72h co-incubation; however, in Figure (29a) we find that within 24h co-incubation, the viral protein is released and induced the immune response. This phenomenon is likely due to the porous structure of the PMLCs. Though the shell was not able to break down within 24h, the enzyme in the medium could access the viral protein through the pores. This is similar to the observations made by Stefaan et al [41]. This likely explains the induction of a stronger immune response within 24h. Figure (29b), (29d) and (29f), represent the mean fluorescence intensity per cell under the different conditions. These results show that the viral protein capsules induced a higher mean fluorescence intensity than the capsules itself, which further confirmed that the combination of antigen and adjuvants stimulate a stronger immune response.

When comparing Figure (29a), (29c) and (29e), each column presents the same observation that the capsules encapsulated by composite MW polymers displays the lowest stimulation level, while capsules composed of low MW polymers induces the highest immune response. Therefore, we found that low MW of P_LARG/DS adjuvant itself was capable of inducing higher immunity.

CD86 is another co-stimulatory molecule that determines DC maturation, as well as the capability for triggering T cell activation to activate the adaptive immune system. Using the same experimental design as above, we studied the induction in the levels of CD86 (Figure 30).

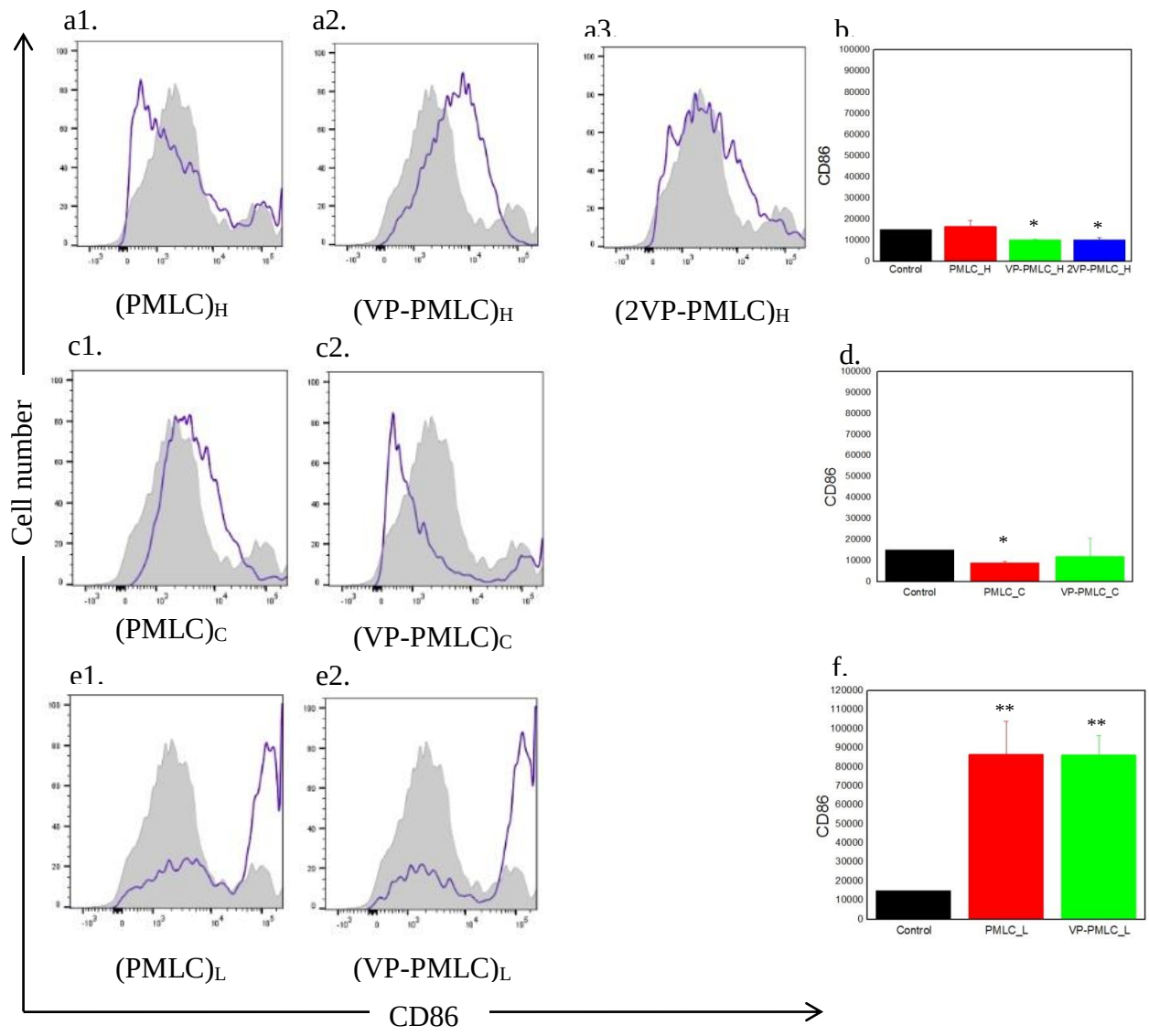

Figure 30. *In vitro* interaction between BMDCs and either PMLCs or VP-PMLCs was analyzed by flow cytometry. Freshly isolated BMDCs were co-incubated with different capsules by the capsule to cell ratio of 20 for 24h. Cells were then stained with surface markers- CD11c, CD40 and CD86. After being gated by $CD11c^{+}$, the expression of CD86 in different conditions is shown. Figure (a) and (b) show CD86 upregulation level with $(PMLC)_H$, represented by the histogram and its mean fluorescent intensity, respectively. Similarly, Figure (c) and (d) show BMDCs co-incubated with $(PMLC)_C$ while Figure (e) and (f) show the interaction between BMDCs and $(PMLC)_L$. The gray color indicates the stimulated level of CD86 relative to the negative control. The conditions shown from left to right are: PMLC alone, VP-PMLCs, 2VP-PMLC, indicated as 1, 2 and 3. One representative experiment from three independent experiments with similar results is shown. $*p < 0.05$, $**p < 0.01$.

CD86, a protein expressed on APCs, provides co-stimulatory signals necessary for T cell activation and survival. In order to know how efficiently the viral protein capsules promote BMDC maturation, cells were co-incubated with either capsules or viral protein capsules for 24h, and the expression of CD86 was detected by flow cytometry. Comparing Figure 30 (a1), (a2) and (a3), the expression of CD86 on mice BMDCs, gated by $CD11c^+$ is slightly higher for $(2VP\text{-}PMLC)_H$ and $(VP\text{-}PMLC)_H$ compared to $(PMLC)_H$. Though the differences are not significant, the curve is different from the PMLCs alone. In Figure (30b), the data indicates that the mean fluorescent intensity does not increase with viral protein capsules, though the curve does shift to the right more, meaning the viral protein capsules might have induced higher activation in some cells; however, others cells still had a low activation level. Observations from Figure 30, (c), (d), (e) and (f) further confirms that the viral protein capsules shows higher CD86 stimulation but not compared to CD40 upregulation.

Taking the encapsulation MW of polymers into consideration, the increase in CD86 expression (Figure 30) shows a similar trend to the expression of CD40 on mice BMDCs, gated by $CD11c^+$, (Figure 29). The $(PMLC)_L$ capsule was able to elicit stronger immune response compared to the $(PMLC)_H$ and $(PMLC)_C$, which again confirmed that low MW of P_LARG/DS pair could induce higher BMDC maturation and enhance immune responses *in vitro*.

4.4 Summary

In this chapter we studied the cytotoxicity, release profile and the immune response of BMDC and DC2.4 dendritic cells to different co-culture conditions *in vitro*. We found that BMDCs co-cultured for 24h with microparticles at a ratio of 20:1 had an overall viability of ~80%, while an increase in the capsule/cell ratio to 100:1 decreased the viability to ~70%. When

considering the different MWs of capsules, low MW capsules had less toxicity (or higher viability) than the other conditions.

We used fluorescent silica beads to mimic the viral protein, and fluorescent dextran to replace original material, and visually investigated the particle structure using CLSM. We found that all capsules were engulfed by DC2.4 dendritic cells within 4h. We observed that silica beads leaked out within 4h for low MW Si-PMLCs; however, leakage of silica beads was observed only after 48h for high MW Si-PMLCs. Moreover, localizing silica beads in the outer layer did not lead to early release, suggesting that the MW of capsules is more important for release.

BMDCs treated with VP-PMLCs showed that low MW capsules and viral proteins located in outer layer were two factors that could efficiently induce an immune response, as seen from the expression of CD40 and CD86. This data also showed that the combination of antigen and adjuvants could stimulate higher immune response.

5. CELLULAR MECHANISMS ACTIVATED BY VP-PMLC: AN *IN VITRO* STUDY

In Chapter 4, we demonstrated that VP-PMLCs upregulate the expression of the DC co-stimulatory molecules CD40 and CD86. In this chapter we investigate *in vitro* the molecular mechanisms and signaling pathways engaged when VP-PMLCs activate the innate immune system.

5.1 Introduction

Activated DCs upregulate the production of a distinct panel of cytokines and co-stimulatory molecules, which eventually leads to initiation of the adaptive immune response in the body [5]. Activation of inflammasome is one of the key intermediate steps initiated by activated DCs in response to harmful stimuli. Inflammasomes are multimeric protein complexes that assemble in the cytosol after sensing damage-associated molecular patterns or pathogen-associated molecular patterns [190].

Therefore, we investigated *in vitro* the cytokine secretion and inflammasome activation in BMDCs upon co-incubation PMLCs. Cytokines (TNF-α, IL-12 and IL-1β) in the cell culture supernatant after 24h incubation using ELISA assay kits. Chemical inhibitors were used to investigate the molecular mechanisms involved in up-regulation of cytokine production.

5.2 Materials and methods

BMDCs were isolated from C57BL/6 mice and cultured as described in Chapter 4.

CA-074 methyl ester (CA-074 ME) and Latrunculin A (Lat. A) were purchased from Sigma Aldrich. Mouse IL-12 ELISA kits (mouse IL-12 ELISA kit) were purchased from Thermo Fisher Scientific. Tumor Necrosis Factor-α (TNF-α) assay kits (mouse TNF-α platinum ELISA kit) and mouse IL-1β assay kits (mouse IL-1β platinum ELISA kit) were purchased from

Invitrogen. All cytokine assays were carried out following the manufacturer's recommended protocols.

Ultrapure water used for all experiments was obtained from a Millipore system with a specific resistance 18.2MΩ/cm.

All experiments were carried out in triplicate. Mice BMDCs were seeded in 96-well flat bottom tissue culture plates at a cell density of ~10^5/well. For all treatment conditions, the ratio of PMLCs and VP-PMLCs to cells was 20:1, and the viral protein concentration was 100 μg/ml, 50 μg/ml, or 10 μg/ml (denoted as VP-100, VP-50 and VP-10, respectively). Co-treated BMDCs were incubated at 37ºC in 5% CO_2 humidified environment for another 24h. For all cytokine assays, BMDCs culture supernatant was used as the negative control. For TNF-α and IL-12 cytokine assays, supernatant from cells stimulated with 1000 ng/ml LPS was used as the positive control. For IL-1β assays, supernatant from cells stimulated with 10 ng/ml LPS was used as the positive control.

For NLRP3 inflammasome activation studies, cathepsin B inhibitor, CA-074 Me, and actin polymerization inhibitor, Lat. A, were used. BMDCs were exposed to either 50 μM of CA-074 Me or 250 nM Lat prior to addition of particles and cells were incubated for 24h.

5.3 Results

5.3.1 Tumor Necrosis Factor-α (TNF-α) secretion

TNF-α is a major pro-inflammatory cell signaling protein involved in early inflammatory events and is one of the major cytokines secreted during the acute phase response [136]. The production of TNF-α induces the expression of other inflammatory molecules, including IL-8 [191], chemokines such as CCL3 (chemokine (C-C motif) ligand 3), CCL4, CCL2 [192], prostaglandins [193], matrix metallopeptidases [194], reactive oxygen species [195], and reactive

nitrogen intermediates [196]. TNF-α is produced mainly by activated macrophages, but it can be produced by many other cell types such as CD4+ lymphocytes, NK cells, neutrophils, mast cells, eosinophils, and neurons.

BMDCs were cultured 6 days, exposed to different concentrations of *SV40* VP1 viral protein for 24h, and cytokine levels in the culture supernatant determined. Figure 31 shows that compared to LPS stimulation, BMDCs co-incubated with *SV40* VP1 viral protein secreted TNF-α only at the highest concentration of VP1 (100 μg/ml). At the lower concentrations, no significant TNF-α was detected in the supernatant.

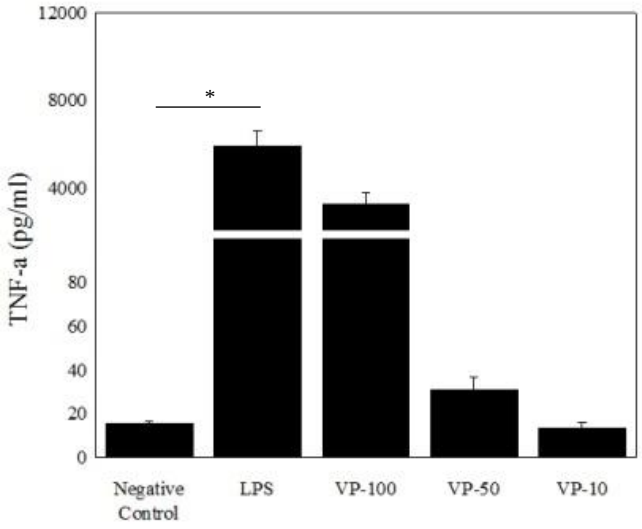

Figure 31. TNF-α secretion in BMDCs exposed to different concentrations (100 μg/ml, 50 μg/ml, or 10 μg/ml) of *SV40* VP1 viral protein. LPS was used as a positive control, untreated cells were used as a negative control. *$p < 0.05$.

The same experimental design was used to co-culture BMDCs with either PMLC, VP-PMLC or 2VP-PMLC at a particle to cell ratio of 20:1 for 24h. Overall, compared to the negative control, none of the capsules significantly induced TNF-α cytokine (Figure 32). Since no cell

death or phagocytosis was observed, these results suggest that P_LARG/DS capsules are not able to induce TNF-α secretion due to their immunocompatibility[197] or thpossible because the capsules induce the expression of other cytokines.

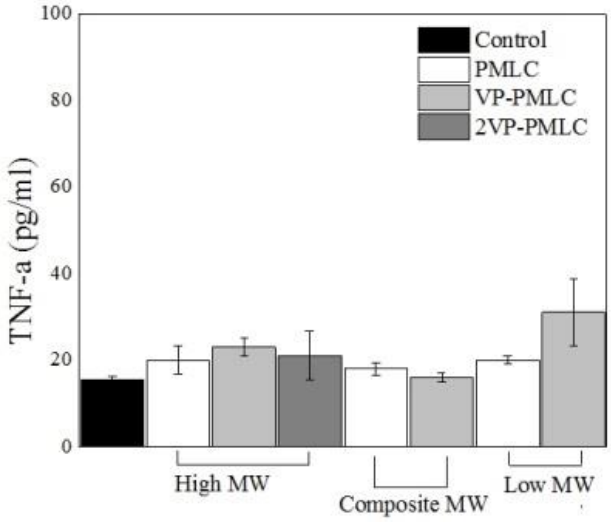

Figure 32. TNF-α secretion in BMDCs incubated with PMLCs (white color), VP-PMLCs (light grey color) and 2VP-PMLCs (dark grey color), respectively, for 24h. The ratio of particle to cell was 20:1. Two molecular weights of P_LARG/DS polyelectrolyte pairs were used to encapsulate viral proteins and untreated cells were used as the negative control.

5.3.2 Interleukin-12 (IL-12) secretion

Interleukin 12 (IL-12) is a proinflammatory cytokine produced by phagocytic cells such as dendritic cells, macrophages, neutrophils, and human B-lymphoblastoids in response to antigenic stimulation. IL-12 is also known as a T cell-stimulating factor, and plays a major role in cellular immunity, notably by inducing lymphocytes to produce IFN-γ [135]. IL-12 signals through heterodimeric receptor complexes that contain IL-12 R β1 paired with IL-12 R β2 for the IL-12 receptor. The activation of T_H1 cells by IL-12 is amplified through the JAK-STAT

signaling pathway and phosphorylation of the transcription factors signal transducer and activator of transcription 1 (STAT1), STAT3, and STAT4.

BMDCs were cultured 6 days, exposed to different concentrations of *SV40* VP1 viral protein for 24h, and IL-12 levels in the culture supernatant determined. Untreated BMDCs were used as the negative control while exposure to 1000 ng/mL of LPS for 12h was used as the positive control. Compared to the LPS control, none of the viral protein samples significantly increased IL-12 levels (Figure 33).

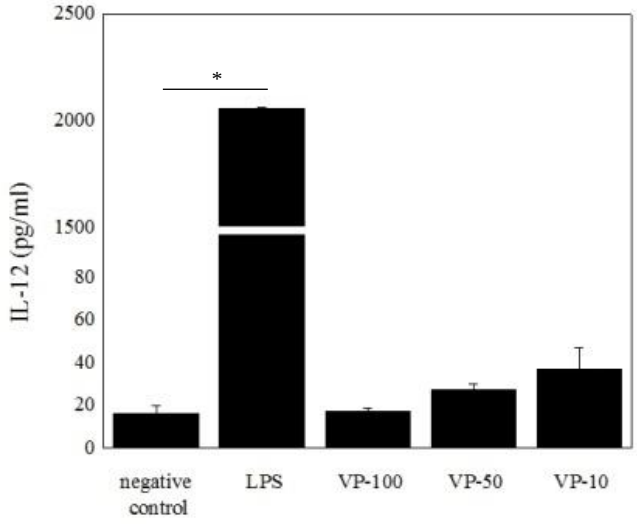

Figure 33. IL-12 secretion with different levels of *SV40* VP1 viral protein. LPS was used as the positive control, and untreated BMDCs were used as the negative control. *$p < 0.05$*

When BMDCs were co-cultured with either PMLC, VP-PMLC or 2VP-PMLC at a 20:1 ratio of particles to cells for 24h, none of the tested capsules significantly induced IL-12 secretion compared to the negative control (Figure 34). Moreover, no cell death or phagocytosis was observed, and since IL-12 is mainly induced by microbial signals such as LPS or CpG

bacterial DNA motifs [198], these results suggest that viral particles did not activate IL-12 signaling.

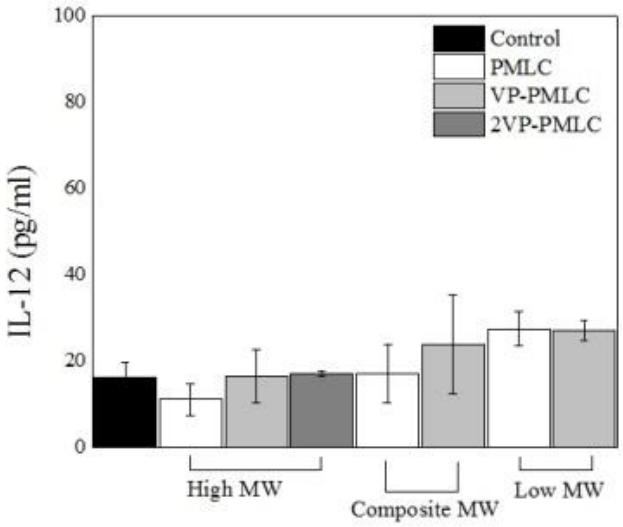

Figure 34. IL-12 secretion in BMDCs incubated with PMLCs (white color), VP-PMLCs (light grey color) and 2VP-PMLCs (dark grey color), respectively, for 24h. The ratio of particle to cell was 20:1. Two molecular weights of P_LARG/DS polyelectrolyte pairs were used to encapsulate the viral protein. Untreated cells were used as the negative control.

5.3.3 Interlukin-1β (IL-1β) Secretion

Most particulate material are known to activate NLRP3, a lymphocyte activating factor mediating the acute phase inflammatory response [129, 131, 148, 199, 200]. The process of NLRP3 inflammasome activation involves a conformational change in NLRP3 into its active form, which then associates with its adaptor protein (apoptosis-associated speck-like protein) through pyrin domain interactions. This complex leads to the recruitment of pro-caspase-1 through caspase activation and recruitment domain interactions [201]. Pro-caspase-1 is then cleaved into its active form, caspase-1, which then converts the biologically inactive pro-IL-1β to

the active cytokine IL-1β [202], which is capable of differentiating naïve T-cells to T_H17 cells. Therefore, the activation of NLRP3 leads to the processing and secretion of IL-1β. LPS, even at low concentrations, can prime dendritic cells to up-regulate pro-IL-1β [132]; however, mature IL-1β secretion is not observed. Therefore, a second stimulation is likely required for IL-1β production.

In this work, BMDCs were co-incubated with PMLC or VP-PMLC either alone or in combination with low dose of LPS (10 ng/ml) at different time points. The experimental design is shown in Figure 35.

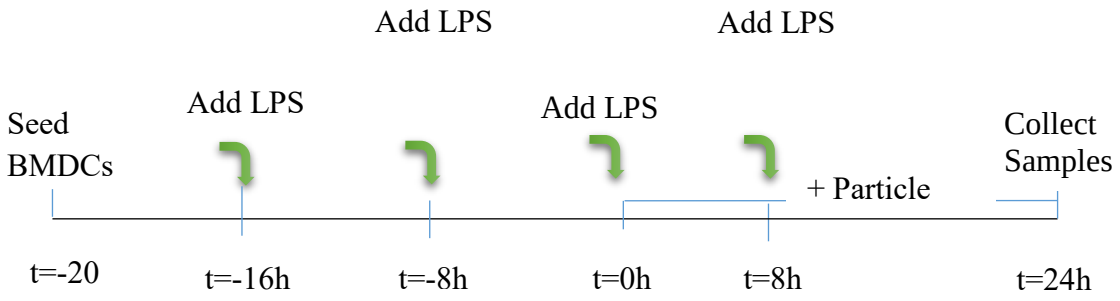

Figure 35. Time line for the *in vitro* stimulation of BMDCs with capsules for IL-1β production

High MW of PMLCs and VP-PMLCs were co-incubated with BMDCs at a particle/cell ratio of 20:1 in 96-well plates. LPS (10 ng/ml) was added to all conditions at different time points (Figure 35). At 24h after addition of the particles, supernatants were collected and used to assay for IL-1β.

Figure 36 shows that BMDCs that received LPS 8h ahead of the capsule addition show maximal IL-1β secretion, though the secretion level for all four LPS addition time points are

relatively similar. Moreover, when considering the effect of VP addition VP, the levels of IL-1β for VP-PMLC (grey color) was higher than PMLC (white color) at all those time points. LPS alone does not elicit a significant induction of IL-1β, which is consistent with previous reports [131]; however, IL-1β is detectable with either co-incubation of PMLC or VP-PMLC alone.

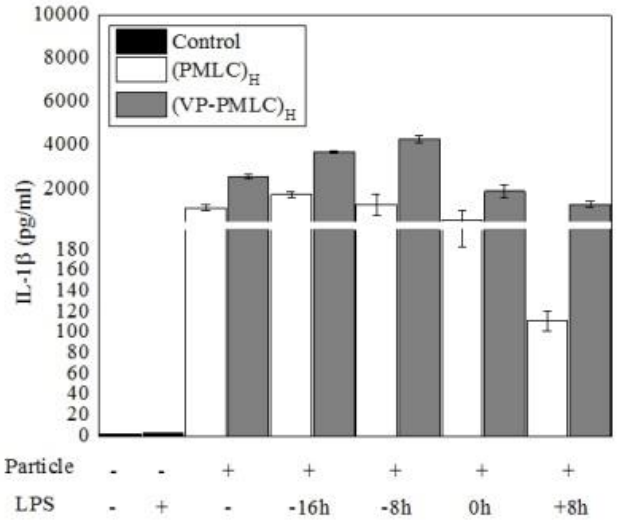

Figure 36. Particle-induced IL-1β secretion in BMDCs incubated with high MW P_LARG/DS polyelectrolyte PMLCs (white color) and VP-PMLCs (grey color), respectively. The ratio of particle to cell was 20:1, and LPS concentration was 10 ng/ml. Untreated cells were used as the negative control.

The same experimental design was used to co-incubate BMDCs with composite MW PMLC and VP-PMLC with composite MW (Figure 37) and low MW (Figure 38) capsules. Figure 37 shows the highest IL-1β secretion is observed when LPS added 8h prior to particle addition, and at all four time points higher levels of IL-1β were detected with VP-PMLC compare to PMLC. And again, LPS alone did not elicit a significant induction of IL-1β (Figure 37).

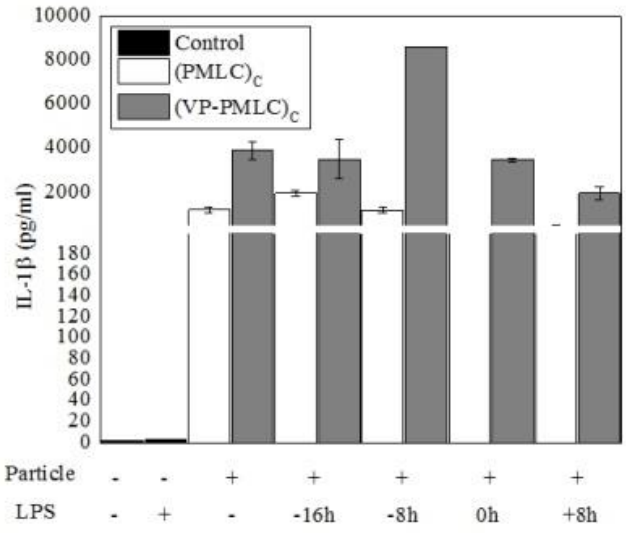

Figure 37. Particle-induced IL-1β secretion in BMDCs incubated with composite MW P_LARG/DS polyelectrolyte PMLCs (white color) and VP-PMLCs (grey color), respectively. The ratio of particle to cell was 20:1, and LPS concentration was 10 ng/ml. Untreated cells were used as the negative control.

Figure 38 shows enhancement of IL-1β secretion by low MW PMLC capsules was similar to the observations with high MW (Figure 36) and composite MW (Figure 37) particles. Comparing Figures 36 - 38, the composite MW particles were the most potent in inducing IL-1β, secretion, followed by high MW and low MW particles. Moreover, these studies also showed that P_LARG/DS microparticles alone could enhance IL-1β secretion, which is in contrast to other studies [131].

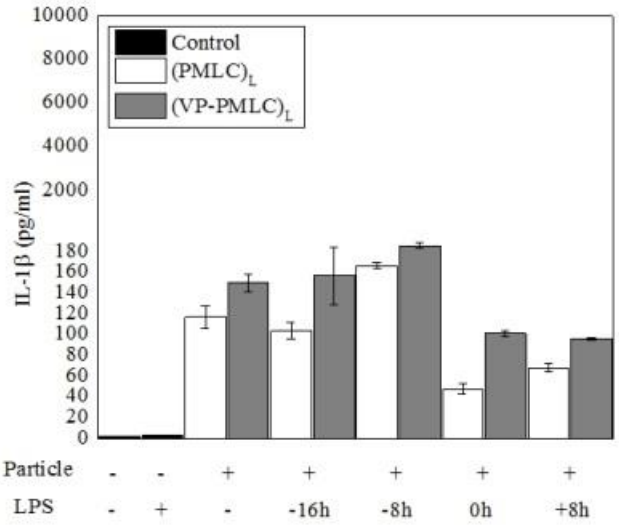

Figure 38. IL-1β secretion in BMDCs incubated with low MW P_LARG/DS polyelectrolyte PMLCs (white color) and VP-PMLCs (grey color), respectively. The ratio of particle to cell was 20:1. The LPS concentration was 10 ng/ml. Untreated cells were used as the negative control.

Figure 39 shows the effect of LPS alone or with soluble antigen (VP1) at different time points on IL-1β secretion. The data show that LPS alone cannot increase IL-1β secretion at any time point. Moreover, even with the addition of LPS, VP1 did not significantly increase IL-1β release. However, Figures 36-38 clearly show that VP-PMLC is capable of increasing IL-1β secretion compared to PMLC. Therefore, these findings suggest that the uptake routes of soluble and particulate antigens are different, and inflammasome activation leading to IL-1β release involves particle phagocytosis.

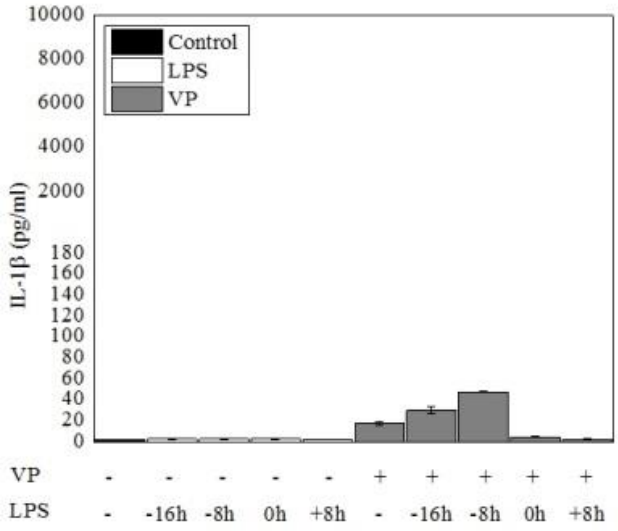

Figure 39. IL-1β secretion in BMDCs incubated either with LPS alone, soluble antigen (*SV40* VP1 viral protein) alone, or VP1 together with the addition of LPS at 16h and 8h ahead, at the same time or 8h later, respectively. The VP concentration was 0.1 mg/ml, and LPS concentration was 10 ng/ml. Untreated cells were used as negative control.

Activation of the NLRP3 inflammasome by microparticles is dependent on particle uptake, lysosomal acidification, and cathepsin B activity [131]. For microparticles with the size around 10μm, actin polymerization has been proposed to be involved in particle uptake [129]. Therefore, we studied the effect of the cathepsin B activity and actin polymerization using chemical inhibitors.

BMDCs were co-incubated either with $(PMLC)_C$ or $(VP\text{-}PMLC)_C$. LPS was added 8h before addition of the particles and incubated for additional 24h. Figure 40 (first and second group of bars) shows the increase in IL-1β secretion in BMDCs co-cultured with PMLCs and the effect of LPS priming, respectively. With the addition of a cathepsin B inhibitor, CA-074 Me (Figure 40, group 3), IL-1β cytokine was essentially abolished. However, addition of an actin polymerization inhibitor, Lat. A, (Figure 40, group 4) did not significantly decrease IL-1β

secretion, and was comparable to that observed with the particles and LPS altogether (Figure 40, group 2).

These results suggest that cathepsin B activity, but not actin polymerization, is required for activation of the NLRP3 inflammasome-signaling complex and IL-1β secretion in BMDCs co-cultured with PMLCs.

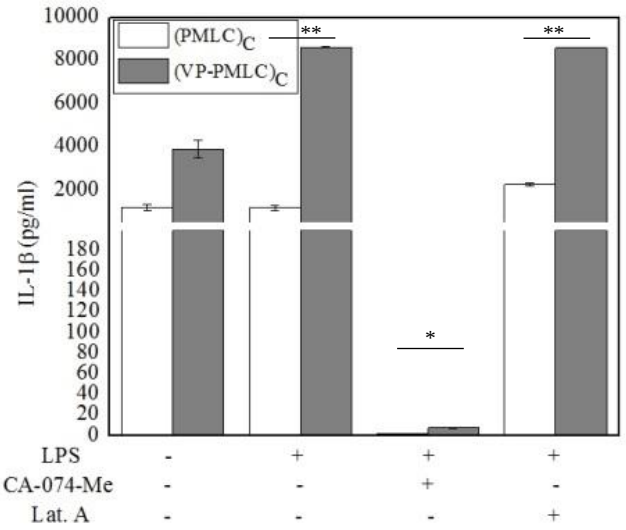

Figure 40. Effect of cathepsin B inhibitor CA-074 Me and actin polymerization inhibitor Lat. A on IL-1β secretion. BMDCs were co-treated with $(PMLC)_C$ and LPS at a particle to cell ratio of 20:1. The LPS concentration was 10 ng/ml, the CA-074 Me concentration was 50μM, and the Lat. A concentration was 250 nM. Untreated cells were used as the negative control. *$p < 0.05$, **$p < 0.01$.

5.4 Summary

In this chapter, we investigated the effect of particles on cytokine release profiles using BMDCs *in vitro*. Changes in the secretion of TNF-α, IL-12 and IL-1β were investigated after 24h incubation. Only a high concentration of *SV40* VP1 viral protein (0.1 mg/ml) induced an increase in TNF-α secretion; however, with the VP concentration at 0.05 mg/ml or lower, no TNF-α

secretion was observed. Mice BMDCs co-incubated for 24h with any of the PMLCs at a particle/cell ratio of 20:1, did not lead to an increase in TNF-α secretion. Neither viral protein, PMLCs nor VP-PMLCs co-incubated with mice BMDCs induced a significant increase in the secretion of IL-12. These results suggest that TNF-α and IL-12 signaling may not be activated upon uptake of viral protein capsules in BMDCs.

On the other hand, BMDCs co-incubated with either LPS and PMLC, LPS and VP-PMLC, or PMLC alone, but not LPS alone or viral protein alone, resulted in increased IL-1β secretion. The highest IL-1β secretion was observed with the addition of LPS 8h prior to the particles. Cathepsin B activation is required for IL-1β secretion with 3μm microparticles, while actin polymerization is not.

6. CONCLUSIONS AND FUTURE WORK

6.1 Conclusions

Recombinant *SV40* viral protein VP1 was successfully expressed suing a baculovirus expression vector system in *Sf9* insect cells and purified using affinity chromatography. VP1 has low toxicity in dendritic cells *in vitro* but also shows poor immunogenicity. A novel viral protein-based polymeric multilayer capsule serving as vaccine vehicle was developed. Biodegradable P_LARG/DS polyelectrolyte pairs and *SV40* VP1 viral protein were successfully assembled onto $CaCO_3$ sacrificial porous microparticles through LbL deposition. The size range of particles formed varied from 1 to 4 μm in diameter.

This study investigated two methods for particle formulation and the use of different molecular weights of P_LARG/DS polyelectrolyte pairs. The highest viral protein encapsulation efficiency obtained was 63% using high molecular weight polyelectrolyte pairs with VP1 deposited only in the 1st layer. However, based on the number of particles formed, the amount of viral protein was similar among all capsules. All VP-PMLCs demonstrated low toxicity *in vitro*. The porous structure of the capsule led to higher surface marker protein expression in dendritic cells *vitro*, with synergism between PLMCs and VP. We further show that the particles increased IL-1β secretion in dendritic cells and this required cathepsin B activity.

Overall, VP-PMLCs, compared to VP1 alone or PMLCs alone, show lower cytotoxicity but higher co-stimulatory activity *in vitro*. When encapsulated using LbL technique, additional layer of VP1 are not important for activity; however, the MW of polyelectrolytes does influence the cytotoxicity, release profile and surface marker expression in immune levels.

Our results demonstrate that *SV40* VP1-based polymeric multilayer capsules can elicit stronger immune response using viral protein. We further show that viral protein encapsulated with low MW polyelectrolytes is an attractive candidate for vaccine delivery. Further studies will focus on improving the protein encapsulation efficiency through different approaches of core synthesis and the *in vitro* signaling pathway.

6.2 Future Work

6.2.1 In vivo *studies using VP-PMLCs*

The work presented here demonstrates effectiveness of the VP-PMLCs *in vitro* using primary dendritic cells and cell lines. The next logical step is to test the effectiveness of VP-PMLCs in mouse models. Since a wide range of immunological tools and reagents for characterization of innate and adaptive immune responses are available, it would be interesting to determine the effect of VP-PLMCs on different immune cells *in vivo*.

6.2.2 Comprehensive investigation of cytokines and signaling pathways activated by VP-PMLCs

In Chapter 5, we identified that IL-1β, but not TNF-α and IL-12, were upregulated in dendritic cells *in vitro.* To understand the cytokines and signaling pathways activated by VP-PMLCs, comprehensive profiling of inflammatory cytokines and chemokines must be carried out. While our work showed the requirement for cathepsin B activity in the upregulation of IL-1β, the role of actin polymerization was not verified for 3 μm particles. This would be a logical next step in delineating the mechanisms underlying increased IL-1β expression with VP-PMLCs. Due to the high surface curvature on P_LARG/DS capsule, different mechanisms of phagocytosis such as lipid draft internalization could be possible. These additional mechanisms could be investigated. For example, CTxB can be used as a marker for lipid drafts [129].

6.2.3 Application to mucosal delivery

Vaccination through the parenteral route shows the fastest and highest bioactivity. However, inconvenience to patients and noncompliance, there is a need for other vaccine delivery routes, such as mucosal delivery. The most efficient way to elicit mucosal immunity is through the administration of vaccines onto the mucosal surfaces [203]. The mucosal membrane, which is vulnerable to infection, is a strong candidate for vaccine delivery not only due to its convenience, but also due to the large surface area at multiple locations (oral, nasal, rectal or vaginal). Nevertheless, there are difficulties associated with measuring the dose that actually enters the body and elucidating complicated mucosal immune responses, including T cell proliferation. The development of mucosal vaccines is still in its infancy as the low bioavailability of soluble antigens in circulation is low. The promising results from this work can be applied for mucosal vaccine delivery.

REFERENCES

1.Federico M (2010) Virus-Like Particles Show Promise as Candidates for New Vaccine Strategies. Future Virology 5:371-374. doi: 10.2217/fvl.10.29

2.Noad R and Roy P (2003) Virus-Like Particles as Immunogens. Trends in Microbiology 11:438-444. doi: 10.1016/s0966-842x(03)00208-7

3.Shakya AK and Nandakumar KS (2013) Applications of Polymeric Adjuvants in Studying Autoimmune Responses and Vaccination against Infectious Diseases. Journal of the Royal Society Interface 10. doi: 10.1098/rsif.2012.0536

4.Lewis JS, Zaveri TD, Crooks CP and Keselowsky BG (2012) Microparticle Surface Modifications Targeting Dendritic Cells for Non-Activating Applications. Biomaterials 33:7221-7232. doi: 10.1016/j.biomaterials.2012.06.049

5.Janeway CA and Medzhitov R (2002) Innate Immune Recognition. Annual Review of Immunology 20:197-216. doi: 10.1146/annurev.immunol.20.083001.084359

6.Beard ME (1984) Molecular-Biology of the Cell. Bioscience 34:449-449. doi: 10.2307/1309637

7.Buonaguro L, Tornesello ML and Buonaguro FM (2010) Virus-Like Particles as Particulate Vaccines. Current Hiv Research 8:299-309. doi: 10.2174/157016210791208659

8.Baxter D (2007) Active and Passive Immunity, Vaccine Types, Excipients and Licensing. Occupational Medicine-Oxford 57:552-556. doi: 10.1093/occmed/kqm110

9.Roy P and Noad R (2008) Virus-Like Particles as a Vaccine Delivery System - Myths and Facts. Human Vaccines 4:5-12. doi: 10.4161/hv.4.1.5559

10.Nathanson N and Langmuir AD (1995) The Cutter Incident - Poliomyelitis Following Formaldehyde-Inactivated Poliovirus Vaccination in the United-States During the Spring of 1955 .2. Relationship of Poliomyelitis to Cutter Vaccine. American Journal of Epidemiology 142:109-140. doi: 10.1093/oxfordjournals.aje.a117611

11.Furione M, Guillot S, Otelea D, Balanant J, Candrea A and Crainic R (1993) Polioviruses with Natural Recombinant Genomes Isolated from Vaccine-Associated Paralytic Poliomylitis. Virology 196:199-208.

12.Georgescu MM, Balanant J, Macadam A, Otelea D, Combiescu M, Combiescu AA, Crainic R and Delpeyroux F (1997) Evolution of the Sabin Type 1 Poliovirus in Humans: Characterization of Strains Isolated from Patients with Vaccine-Associated Paralytic Poliomyelitis. Journal of Virology 71:7758-7768.

13.Moyle PM and Toth I (2013) Modern Subunit Vaccines: Development, Components, and Research Opportunities. Chemmedchem 8:360-376. doi: 10.1002/cmdc.201200487

14.Nascimento IP and Leite LCC (2012) Recombinant Vaccines and the Development of New Vaccine Strategies. Brazilian Journal of Medical and Biological Research 45:1102-1111. doi: 10.1590/s0100-879x2012007500142

15.Grgacic EVL and Anderson DA (2006) Virus-Like Particles: Passport to Immune Recognition. Methods 40:60-65. doi: 10.1016/j.ymeth.2006.07.018

16.Schijns V (2003) Mechanisms of Vaccine Adjuvant Activity: Initiation and Regulation of Immune Responses by Vaccine Adjuvants. Vaccine 21:829-831. doi: 10.1016/s0264-410x(02)00527-3

17.Gallucci S, Lolkema M and Matzinger P (1999) Natural Adjuvants: Endogenous Activators of Dendritic Cells. Nature Medicine 5:1249-1255. doi: 10.1038/15200

18.Savelkoul HFJ, Ferro VA, Strioga MM and Schijns V (2015) Choice and Design of Adjuvants for Parenteral and Mucosal Vaccines. Vaccines 3:148-171. doi: 10.3390/vaccines3010148

19.Coffman RL, Sher A and Seder RA (2010) Vaccine Adjuvants: Putting Innate Immunity to Work. Immunity 33:492-503. doi: 10.1016/j.immuni.2010.10.002

20.Gupta RK, Chang AC and Siber GR (1998) Biodegradable Polymer Microspheres as Vaccine Adjuvants and Delivery Systems. In: Brown F and Haaheim LR (eds) Modulation of the Immune Response to Vaccine Antigens, Karger, Basel pp. 63-78

21.Mohan T, Verma P and Rao DN (2013) Novel Adjuvants & Delivery Vehicles for Vaccines Development: A Road Ahead. Indian Journal of Medical Research 138:779-795.

22.Lollo G, Gonzalez-Paredes A, Garcia-Fuentes M, Calvo P, Torres D and Alonso MJ (2017) Polyarginine Nanocapsules as a Potential Oral Peptide Delivery Carrier. Journal of Pharmaceutical Sciences 106:611-618. doi: 10.1016/j.xphs.2016.09.029

23.Cook MT, Tzortzis G, Khutoryanskiy VV and Charalampopoulos D (2013) Layer-by-Layer Coating of Alginate Matrices with Chitosan-Alginate for the Improved Survival and Targeted Delivery of Probiotic Bacteria after Oral Administration. Journal of Materials Chemistry B 1:52-60. doi: 10.1039/c2tb00126h

24.Lindblad EB (2004) Aluminium Compounds for Use in Vaccines. Immunology and Cell Biology 82:497-505. doi: 10.1111/j.1440-1711.2004.01286.x

25.O'Hagan DT (2007) MF59 is a Safe and Potent Vaccine Adjuvant that Enhances Protection against Influenza Virus Infection. Expert Review of Vaccines 6:699-710. doi: 10.1586/14760584.6.5.699

26.Billiau A and Matthys P (2001) Modes of Action of Freund's Adjuvants in Experimental Models of Autoimmune Diseases. Journal of Leukocyte Biology 70:849-860.

27.Spangler BD (1992) Structure and Function of Cholera-Toxin and the Related Escherichia-Coli Heat-Labile Enterotoxin. Microbiological Reviews 56:622-647.

28.Woodrow KA, Bennett KM and Lo DD (2012) Mucosal Vaccine Design and Delivery. In: Yarmush ML (ed) Annual Review of Biomedical Engineering, Vol 14, Annual Reviews, Palo Alto pp. 17-46

29.Dziarski R (2003) Recognition of Bacterial Peptidoglycan by the Innate Immune System. Cellular and Molecular Life Sciences 60:1793-1804. doi: 10.1007/s00018-003-3019-6

30.Rainone V, Dubois G, Temchura V, Uberla K, Nebuloni M, Lauri E, Trabattoni D, Veas F and Clerici M (2012) CCL28 Induces Mucosal Homing of HIV-1-Specific IgA-Secreting Plasma Cells in Mice Immunized with HIV-1 Virus-Like Particles. Retrovirology 9. doi: 10.1186/1742-4690-9-s2-p19

31.Song S, Wang Y, Zhang Y, Wang F, He Y, Ren D, Guo Y and Sun S (2007) Augmented Induction of CD8(+) Cytotoxic T-Cell Response and Antitumor Effect by DCs Pulsed with Virus-Like Particles Packaging with CpG. Cancer Letters 256:90-100. doi: 10.1016/j.canlet.2007.06.004

32.Fischer NO, Rasley A, Corzett M, Hwang MH, Hoeprich PD and Blanchette CD (2013) Colocalized Delivery of Adjuvant and Antigen Using Nanolipoprotein Particles Enhances the Immune Response to Recombinant Antigens. Journal of the American Chemical Society 135:2044-2047. doi: 10.1021/ja3063293

33.Storni T, Lechner F, Erdmann I, Bachi T, Jegerlehner A, Dumrese T, Kundig TM, Ruedl C and Bachmann MF (2002) Critical Role for Activation of Antigen-Presenting Cells in Priming of

Cytotoxic T Cell Responses after Vaccination with Virus-Like Particles. Journal of Immunology 168:2880-2886.

34.Yan GP, Zong RF, Li LA, Fu T, Liu F and Yu XH (2010) Anticancer Drug-Loaded Nanospheres Based on Biodegradable Amphiphilic Epsilon-Caprolactone and Carbonate Copolymers. Pharmaceutical Research 27:2743-2752. doi: 10.1007/s11095-010-0275-7

35.Gallovic MD, Montjoy DG, Collier MA, Do C, Wyslouzil BE, Bachelder EM and Ainslie KM (2016) Chemically Modified Inulin Microparticles Serving Dual Function as a Protein Antigen Delivery Vehicle and Immunostimulatory Adjuvant. Biomaterials Science 4:483-493. doi: 10.1039/c5bm00451a

36.Gordon S, Saupe A, McBurney W, Rades T and Hook S (2008) Comparison of Chitosan Nanoparticles and Chitosan Hydrogels for Vaccine Delivery. Journal of Pharmacy and Pharmacology 60:1591-1600. doi: 10.1211/jpp/60.12.0004

37.Hsu LW, Lee PL, Chen CT, Mi FL, Juang JH, Hwang SM, Ho YC and Sung HW (2012) Elucidating the Signaling Mechanism of an Epithelial Tight-Junction Opening Induced by Chitosan. Biomaterials 33:6254-6263. doi: 10.1016/j.biomaterials.2012.05.013

38.De Geest BG, Willart MA, Hammad H, Lambrecht BN, Pollard C, Bogaert P, De Filette M, Saelens X, Vervaet C, Remon JP, Grooten J and De Koker S (2012) Polymeric Multilayer Capsule-Mediated Vaccination Induces Protective Immunity Against Cancer and Viral Infection. Acs Nano 6:2136-2149. doi: 10.1021/nn205099c

39.Bertram U, Bernard M-C, Haensler J, Maincent P and Bodmeier R (2010) In Situ Glling Nasal Inserts for Influenza Vaccine Delivery. Drug Development and Industrial Pharmacy 36:581-593. doi: 10.3109/03639040903382673

40.Yamaki T, Kamiya Y, Ohtake K, Uchida M, Seki T, Ueda H, Kobayashi J, Morimoto Y and Natsume H (2014) A Mechanism Enhancing Macromolecule Transport Through Paracellular Spaces Induced by Poly-L-Arginine: Poly-L-Arginine Induces the Internalization of Tight Junction Proteins via Clathrin-Mediated Endocytosis. Pharmaceutical Research 31:2287-2296. doi: 10.1007/s11095-014-1324-4

41.De Koker S, De Geest BG, Singh SK, De Rycke R, Naessens T, Van Kooyk Y, Demeester J, De Smedt SC and Grooten J (2009) Polyelectrolyte Microcapsules as Antigen Delivery Vehicles To Dendritic Cells: Uptake, Processing, and Cross-Presentation of Encapsulated Antigens. Angewandte Chemie-International Edition 48:8485-8489. doi: 10.1002/anie.200903769

42.Chroboczek J, Szurgot I and Szolajska E (2014) Virus-Like Particles as Vaccine. Acta Biochimica Polonica 61:531-539.

43.Buonaguro L, Tagliamonte M, Tornesello ML and Buonaguro FM (2011) Developments in Virus-Like Particle-Based Vaccines for Infectious Diseases and Cancer. Expert Review of Vaccines 10:1569-1583. doi: 10.1586/erv.11.135

44.Jennings GT and Bachmann MF (2008) Coming of Age of Virus-Like Particle Vaccines. Biological Chemistry 389:521-536. doi: 10.1515/bc.2008.064

45.Michel ML and Tiollais P (2010) Hepatitis B Vaccines: Protective Efficacy and Therapeutic Potential. Pathologie Biologie 58:288-295. doi: 10.1016/j.patbio.2010.01.006

46.Leenders WPJ and Debruin WCC (1994) Cloning and Production of Functional Active Recombinant Hepatitis-B Virus Surface-Antigen Binding-Protein. Biochemical and Biophysical Research Communications 205:52-59. doi: 10.1006/bbrc.1994.2628

47.Alvarez AMR, Perez-Vilar S, Pacis-Tirso C, Contreras M, El Omeiri N, Ruiz-Matus C and Velandia-Gonzalez M (2017) Progress in Vaccination towards Hepatitis B Control and

Elimination in the Region of the Americas. Bmc Public Health 17:10. doi: 10.1186/s12889-017-4227-6

48.Sandalon Z, DalyotHerman N, Oppenheim AB and Oppenheim A (1997) In Vitro Assembly of SV40 Virions and Pseudovirions: Vector Development for Gene Therapy. Human Gene Therapy 8:843-849. doi: 10.1089/hum.1997.8.7-843

49.Sweet BH and Hilleman MR (1960) The Vacuolating Virus, SV40. Proceedings of the Society for Experimental Biology and Medicine 105:420-427.

50.Hull RN and Minner JR (1957) New Viral Agents Rrcovered from Tissue Cultures of Monkey Kidney Cells .2. Problems of Isolation and Identification. Annals of the New York Academy of Sciences 67:413-423. doi: 10.1111/j.1749-6632.1957.tb46064.x

51.Abramczuk J, Pan S, Maul G and Knowles BB (1984) Tumor-Induction by Simian Virus-40 in Mice is Controlled by Long-Term Persistence on the Viral Genome and the Immune-Response of the Host. Journal of Virology 49:540-548.

52.Strickler HD, Goedert JJ, Butel JS, Daniel R, Freymuth F, Gibbs A, Griffiths DJ, Jablons D, Jasani B, Jones C, Lednicky JA, Miller CW, Radu C, Richards WG, Shah KV, You L, Corson JM, Gerwin B, Harris C, Sugarbaker DJ, Egan W, Lewis AM, Krause PR, Peden K, Levine AS, Melnick S, Cosentino M, da Costa M, Devairrakam V, Ji J, Palefsky J, Rasmussen L, Shea K, Wacholder S, Waters D, Wright T and Int SVWG (2001) A Multicenter Evaluation of Assays for Detection of SV40 DNA and Results in Masked Mesothelioma Specimens. Cancer Epidemiology Biomarkers & Prevention 10:523-532.

53.Corallini A, Mazzoni E, Taronna A, Manfrini M, Carandina G, Guerra G, Guaschino R, Vaniglia F, Magnani C, Casali F, Dolcetti R, Palmonari C, Rezza G, Martini F, Barbanti-Brodano G and Tognon MG (2012) Specific Antibodies Reacting with Simian Virus 40 Capsid

Protein Mimotopes in Serum Samples from Healthy Blood Donors. Human Immunology 73:502-510. doi: 10.1016/j.humimm.2012.02.009

54.Barbanti-Brodano G, Sabbioni S, Martini F, Negrini M, Corallini A and Tognon M (2004) Simian Virus 40 Infection in Humans and Association with Human Diseases: Results and Hypotheses. Virology 318:1-9. doi: 10.1016/j.virol.2003.09.004

55.Kawano M, Matsui M and Handa H (2013) SV40 Virus-Like Particles as an Effective Delivery System and Its Application to a Vaccine Carrier. Expert Review of Vaccines 12:199-210. doi: 10.1586/erv.12.149

56.Tsai B and Qian MD (2010) Cellular Entry of Polyomaviruses. In: Johnson JE (ed) Cell Entry by Non-Enveloped Viruses, pp. 177-194

57.Stehle T, Gamblin SJ, Yan YW and Harrison SC (1996) The Structure of Simian Virus 40 Refined at 3.1 Angstrom Resolution. Structure 4:165-182. doi: 10.1016/s0969-2126(96)00020-2

58.O'Farrell PZ and Goodman HM (1976) Resolution of Simian Virus 40 Proteins in Whole Cell Extracts by Two-Dimensional Electrophoresis: Heterogeneity of the Major Capsid Protein. Cell 9:289-98.

59.Rayment I, Baker TS, Caspar DLD and Murakami WT (1982) The Structure of Polyoma-Virus Capsids at 22.5-A Resolution. Biophysical Journal 37:A8-A8.

60.Oppenheim A, Ben-Nun-Shaul O, Mukherjee S and Abd-El-Latif M (2008) SV40 Assembly In Vivo and In Vitro. Computational and Mathematical Methods in Medicine 9:265-276. doi: 10.1080/17486700802168312

61.Toscano MG and de Haan P (2018) How Simian Virus 40 Hijacks the Intracellular Protein Trafficking Pathway to Its Own Benefit ... and Ours. Frontiers in Immunology 9:9. doi: 10.3389/fimmu.2018.01160

62.Pelkmans L and Helenius A (2003) Insider Information: What Viruses tell Us about Endocytosis. Current Opinion in Cell Biology 15:414-422. doi: 10.1016/s0955-0674(03)00081-4

63.Stehle T, Yan YW, Benjamin TL and Harrison SC (1994) Structure of Murine Polyomavirus Complexed with an Oligosaccharide Receptor Fragment. Nature 369:160-163. doi: 10.1038/369160a0

64.Haynes JI, Chang DC and Consigli RA (1993) Mutations in the Putative Calcium-Binding Domain of Polyomavirus VP1 Affect Capsid Assembly. Journal of Virology 67:2486-2495.

65.Mukherjee S, Abd-El-Latif M, Bronstein M, Ben-nun-Shaul O, Kler S and Oppenheim A (2007) High Cooperativity of the SV40 Major Capsid Protein VP1 in Virus Assembly. Plos One 2:9. doi: 10.1371/journal.pone.0000765

66.Zhang WJ, Zhang XE and Li F (2018) Virus-Based Nanoparticles of Simian Virus 40 in the Field of Nanobiotechnology. Biotechnology Journal 13:7. doi: 10.1002/biot.201700619

67.Kanesashi SN, Ishizu K, Kawano M, Han S, Tomita S, Watanabe H, Kataoka K and Handa K (2003) Simian Virus 40 VP1 Capsid Protein Forms Polymorphic Assemblies In Vitro. Journal of General Virology 84:1899-1905. doi: 10.1099/vir.0.19067-0

68.Brady JN, Winston VD and Consigli RA (1977) Dissociation of Polyoma-Virus by Chelation of Calcium-ions Found Associated with Purified Virions. Journal of Virology 23:717-724.

69.Singh M and O'Hagan D (1999) Advances in Vaccine Adjuvants. Nature Biotechnology 17:1075-1081. doi: 10.1038/15058

70.Ishizu KI, Watanabe H, Han SI, Kanesashi SN, Hoque M, Yajima H, Kataoka K and Handa H (2001) Roles of Disulfide Linkage and Calcium Ion-Mediated Interactions in Assembly and Disassembly of Virus-Like Particles Composed of Simian Virus 40 VP1 Capsid Protein. Journal of Virology 75:61-72. doi: 10.1128/jvi.75.1.61-72.2001

71.Da Silva DM, Pastrana DV, Schiller JT and Kast WM (2001) Effect of Preexisting Neutralizing Antibodies on the Anti-Tumor Immune Response Induced by Chimeric Human Papillomavirus Virus-Like Particle Vaccines. Virology 290:350-360. doi: 10.1006/viro.2001.1179

72.Peacey M, Wilson S, Baird MA and Ward VK (2007) Versatile RHDV Virus-Like Particles: Incorporation of Antigens by Genetic Modification and Chemical Conjugation. Biotechnology and Bioengineering 98:968-977. doi: 10.1002/bit.21518

73.Leavitt AD, Roberts TM and Garcea RL (1985) Polyoma-Virus Major Capsid Protein, VP1 - Purification after High-Level Expression in Escherichia-Coli. Journal of Biological Chemistry 260:2803-2809.

74.Burton KS and Consigli RA (1996) Methylation of the Polyomavirus Major Capsid Protein VP1. Virus Research 40:141-147. doi: 10.1016/0168-1702(95)01266-4

75.Forstova J, Krauzewicz N, Wallace S, Street AJ, Dilworth SM, Beard S and Griffin BE (1993) Cooperation of Structural Proteins During Late Events in the Life-Cycle of Polyomavirus. Journal of Virology 67:1405-1413.

76.Druzinec D, Salzig D, Brix A, Kraume M, Vilcinskas A, Kollewe C and Czermak P (2013) Optimization of Insect Cell Based Protein Production Processes - Online Monitoring, Expression Systems, Scale Up. In: Vilcinskas A (ed) Yellow Biotechnology Ii: Insect Biotechnology in Plant Protection and Industry, Springer-Verlag Berlin, Berlin pp. 65-100

77.An K, Gillock ET, Sweat JA, Reeves WM and Consigli RA (1999) Use of the Baculovirus System to Assemble Polyomavirus Capsid-Like Particles with Different Polyomavirus Structural Proteins: Analysis of the Recombinant Assembled Capsid-Like Particles. Journal of General Virology 80:1009-1016.

78.Kitai Y, Fukuda H, Enomoto T, Asakawa Y, Suzuki T, Inouye S and Handa H (2011) Cell Selective Targeting of a Simian Virus 40 Virus-Like Particle Conjugated to Epidermal Growth Factor. Journal of Biotechnology 155:251-256. doi: 10.1016/j.jbiotec.2011.06.030

79.Enomoto T, Kawano M, Fukuda H, Sawada W, Inoue T, Haw KC, Kita Y, Sakamoto S, Yamaguchi Y, Imai T, Hatakeyama M, Saito S, Sandhu A, Matsui M, Aoki I and Handa H (2013) Viral Protein-Coating of Magnetic Nanoparticles Using Simian Virus 40 VP1. Journal of Biotechnology 167:8-15. doi: 10.1016/j.jbiotec.2013.06.005

80.Win SJ, McMillan DGG, Errington-Mais F, Ward VK, Young SL, Baird MA and Melcher AA (2012) Enhancing the Immunogenicity of Tumour Lysate-Loaded Dendritic Cell Vaccines by Conjugation to Virus-Like Particles. British Journal of Cancer 106:92-98. doi: 10.1038/bjc.2011.538

81.Yang ZS, Xu MM, Jia ZH, Zhang YT, Wang L, Zhang HR, Wang JY, Song M, Zhao YP, Wu ZZ, Zhao LQ, Yin ZN and Hong ZY (2017) A Novel Antigen Delivery System Induces Strong Humoral and CTL Immune Responses. Biomaterials 134:51-63. doi: 10.1016/j.biomaterials.2017.04.035

82.Shah A, Gani A, Ahmad M, Ashwar BA and Masoodi FA (2016) Beta-Glucan as an Encapsulating Agent: Effect on Probiotic Survival in Simulated Gastrointestinal Tract. International Journal of Biological Macromolecules 82:217-222. doi: 10.1016/j.ijbiomac.2015.11.017

83.Dierendonck M, Fierens K, De Rycke R, Lybaert L, Maji S, Zhang ZY, Zhang QL, Hoogenboom R, Lambrecht BN, Grooten J, Remon JP, De Koker S and De Geest BG (2014) Nanoporous Hydrogen Bonded Polymeric Microparticles: Facile and Economic Production of

Cross Presentation Promoting Vaccine Carriers. Advanced Functional Materials 24:4634-4644. doi: 10.1002/adfm.201400763

84.De Koker S, De Cock LJ, Rivera-Gil P, Parak WJ, Velty RA, Vervaet C, Remon JP, Grooten J and De Geest BG (2011) Polymeric Multilayer Capsules Delivering Biotherapeutics. Advanced Drug Delivery Reviews 63:748-761. doi: 10.1016/j.addr.2011.03.014

85.Decher G (1997) Fuzzy Nanoassemblies: Toward Layered Polymeric Multicomposites. Science 277:1232-1237. doi: 10.1126/science.277.5330.1232

86.Zhou J, Pishko MV and Lutkenhaus JL (2014) Thermoresponsive Layer-by-Layer Assemblies for Nanoparticle-Based Drug Delivery. Langmuir 30:5903-5910. doi: 10.1021/la501047m

87.Yu X and Pishko MV (2011) Nanoparticle-Based Biocompatible and Targeted Drug Delivery: Characterization and in Vitro Studies. Biomacromolecules 12:3205-3212. doi: 10.1021/bm200681m

88.Sexton A, Whitney PG, Chong SF, Zelikin AN, Johnston APR, De Rose R, Brooks AG, Caruso F and Kent SJ (2009) A Protective Vaccine Delivery System for In Vivo T Cell Stimulation Using Nanoengineered Polymer Hydrogel Capsules. Acs Nano 3:3391-3400. doi: 10.1021/nn900715g

89.Su XF, Kim BS, Kim SR, Hammond PT and Irvine DJ (2009) Layer-by-Layer-Assembled Multilayer Films for Transcutaneous Drug and Vaccine Delivery. Acs Nano 3:3719-3729. doi: 10.1021/nn900928u

90.Torchilin VP (2001) Structure and Design of Polymeric Surfactant-Based Drug Delivery Systems. Journal of Controlled Release 73:137-172. doi: 10.1016/s0168-3659(01)00299-1

91.Zhang Z, Gao XY, Zhang AP, Wu XW, Chen L, He CL, Zhuang XL and Chen XS (2012) Biodegradable pH-Dependent Thermo-Sensitive Hydrogels for Oral Insulin Delivery. Macromolecular Chemistry and Physics 213:713-719. doi: 10.1002/macp.201100604

92.Richardson TP, Peters MC, Ennett AB and Mooney DJ (2001) Polymeric System for Dual Growth Factor Delivery. Nature Biotechnology 19:1029-1034. doi: 10.1038/nbt1101-1029

93.Yang YH, Bolling L, Priolo MA and Grunlan JC (2013) Super Gas Barrier and Selectivity of Graphene Oxide-Polymer Multilayer Thin Films. Advanced Materials 25:503-508. doi: 10.1002/adma.201202951

94.De Koker S, Naessens T, De Geest BG, Bogaert P, Demeester J, De Smedt S and Grooten J (2010) Biodegradable Polyelectrolyte Microcapsules: Antigen Delivery Tools with Th17 Skewing Activity after Pulmonary Delivery. Journal of Immunology 184:203-211. doi: 10.4049/jimmunol.0803591

95.Clark SL and Hammond PT (2000) The Role of Secondary Interactions in Selective Electrostatic Multilayer Deposition. Langmuir 16:10206-10214. doi: 10.1021/la000418a

96.Kreft O, Prevot M, Mohwald H and Sukhorukov GB (2007) Shell-in-Shell Microcapsules: A Novel Tool for Integrated, Spatially Confined Enzymatic Reactions. Angewandte Chemie-International Edition 46:5605-5608. doi: 10.1002/anie.200701173

97.Kim BS, Oh JM, Kim KS, Seo KS, Cho JS, Khang G, Lee HB, Park K and Kim MS (2009) BSA-FITC-Loaded Microcapsules for In Vivo Delivery. Biomaterials 30:902-909. doi: 10.1016/j.biomaterials.2008.10.030

98.Volodkin DV, Petrov AI, Prevot M and Sukhorukov GB (2004) Matrix Polyelectrolyte Microcapsules: New System for Macromolecule Encapsulation. Langmuir 20:3398-3406. doi: 10.1021/la036177z

99. Petrov AI, Volodkin DV and Sukhorukov GB (2005) Protein-Calcium Carbonate Coprecipitation: A Tool for Protein Encapsulation. Biotechnology Progress 21:918-925. doi: 10.1021/bp0495825

100. Flemke J, Maywald M and Sieber V (2013) Encapsulation of Living E. coli Cells in Hollow Polymer Microspheres of Highly Defined Size. Biomacromolecules 14:207-214. doi: 10.1021/bm3016362

101. Yu HD, Wang DS and Han MY (2007) Top-Down Solid-Phase Fabrication of Nanoporous Cadmium Oxide Architectures. Journal of the American Chemical Society 129:2333-2337. doi: 10.1021/ja066884p

102. Antipov AA, Shchukin D, Fedutik Y, Petrov AI, Sukhorukov GB and Mohwald H (2003) Carbonate Microparticles for Hollow Polyelectrolyte Capsules Fabrication. Colloids and Surfaces a-Physicochemical and Engineering Aspects 224:175-183. doi: 10.1016/s0927-7757(03)00195-x

103. Volodkin DV, Schmidt S, Fernandes P, Larionova NI, Sukhorukov GB, Duschl C, Mohwald H and von Klitzing R (2012) One-Step Formulation of Protein Microparticles with Tailored Properties: Hard Templating at Soft Conditions. Advanced Functional Materials 22:1914-1922. doi: 10.1002/adfm.201103007

104. Mahapatro A and Singh DK (2011) Biodegradable Nanoparticles are Excellent Vehicle for Site Directed In-Vivo Delivery of Drugs and Vaccines. Journal of Nanobiotechnology 9:11. doi: 10.1186/1477-3155-9-55

105. De Geest BG, Vandenbroucke RE, Guenther AM, Sukhorukov GB, Hennink WE, Sanders NN, Demeester J and De Smedt SC (2006) Intracellularly Degradable Polyelectrolyte Microcapsules. Advanced Materials 18:1005-+. doi: 10.1002/adma.200502128

106. Gao H, Goriacheva OA, Tarakina NV and Sukhorukov GB (2016) Intracellularly Biodegradable Polyelectrolyte/Silica Composite Microcapsules as Carriers for Small Molecules. Acs Applied Materials & Interfaces 8:9651-9661. doi: 10.1021/acsami.6b01921

107. De Koker S, De Geest BG, Cuvelier C, Ferdinande L, Deckers W, Hennink WE, De Smedt S and Mertens N (2007) In Vivo Cellular Uptake, Degradation, and Biocompatibility of Polyelectrolyte Microcapsules. Advanced Functional Materials 17:3754-3763. doi: 10.1002/adfm.200700416

108. Dragojevic S, Ryu JS and Raucher D (2015) Polymer-Based Prodrugs: Improving Tumor Targeting and the Solubility of Small Molecule Drugs in Cancer Therapy. Molecules 20:21750-21769. doi: 10.3390/molecules201219804

109. Mattner F, Fleitmann JK, Lingnau K, Schmidt W, Egyed A, Fritz J, Zauner W, Wittmann B, Gorny I, Berger M, Kirlappos H, Otava A, Birnstiel ML and Buschle M (2002) Vaccination with Poly-L-Arginine as Immunostimulant for Peptide Vaccines: Induction of Potent and Long-Lasting T-Cell Responses against Cancer Antigens. Cancer Research 62:1477-1480.

110. Reddy ST, Swartz MA and Hubbell JA (2006) Targeting Dendritic Cells with Biomaterials: Developing the Next Generation of Vaccines. Trends in Immunology 27:573-579. doi: 10.1016/j.it.2006.10.005

111. Ai H, Jones SA and Lvov YM (2003) Biomedical Applications of Electrostatic Layer-by-Layer Nano-Assembly of Polymers, Enzymes, and Nanoparticles. Cell Biochemistry and Biophysics 39:23-43. doi: 10.1385/cbb:39:1:23

112. Chua BY, Al Kobaisi M, Zeng WG, Mainwaring D and Jackson DC (2012) Chitosan Microparticles and Nanoparticles as Biocompatible Delivery Vehicles for Peptide and Protein-

Based Immunocontraceptive Vaccines. Molecular Pharmaceutics 9:81-90. doi: 10.1021/mp200264m

113. Moser BA, Steinhardt RC and Esser-Kahn AP (2017) Surface Coating of Nanoparticles Reduces Background Inflammatory Activity while Increasing Particle Uptake and Delivery. Acs Biomaterials Science & Engineering 3:206-213. doi: 10.1021/acsbiomaterials.6b00473

114. Champion JA, Walker A and Mitragotri S (2008) Role of Particle Size in Phagocytosis of Polymeric Microspheres. Pharmaceutical Research 25:1815-1821. doi: 10.1007/s11095-008-9562-y

115. Rowley DA and Fitch FW (2012) The Road to the Discovery of Dendritic Cells, a Tribute to Ralph Steinman. Cellular Immunology 273:95-98. doi: 10.1016/j.cellimm.2012.01.002

116. Banchereau J and Steinman RM (1998) Dendritic Cells and the Control of Immunity. Nature 392:245-252. doi: 10.1038/32588

117. Hu W and Pasare C (2013) Location, Location, Location: Tissue-Specific Regulation of Immune Responses. Journal of Leukocyte Biology 94:409-421. doi: 10.1189/jlb.0413207

118. Kambayashi T and Laufer TM (2014) Atypical MHC Class II-Expressing Antigen-Presenting Cells: Can Anything Replace a Dendritic Cell? Nature Reviews Immunology 14:719-730. doi: 10.1038/nri3754

119. Labrousse AM, Meunier E, Record J, Labernadie A, Beduer A, Vieu C, Ben Safta T and Maridonneau-Parini I (2011) Frustrated Phagocytosis on Micro-Patterned Immune Complexes to Characterize Lysosome Movements in Live Macrophages. Frontiers in Immunology 2:10. doi: 10.3389/fimmu.2011.00051

120. Sprent J (1995) Antigen-Presrnting Cells - Professionals and Amateurs. Current Biology 5:1095-1097. doi: 10.1016/s0960-9822(95)00219-3

121. Mosser DM and Edwards JP (2010) Exploring the Full Spectrum of Macrophage Activation. Nature Reviews Immunology 10:460-460. doi: 10.1038/nri2788

122. Regnault A, Lankar D, Lacabanne V, Rodriguez A, Thery C, Rescigno M, Saito T, Verbeek S, Bonnerot C, Ricciardi-Castagnoli P and Amigorena S (1999) Fc Gamma Receptor-Mediated Induction of Dendritic Cell Maturation and Major Histocompatibility Complex Class I-Restricted Antigen Presentation after Immune Complex Internalization. Journal of Experimental Medicine 189:371-380. doi: 10.1084/jem.189.2.371

123. Trombetta ES and Mellman I (2005) Cell Biology of Antigen Processing In Vitro and In Vivo. Annual Review of Immunology, Annual Reviews, Palo Alto pp. 975-1028

124. Zhang ZP, Tongchusak S, Mizukami Y, Kang YJ, Ioji T, Touma M, Reinhold B, Keskin DB, Reinherz EL and Sasada T (2011) Induction of Anti-Tumor Cytotoxic T cell Responses through PLGA-Nanoparticle Mediated Antigen Delivery. Biomaterials 32:3666-3678. doi: 10.1016/j.biomaterials.2011.01.067

125. Wang QC, Feng ZH, Zhou YX and Nie QH (2005) Induction of Hepatitis C Virus-Specific Cytotoxic T and B Cell Responses by Dendritic Cells Expressing a Modified Antigen Targeting Receptor. World Journal of Gastroenterology 11:557-560.

126. Sun BB, Ji ZX, Liao YP, Chang CH, Wang X, Ku J, Xue CY, Mirshafiee V and Xia T (2017) Enhanced Immune Adjuvant Activity of Aluminum Oxyhydroxide Nanorods through Cationic Surface Functionalization. Acs Applied Materials & Interfaces 9:21697-21705. doi: 10.1021/acsami.7b05817

127. Meder F, Daberkow T, Treccani L, Wilhelm M, Schowalter M, Rosenauer A, Madler L and Rezwan K (2012) Protein Adsorption on Colloidal Alumina Particles Functionalized with

Amino, Carboxyl, Sulfonate and Phosphate Groups. Acta Biomaterialia 8:1221-1229. doi: 10.1016/j.actbio.2011.09.014

128. Valkonen M and Kantele J (1972) Role of Target Geometry in 14 MEV Neutron-Capture Cross-Section Measurements. Nuclear Instruments & Methods 103:549-&. doi: 10.1016/0029-554x(72)90014-6

129. Vaine CA, Patel MK, Zhu JT, Lee E, Finberg RW, Hayward RC and Kurt-Jones EA (2013) Tuning Innate Immune Activation by Surface Texturing of Polymer Microparticles: The Role of Shape in Inflammasome Activation. Journal of Immunology 190:3525-3532. doi: 10.4049/jimmunol.1200492

130. Lewis JS, Roche C, Zhang Y, Brusko TM, Wasserfall CH, Atkinson M, Clare-Salzler MJ and Keselowsky BG (2014) Combinatorial Delivery of Immunosuppressive Factors to Dendritic Cells Using Dual-Sized Microspheres. Journal of Materials Chemistry B 2:2562-2574. doi: 10.1039/c3tb21460e

131. Sharp FA, Ruane D, Claass B, Creagh E, Harris J, Malyala P, Singh M, O'Hagan DT, Petrilli V, Tschopp J, O'Neill LAJ and Lavelle EC (2009) Uptake of Particulate Vaccine Adjuvants by Dendritic Cells Activates the NALP3 Inflammasome. Proceedings of the National Academy of Sciences of the United States of America 106:870-875. doi: 10.1073/pnas.0804897106

132. Wesa AK and Galy A (2001) IL-1 Beta Induces Dendritic Cells to Produce IL-12. International Immunology 13:1053-1061. doi: 10.1093/intimm/13.8.1053

133. Storni T, Kundig TM, Senti G and Johansen P (2005) Immunity in Response to Particulate Antigen-Delivery Systems. Advanced Drug Delivery Reviews 57:333-355. doi: 10.1016/j.addr.2004.09.008

134. Dinarello CA (2018) Overview of the IL-1 Family in Innate Inflammation and Acquired Immunity. Immunological Reviews 281:8-27. doi: 10.1111/imr.12621

135. Li HYS and Watowich SS (2014) Innate Immune Regulation by STAT-Mediated Transcriptional Mechanisms. Immunological Reviews 261:84-101. doi: 10.1111/imr.12198

136. Turner MD, Nedjai B, Hurst T and Pennington DJ (2014) Cytokines and Chemokines: At the Crossroads of Cell Signalling and Inflammatory Disease. Biochimica Et Biophysica Acta-Molecular Cell Research 1843:2563-2582. doi: 10.1016/j.bbamcr.2014.05.014

137. Trinchieri G, Pflanz S and Kastelein RA (2003) The IL-12 Family of Heterodimeric Cytokines: New Players in the Regulation of T Cell Responses. Immunity 19:641-644. doi: 10.1016/s1074-7613(03)00296-6

138. Vignali DAA and Kuchroo VK (2012) IL-12 Family Cytokines: Immunological Playmakers. Nature Immunology 13:722-728. doi: 10.1038/ni.2366

139. Fritz JH, Ferrero RL, Philpott DJ and Girardin SE (2006) Nod-Like Proteins in Immunity, Inflammation and Disease. Nature Immunology 7:1250-1257. doi: 10.1038/ni1412

140. Latz E, Xiao TS and Stutz A (2013) Activation and Regulation of the Inflammasomes. Nature Reviews Immunology 13:397-411. doi: 10.1038/nri3452

141. Leemans JC, Cassel SL and Sutterwala FS (2011) Sensing Damage by the NLRP3 Inflammasome. Immunological Reviews 243:152-162. doi: 10.1111/j.1600-065X.2011.01043.x

142. Tschopp J and Schroder K (2010) NLRP3 Inflammasome Activation: The Convergence of multiple signalling pathways on ROS production? Nat Rev Immunol 10:210-5. doi: 10.1038/nri2725

143. Guo LY, Wei G, Zhu JF, Liao W, Leonard WJ, Zhao KJ and Paul W (2009) IL-1 Family Members and STAT Activators Induce Cytokine Production by Th2, Th17, and Th1 Cells.

Proceedings of the National Academy of Sciences of the United States of America 106:13463-13468. doi: 10.1073/pnas.0906988106

144. Pelegrin P and Surprenant A (2006) Pannexin-1 Mediates Large Pore Formation and Interleukin-1 Beta Release by the ATP-Gated P2X(7) Receptor. Embo Journal 25:5071-5082. doi: 10.1038/sj.emboj.7601378

145. Hornung V, Bauernfeind F, Halle A, Samstad EO, Kono H, Rock KL, Fitzgerald KA and Latz E (2008) Silica Crystals and Aluminum Salts Activate the NALP3 Inflammasome through Phagosomal Destabilization. Nature Immunology 9:847-856. doi: 10.1038/ni.1631

146. Zhou RB, Tardivel A, Thorens B, Choi I and Tschopp J (2010) Thioredoxin-Interacting Protein Links Oxidative Stress to Inflammasome Activation. Nature Immunology 11:136-U51. doi: 10.1038/ni.1831

147. Wang YF, Rahman D and Lehner T (2012) A Comparative Study of Stress-Mediated Immunological Functions with the Adjuvanticity of Alum. Journal of Biological Chemistry 287:17152-17160. doi: 10.1074/jbc.M112.347179

148. Neumann S, Burkert K, Kemp R, Rades T, Dunbar PR and Hook S (2014) Activation of the NLRP3 Inflammasome is not a Feature of All Particulate Vaccine Adjuvants. Immunology and Cell Biology 92:535-542. doi: 10.1038/icb.2014.21

149. McAuley JL, Tate MD, MacKenzie-Kludas CJ, Pinar A, Zeng WG, Stutz A, Latz E, Brown LE and Mansell A (2013) Activation of the NLRP3 Inflammasome by IAV Virulence Protein PB1-F2 Contributes to Severe Pathophysiology and Disease. Plos Pathogens 9:14. doi: 10.1371/journal.ppat.1003392

150. Lebre F, Sridharan R, Sawkins MJ, Kelly DJ, O'Brien FJ and Lavelle EC (2017) The Shape and Size of Hydroxyapatite Particles Dictate Inflammatory Responses Following Implantation. Scientific Reports 7:13. doi: 10.1038/s41598-017-03086-0

151. Munoz-Planillo R, Kuffa P, Martinez-Colon G, Smith BL, Rajendiran TM and Nunez G (2013) K+ Efflux Is the Common Trigger of NLRP3 Inflammasome Activation by Bacterial Toxins and Particulate Matter. Immunity 38:1142-1153. doi: 10.1016/j.immuni.2013.05.016

152. Wilmar A, Lonez C, Vermeersch M, Andrianne M, Perez-Morga D, Ruysschaert JM, Vandenbranden M, Leo O and Temmerman ST (2012) The Cationic Lipid, DiC14 Amidine, Extends the Adjuvant Properties of Aluminum Salts through a TLR-4- and Caspase-1-Independent Mechanism. Vaccine 30:414-424. doi: 10.1016/j.vaccine.2011.10.071

153. Gupta RK and Siber GR (1995) Adjuvants for Human Vaccines - Current Status, Problems and Future-Prospects. Vaccine 13:1263-1276. doi: 10.1016/0264-410x(95)00011-o

154. Schneider J, Gilbert SC, Blanchard TJ, Hanke T, Robson KJ, Hannan CM, Becker M, Sinden R, Smith GL and Hill AVS (1998) Enhanced Immunogenicity for CD8+ T Cell Induction and Complete Protective Efficacy of Malaria DNA Vaccination by Boosting with Modified Vaccinia Virus Ankara. Nature Medicine 4:397-402. doi: 10.1038/nm0498-397

155. Invitrogen (2010) Bac-to-Bac® Baculovirus Expression System.78.

156. Dong LC, Hoffman AS and Yan Q (1994) Dextran Permeation through Poly(N-Isopropylacrylamide) Hydrogels. Journal of Biomaterials Science-Polymer Edition 5:473-484. doi: 10.1163/156856294x00158

157. Noble K and Wray S (2002) The Role of the Sarcoplasmic Reticulum (SR) in Developing Uterine Smooth Muscle. Journal of Physiology-London 543:78P-78P.

158. Salunke DM, Caspar DLD and Garcea RL (1989) Polymorphism in the Assembly of Polyomavirus Capsid Protein VP1. Biophysical Journal 56:887-900.

159. Borodina T, Markvicheva E, Kunizhev S, Moehwald H, Sukhorukov GB and Kreft O (2007) Controlled Release of DNA from Self-Degrading Microcapsules. Macromolecular Rapid Communications 28:1894-1899. doi: 10.1002/marc.200700409

160. Zebli B, Susha AS, Sukhorukov GB, Rogach AL and Parak WJ (2005) Magnetic Targeting and Cellular Uptake of Polymer Microcapsules Simultaneously Functionalized with Magnetic and Luminescent Nanocrystals. Langmuir 21:4262-4265. doi: 10.1021/la0502286

161. Rejman J, Oberle V, Zuhorn IS and Hoekstra D (2004) Size-Dependent Internalization of Particles via the Pathways of Clathrin-and Caveolae-Mediated Endocytosis. Biochemical Journal 377:159-169. doi: 10.1042/bj20031253

162. Mauser T, Dejugnat C, Mohwald H and Sukhorukov GB (2006) Microcapsules Made of Weak Polyelectrolytes: Templating and Stimuli-Responsive Properties. Langmuir 22:5888-5893. doi: 10.1021/la060088f

163. Itoh Y, Matsusaki M, Kida T and Akashi M (2006) Enzyme-Responsive Release of Encapsulated Proteins from Biodegradable Hollow Capsules. Biomacromolecules 7:2715-2718. doi: 10.1021/bm060289y

164. Yu AM, Wang YJ, Barlow E and Caruso F (2005) Mesoporous Silica Particles as Templates for Preparing Enzyme-Loaded Biocompatible Microcapsules. Advanced Materials 17:1737-+. doi: 10.1002/adma.200402045

165. Dierendonck M, De Koker S, Cuvelier C, Grooten J, Vervaet C, Remon JP and De Geest BG (2010) Facile Two-Step Synthesis of Porous Antigen-Loaded Degradable Polyelectrolyte

Microspheres. Angewandte Chemie-International Edition 49:8620-8624. doi: 10.1002/anie.201001046

166. Dierendonck M, De Koker S, De Rycke R, Bogaert P, Grooten J, Vervaet C, Remon JP and De Geest BG (2011) Single-Step Formation of Degradable Intracellular Biomolecule Microreactors. Acs Nano 5:6886-6893. doi: 10.1021/nn200901g

167. Yan S, Zhu J, Wang Z, Yin J, Zheng Y and Chen X (2011) Layer-by-Layer Assembly of Poly(L-Glutamic Acid)/Chitosan Microcapsules for High Loading and Sustained Release of 5-Fluorouracil. European Journal of Pharmaceutics and Biopharmaceutics 78:336-345. doi: 10.1016/j.ejpb.2010.12.031

168. Yu X and Pishko MV (2011) Release of Paclitaxel from pH Sensitive and Biodegradable Dextran based Hydrogels. Soft Matter 7:8898. doi: 10.1039/c1sm05729d

169. Sukhorukov GB, Donath E, Davis S, Lichtenfeld H, Caruso F, Popov VI and Mohwald H (1998) Stepwise Polyelectrolyte Assembly on Particle Surfaces: a Novel Approach to Colloid Design. Polymers for Advanced Technologies 9:759-767. doi: 10.1002/(sici)1099-1581(1998100)9:10/11<759::aid-pat846>3.0.co;2-q

170. Moya S, Dahne L, Voigt A, Leporatti S, Donath E and Mohwald H (2001) Polyelectrolyte Multilayer Capsules Templated on Biological Cells: Core Oxidation Influences Layer Chemistry. Colloids and Surfaces a-Physicochemical and Engineering Aspects 183:27-40. doi: 10.1016/s0927-7757(01)00537-4

171. Foged C, Brodin B, Frokjaer S and Sundblad A (2005) Particle Size and Surface Charge Affect Particle Uptake by Human Dendritic Cells in an In Vitro Model. International Journal of Pharmaceutics 298:315-322. doi: 10.1016/j.ijpharm.2005.03.035

172. Volodkin DV, Larionova NI and Sukhorukov GB (2004) Protein Encapsulation via Porous CaCO3 Microparticles Templating. Biomacromolecules 5:1962-1972. doi: 10.1021/bm049669e

173. Yu J, Sanyal O, Izbicki AP and Lee I (2015) Development of Layered Multiscale Porous Thin Films by Tuning Deposition Time and Molecular Weight of Polyelectrolytes. Macromolecular Rapid Communications 36:1669-1674. doi: 10.1002/marc.201500250

174. She Z, Antipina MN, Li J and Sukhorukov GB (2010) Mechanism of Protein Release from Polyelectrolyte Multilayer Microcapsules. Biomacromolecules 11:1241-1247. doi: 10.1021/bm901450r

175. Braciale TJ, Morrison LA, Sweetser MT, Sambrook J, Gething MJ and Braciale VL (1987) Antigen Presentation Pathways to Class-I and Class-II MHC-Restricted T Lymphocytes. Immunological Reviews 98:95-114. doi: 10.1111/j.1600-065X.1987.tb00521.x

176. Hamilos DL (1989) Antigen Presenting Cells. Immunologic Research 8:98-117. doi: 10.1007/bf02919073

177. Moss WJ and Griffin DE (2012) Measles. Lancet 379:153-164. doi: 10.1016/s0140-6736(10)62352-5

178. Decker MD and Edwards KM (2000) Acellular Pertussis Vaccines. Pediatric Clinics of North America 47:309-+. doi: 10.1016/s0031-3955(05)70209-1

179. Akira S, Uematsu S and Takeuchi O (2006) Pathogen Recognition and Innate Immunity. Cell 124:783-801. doi: 10.1016/j.cell.2006.02.015

180. Fischer D, Li YX, Ahlemeyer B, Krieglstein J and Kissel T (2003) In Vitro Cytotoxicity Testing of Polycations: Influence of Polymer Structure on Cell Viability and Hemolysis. Biomaterials 24:1121-1131. doi: 10.1016/s0142-9612(02)00445-3

181. Wesslen T (1970) SV40-Tumorigenesis in Mouse. Acta Pathologica Et Microbiologica Scandinavica Section B-Microbiology and Immunology 78:479-&.

182. Banchereau J, Briere F, Caux C, Davoust J, Lebecque S, Liu YT, Pulendran B and Palucka K (2000) Immunobiology of Dendritic Cells. Annual Review of Immunology 18:767-+. doi: 10.1146/annurev.immunol.18.1.767

183. Baud V and Karin M (2001) Signal Transduction by Tumor Necrosis Factor and Its Relatives. Trends in Cell Biology 11:372-377. doi: 10.1016/s0962-8924(01)02064-5

184. vanKooten C and Banchereau J (1997) Functions of CD40 on B cells, Dendritic Cells and Other Cells. Current Opinion in Immunology 9:330-337. doi: 10.1016/s0952-7915(97)80078-7

185. Cella M, Scheidegger D, PalmerLehmann K, Lane P, Lanzavecchia A and Alber G (1996) Ligation of CD40 on Dendritic Cells Triggers Production of High Levels of Interleukin-12 and Enhances T Cell Stimulatory Capacity: T-T Help via APC Activation. Journal of Experimental Medicine 184:747-752. doi: 10.1084/jem.184.2.747

186. Bennett SRM, Carbone FR, Karamalis F, Flavell RA, Miller J and Heath WR (1998) Help for Cytotoxic-T-cell Responses is Mediated by CD40 Signalling. Nature 393:478-480.

187. Cruse JM, Wang H, Lewis RE and Morrison RS (2003) Expression of CD80 and CD86 in CD34+-Derived Dendritic Cells: the Role of TNF-Alpha. Faseb Journal 17:C147-C147.

188. Wendland T, Mauri D, Frutig K, Frei E, Brander K and Pichler WJ (1997) Induction of Human Cytotoxic CD4+ T Cells: Role of CD80 and CD86 Expression on Antigen Presenting Cells. Journal of Allergy and Clinical Immunology 99:1246-1246.

189. Acharya AP, Carstens MR, Lewis JS, Dolgova N, Xia CQ, Clare-Salzler MJ and Keselowsky BG (2016) A Cell-Based Microarray to Investigate Combinatorial Effects of

Microparticle-Encapsulated Adjuvants on Dendritic Cell Activation. Journal of Materials Chemistry B 4:1672-1685. doi: 10.1039/c5tb01754h

190. Lamkanfi M and Dixit VM (2014) Mechanisms and Functions of Inflammasomes. Cell 157:1013-1022. doi: 10.1016/j.cell.2014.04.007

191. Kim SH, Kim DH, Lavender P, Seo JH, Kim YS, Park JS, Kwak SJ and Jee YK (2009) Repression of TNF-Alpha-Induced IL-8 Expression by the Glucocorticoid Receptor-Beta Involves Inhibition of Histone H4 Acetylation. Experimental and Molecular Medicine 41:297-306. doi: 10.3858/emm.2009.41.5.033

192. Iwai-Shimada M, Takahashi T, Kim MS, Fujimura M, Ito H, Toyama T, Naganuma A and Hwang GW (2016) Methylmercury Induces the Expression of TNF-Alpha Selectively in the Brain of Mice. Scientific Reports 6:8. doi: 10.1038/srep38294

193. Spengler RN, Spengler ML, Strieter RM, Remick DG, Larrick JW and Kunkel SL (1989) Modulation of Tumor Necrosis Factor-Alpha Gene-Expression Desensilization of Prostaglandin-E2-Induced Suppression. Journal of Immunology 142:4346-4350.

194. Zhou L, Yan CL, Gieling RG, Kida Y, Garner W, Li W and Han YP (2009) Tumor Necrosis Factor-Alpha Induced Expression of Matrix Metalloproteinase-9 through p21-Activated Kinase-1. Bmc Immunology 10:15. doi: 10.1186/1471-2172-10-15

195. Woo CH, Eom YW, Yoo MH, You HJ, Han HJ, Song WK, Yoo YJ, Chun JS and Kim JH (2000) Tumor Necrosis Factor-Alpha Generates Reactive Oxygen Species via a Cytosolic Phospholipase A(2)-Linked Cascade. Journal of Biological Chemistry 275:32357-32362. doi: 10.1074/jbc.M005638200

196. Cox GW, Melillo G, Chattopadhyay U, Mullet D, Fertel RH and Varesio L (1992) Tumor Necrosis Factor-Alpha-Dependent Production of Reactive Nitrogen Intermediates IFN-Gamma

Plus IL-2-Induced Murine Macrophage Tumoricidal Activity. Journal of Immunology 149:3290-3296.

197. Zyuzin MV, Diez P, Goldsmith M, Carregal-Romero S, Teodosio C, Rejman J, Feliu N, Escudero A, Almendral MJ, Linne U, Peer D, Fuentes M and Parak WJ (2017) Comprehensive and Systematic Analysis of the Immunocompatibility of Polyelectrolyte Capsules. Bioconjugate Chemistry 28:556-564. doi: 10.1021/acs.bioconjchem.6b00657

198. Klinman DM, Yi AK, Beaucage SL, Conover J and Krieg AM (1996) CpG Motifs Present in Bacterial DNA Rapidly Induce Lymphocytes to Secrete Interleukin 6, Interleukin 12, and Interferon Gamma. Proceedings of the National Academy of Sciences of the United States of America 93:2879-2883. doi: 10.1073/pnas.93.7.2879

199. Li HF, Willingham SB, Ting JPY and Re F (2008) Cutting Edge: Inflammasome Activation by Alum and Alum's Adjuvant Effect are Mediated by NLRP3. Journal of Immunology 181:17-21. doi: 10.4049/jimmunol.181.1.17

200. Ciraci C, Janczy JR, Sutterwala FS and Cassel SL (2012) Control of Innate and Adaptive Immunity by the Inflammasome. Microbes and Infection 14:1263-1270. doi: 10.1016/j.micinf.2012.07.007

201. Mariathasan S and Monack DM (2007) Inflammasome Adaptors and Sensors: Intracellular Regulators of Infection and Inflammation. Nature Reviews Immunology 7:31-40. doi: 10.1038/nri1997

202. Burns K, Martinon F and Tschopp J (2003) New Insights into the Mechanism of IL-1 Beta Maturation. Current Opinion in Immunology 15:26-30. doi: 10.1016/s0952-7915(02)00017-1

203. Lamm ME (1997) Interaction of Antigens and Antibodies at Mucosal surfaces. Annual Review of Microbiology 51:311-340. doi: 10.1146/annurev.micro.51.1.311

204. De Temmerman M-L, Demeester J, De Vos F and De Smedt SC (2011) Encapsulation Performance of Layer-by-Layer Microcapsules for Proteins. Biomacromolecules 12:1283-1289. doi: 10.1021/bm101559w

APPENDIX A FLUORESCENT-PMLC ENCAPSULATION

Chitosan is a nontoxic linear polysaccharide composed of β-1,4-linked D-glucosamine. It's a naturally occurring polymer, derived from the deacetylation of chitin which was found in the exoskeletons of crustaceans and insects. Due to its biodegradable and biocompatible properties, it's commonly used for pharmaceutical and medical applications.

Additionally, while considering the suitable polyelectrolytes for surface modification, chitosan is always evident. Because of its ability to open tight junctions and adhere on the mucosal surface [28], the weak positive charge also makes it capable of being a polycation. However, it could be dissolved in water only when the pH value is lower than 4. Therefore, it could not be used in our system, because the low pH surrounding resulted in the core decomposed simultaneously, scanning electron microscopy image was shown in Figure 41. From the SEM image, the structure is not microsphere as we expected and even the morphology is unlike other PMLCs after core removal.

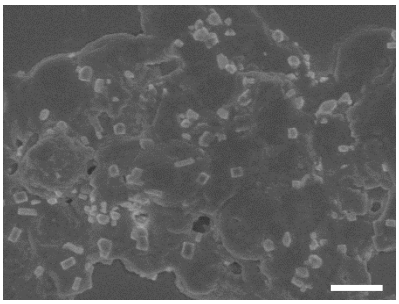

Figure 41. FE-SEM image of the PMLCs encapsulated BSA with 3 bilayers and followed by deposited chitosan as the surface modification, scale bar, 3 μm.

APPENDIX B BOVINE SERUM ALBUMIN ENCAPSULATION

Bovine Serum Albumin (BSA), with MW of 66.5 kDa, pI value of 4.7 and 7 nm in diameter, was first used as an model antigen temporarily, serving for primary verification and study of the PMLCs.

To study the structure of the particles, BSA was labeled with fluorescent isothiocyanate (FITC). FITC was first dissolved in 0.1 M carbonate-bicarbonate buffer, and FITC-BSA was bound at a molar ratio of 10:1, after incubating for 2 hours at room temperature, the solution was then collected by flowing through the Sephadex G-25M column gel bed.

Confocal Laser Scanning Microscopy was used to investigate the distribution of encapsulation. One drop of well-suspended FITC-PMLCs was spread and placed on a glass slide covered by #1.5 coverslip. Confocal micrographs were taken with Olympus FV1000 Confocal Microscope and equipped with a 100x oil immersion objective with a numerical aperture of 1.4. The excitation wavelength was 488nm for detecting FITC labeled protein and 633 nm for detecting Alexa Fluor® 647.

In order to verify the adsorption mechanism, the FITC-BSA was encapsulated to PMLCs. From the CLSM images, shown in Figure 42, the profile presents higher fluorescence intensity from the edge than from the center. Meanwhile, it reveals that the FITC-BSA with a hydrodynamic diameter of about 12nm is able to penetrate through porous structure into the $CaCO_3$ microparticles.

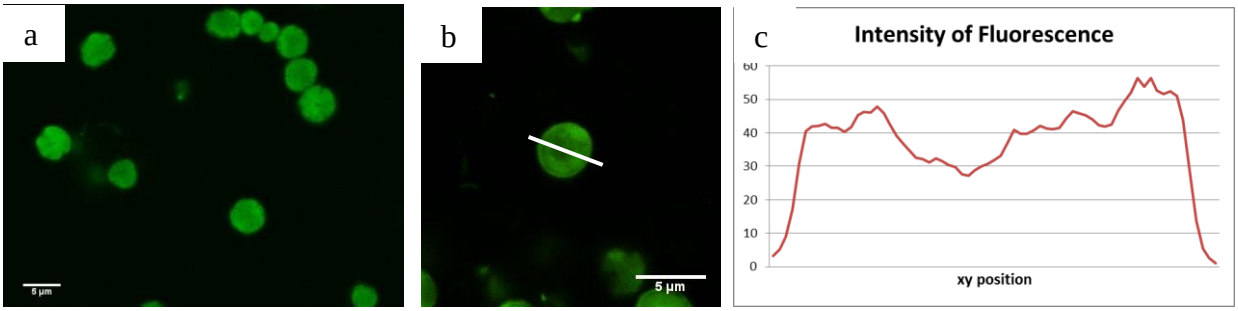

Figure 42. CLSM images of PMLCs encapsulated FITC-BSA with 2.5 bilayers (a, b), and (c) is the fluorescence profile for image (b).

The effect of the size of protein on encapsulation efficiency was also investigated. Bovine serum albumin with 7 nm in diameter was fabricated into PMLC with the same approach as $(VP\text{-}PMLC)_H$. The encapsulation efficiency was 50%, which was lower than that of $(VP\text{-}PMLC)_H$. A possible reason could be the limited diffusion of larger biomacromolecules through the capsule [204]. Therefore, viral protein with a larger size appears to be a better candidate for PMLC encapsulation.